1992

Incorporating Reservoir Characteristics for Automatic History Matching.

Keith J. Halford
Louisiana State University and Agricultural & Mechanical College

Order Number 9301058

Incorporating reservoir characteristics for automatic history matching

Halford, Keith J., Ph.D.

The Louisiana State University and Agricultural and Mechanical Col., 1992

U·M·I
300 N. Zeeb Rd.
Ann Arbor, MI 48106

INCORPORATING RESERVOIR CHARACTERISTICS FOR AUTOMATIC HISTORY MATCHING

A Dissertation

Submitted to the Graduate Faculty of the
Louisiana State University and
Agricultural and Mechanical College
in partial fulfillment of the
requirements for the degree of
Doctor of Philosophy

in

The Department of Petroleum Engineering

by
Keith J. Halford
B.S., Louisiana State University, 1984
M.S., Louisiana State University, 1985
May, 1992

ACKNOWLEDGEMENT

The author wishes to express his gratitude and appreciation to Dr. Zaki Bassiouni, Chairman of the Petroleum Engineering Department at Louisiana State University, under whose guidance and supervision this work was completed. He also wants to thank his patient and reasonably tolerant wife.

TABLE OF CONTENTS

		page
ACKNOWLEDGEMENT		ii
LIST OF TABLES		vi
LIST OF FIGURES		viii
ABSTRACT		xiii
CHAPTER		
I.	INTRODUCTION	1
II.	AUTOMATIC HISTORY-MATCHING : KEY INGREDIENTS	4
	2.1. Objective function	4
	2.2. History-matching parameters	5
III.	SEARCH ALGORITHMS	10
	3.1. Steepest descent	12
	3.2. Newton's method	14
	3.2.1. Gauss-Newton	16
	3.2.2. Levenberg-Marquardt	16
	3.2.3. Quasi-Newton	22
IV.	EXPANDED OBJECTIVE FUNCTION	23
	4.1. Comparison of measured observations	24
	4.2. Comparison of synthesized observations	25
V.	INCORPORATING RESERVOIR CHARACTERISTICS IN HISTORY-MATCHING PARAMETERS	30
	5.1. Iso-value contours	30
	5.2. Weight matrix applications	40
	5.2.1. Exponential modifier	40
	5.2.2. Average values	42
	5.3. Relative permeability	43

VI. AUTOMATIC HISTORY-MATCHING ALGORITHM 46

6.1. Coordinate systems 46
6.2. Zonation 50
6.3. Weight matrices 53
6.4. History-matching parameters 54
6.5. History aquisition 60
6.6. Search algorithm 62

VII. HISTORY MATCH OF BERYL RESERVOIR -- A HYPOTHETICAL CASE 66

7.1. The Beryl reservoir 66
7.2. History matching with ideal parameters 73
7.3. History matching with realistic parameters 77

VIII. HISTORY MATCH OF SPARTA "B" RESERVOIR -- FORDOCHE FIELD 82

8.1. The Sparta "B" reservoir 82
8.2 Production and Pressure History 84
8.3 Automatic History Matching 86

IX. CONCLUSIONS 106

REFERENCES 109

APPENDICES

A. SIMULATION OF "1,200-FOOT" AQUIFER 115

A.1. Model Grid 115
A.2. Model Boundaries 116
A.3. Period Investigated. 117
A.4. History Match and Sensitivity Analysis 117

B. MODIFICATIONS TO BOAST II. 126

B.1. BOAST as a subroutine. 126
B.2. SIP, strongly implicit procedure, matrix solver added. 126
B.3. Subroutines SOLONE and SOLTWO 126

B.4. Subroutine QRATE 127
B.5. No free gas option 128

C. HISTORY MATCH OF SPARTA "A" RESERVOIR -- FORDOCHE FIELD 129

C.1 The Sparta "A" 129
C.2 Production History 131
C.3 Automatic History Matching 131

VITA 150

LIST OF TABLES

Table		Page
4.1	An example of 118 observations with 7 data types.	24
6.1	Reservoir characteristics that can be modified by OPTIM and their associated identifiers.	55
6.2	History-matching parameter options.	55
6.3	An example of history-matching parameter report from OPTIM.	56
6.4	Observation types OPTIM compares to calculated values and their associated identifiers.	61
7.1	Summary of Beryl reservoir, fluid properties, and aquifer characteristics.	70
7.2	Reservoir production summary for the Beryl reservoir.	71
7.3	Observation types used to history-match the Beryl reservoir.	75
7.4	Error statistics for the Beryl reservoir simulated with an ideal and a realistic parameter set at selected iterations.	79
8.1	Summary of Sparta "B" reservoir, fluid properties, and aquifer characteristics.	83
8.2	Production from the Sparta "B" by well from March 1973 to September 1989.	85
8.3	Observation types used to history-match the Sparta "B".	86
8.4	Error statistics, in Bbls/d, for the Sparta "B" initial model, history-match, prediction, and overall.	87
8.5	Cumulative calculated and measured production from the Sparta "B".	88

C.1 Summary of Sparta "A" reservoir, fluid properties, and aquifer characteristics. 130

C.2 Production from the Sparta "A" by well from January 1970 to September 1989. 133

C.3 Cumulative calculated and measured production from the Sparta "A". 133

LIST OF FIGURES

Figure		Page
2.1	Three permeability distributions generated by zone multipliers, a sensitivity vector, and a weight matrix.	7
3.1	"1,200-foot" aquifer model's sensitivity to changes in Kxy and Kz.	11
3.2	Steepest-descent search paths for three cases.	13
3.3	Gauss-Newton search paths for four cases.	17
3.4	The differences between steepest-descent and Gauss-Newton search paths for a case.	18
3.5	The effect of Levenberg radius, LR, on search direction and range.	20
3.6	Errors in search direction and range, p, from the Gauss-Newton approximation.	21
4.1	Three different matches with a root-mean-square error of 650 psi.	28
4.2	An example of appropriately and inappropriately approximating a potential surface with a plane defined by three water-level measurements.	29
5.1	An example iso-value contour and zone of influence associated with seg 3.	32
5.2	Defining dividing planes.	34
5.3	Determining distance to a segment and polarity of segments within an iso-line.	36
5.4	Two permeability distributions generated with the iso-value line of figure 5.1.	39

5.5 A three-dimensional example of dividing planes on an iso-line. 41

5.6 Defining relative permeability curves with a hyperbolic tangent function and the effect of varying fitting parameters a and b. 45

6.1 Cartesian coordinate system superimposed on a column, row, and layer system. 47

6.2 Obtaining calculated observation by interpolation. 49

6.3 Defining a model zone with a closed contour. 51

6.4 Dividing a model into zones with a structure map. 52

6.5 Effect of log transforms and scaling on parameter sensitivity. 59

6.6 Flow chart of OPTIM coupled with BOAST II. 65

7.1 Structure map and model grid for the Beryl reservoir, a hypothetical field. 67

7.2 Isopach maps of the upper Beryl, lower Beryl, and net sand. 68

7.3 Porosity and permeability distributions in the Beryl reservoir. 69

7.4 The true history of the Beryl and histories approximated with an ideal parameter set and a realistic parameter set. 72

7.5 Change in model error and parameter multipliers for an ideal and a realistic parameter set. 74

7.6 Relative permeability curves from models produced with an ideal parameter set and with a realistic parameter set. 76

7.7	History-matched horizontal permeability, Kxy, distribution based on realistic parameter set.	78
7.8	Production and pressure history from well By-2, the well fitted best with a realistic parameter set.	80
7.9	Production and pressure history from well By-5, the well fitted worst with a realistic parameter set.	81
8.1	Structure map and model grid for the Sparta "B".	90
8.2	Isopach maps of Sparta "B" upper sand, intermediate shale, and lower sand.	91
8.3	Cross-sections A-A' and B-B' through the Sparta "B". See figure 8.1 for sections traces.	92
8.4	Porosity maps of Sparta "B" upper and lower sands.	93
8.5	Initial permeability maps of Sparta "B" upper and lower sands.	94
8.6	Observation error introduced by step-wise approximation of production rates.	95
8.7	Total production from the Sparta "B".	96
8.8	Change in model error and parameter multipliers for the Sparta "B".	97
8.9	History-matched permeability maps of Sparta "B" upper and lower sands.	98
8.10	Relative permeability curves for the Sparta "B".	99
8.11	Production from well Sm-4 in the Sparta "B".	100
8.12	Production from well Sm-7 in the Sparta "B".	101
8.13	Production from well Sm-9 in the Sparta "B".	102

8.14 Production from well Bl-4 in the Sparta "B". 103

8.15 Displaceable oil distribution in the Sparta "B" in 1973 and 1978. 104

8.16 Displaceable oil distribution in the Sparta "B" in 1982 and 1990. 105

A.1 Model grid and extent. 119

A.2 Conceptual model for the "1,200-foot" aquifer and adjacent units. 120

A.3 Simulated potentiometric surface of the "400- and 600-foot" aquifers (layer 1) in 1984. 121

A.4 Pumpage by aquifer from 1946 through 1988. 122

A.5 Simulated and measured water levels for wells An-16, EB-780A, and EB-780B south of the Baton Rouge fault. 123

A.6 Simulated and measured water levels for wells EB-146 and EB-782B in Baton Rouge. 124

A.7 Model sensitivity to changes in transmissivity, vertical leakance, and storage coefficient. 125

C.1 Structure map and model grid for the Sparta "A". 134

C.2 Isopach maps of Sparta "A" upper sand and middle sand. 135

C.3 Isopach maps of Sparta "A" lower sand and total sand. 136

C.4 Isopach maps of Sparta "A" upper shale and lower shale. 137

C.5 Cross-sections A-A' and B-B' through the Sparta "A". See figure C.1 for sections traces. 138

C.6 Porosity maps of Sparta "A" upper and middle sands. 139

C.7 Porosity map of Sparta "A" lower sand and the history-matched horizontal permeability distribution of all sands . 140

C.8 Relative permeability curves for the Sparta "A". 141

C.9 Total production from the Sparta "A". 142

C.10 Production from well An-2 in the Sparta "A". 143

C.11 Production from well Sm-5 in the Sparta "A". 144

C.12 Production from well Sm-6 in the Sparta "A". 145

C.13 Production from well Sm-7 in the Sparta "A". 146

C.14 Displaceable oil distribution in the Sparta "A" in 1970 and 1974. 147

C.15 Displaceable oil distribution in the Sparta "A" in 1978 and 1982. 148

C.16 Displaceable oil distribution in the Sparta "A" in 1986 and 1990. 149

ABSTRACT

Automatic history-matching is refined in this work by expanding the objective function and incorporating reservoir characteristics in the process of parameter selection. Iso-value contours are used to incorporate reservoir characteristics within history-matching parameters. These improvements are implemented in an automatic history matching algorithm, OPTIM, that is coupled with BOAST II. Case histories of both hypothetical and real reservoirs demonstrated the effectiveness of incorporating reservoir characteristics in automatic history-matching parameters.

CHAPTER I
INTRODUCTION

History matching attempts to estimate unknown reservoir properties based on past production. A reasonable approximation of these unknowns is needed if future production estimates are to be believed. Automatic history matching provides a better way of determining these unknowns than trial-and-error methods. The automatic history match approach includes a rigorous, quantitative description, a sensitivity analysis of each estimated property, and an algorithm's indifference to tedium.

Successful automatic history matching requires:

(1) stating an equation, the objective function, which provides the non-arbitrary basis of comparison between reservoir simulation results and field measurements;

(2) grouping unknown reservoir properties into easily adjustable parameters; and

(3) formulating an appropriate "search" technique that estimates the unknown reservoir properties based on minimization of the objective function.

The earliest automatic history-matching programs used a pressure-based objective function. The parameters were defined by zones and least-squares data fitting was used (Jacquard and Jains, 1965). Jahns (1966) used these methods coupled with a Gauss-Newton search algorithm and solved the parameter values iteratively.

A few investigators have tried avoiding the iterative component of automatic history matching. Coats et al. (1970) assumed the region of interest could be bounded and treated as linear, but the reservoir descriptions were questionable (Farouq Ali and Berkowitz, 1988). Veatch and Thomas (1971) sought the inverse solution directly by solving for porosity and permeability distributions close to the wells, and then extending the solution outward. Unfortunately, small pressure measurement errors greatly changed the estimated reservoir description (Farouq Ali and Berkowitz, 1988).

Simulation of groundwater problems has also furthered automatic history matching since the associated problems are similar to those found in petroleum engineering. Most petroleum reservoirs and associated aquifers are bounded by impermeable beds and can be assumed to be static prior to production. However, the boundary conditions on groundwater problems differ since there is always some flow either through or into a freshwater system. Consequently, the flux through a system is one of the unknown aquifer properties that must be estimated.

Recent groundwater literature has focused on the believability and relative worth of parameter estimating schemes. Kuiper (1986) compared maximum likelihood, kriging, and optimization methods for determining permeability distributions. He found optimization to be simpler and to work as well or better than the other methods. Hill (1989) applied the methods of Cooley and Vecchia (1987) to check plausibility of the inverse solution.

Automatic history matching is refined in this work by expanding the objective function and incorporating reservoir characteristics in the process of parameter selection. An expanded objective function incorporating several measurement types can make an automatic history-matching algorithm more sensitive to the parameters being estimated and reduce the implausibility of some estimates.

CHAPTER II

AUTOMATIC HISTORY MATCHING : KEY INGREDIENTS

2.1 Objective Function

The objective function is a vital component of an automatic history-matching scheme because it is the only reference to reality. If a poorly defined objective function is used, automatic history-matching algorithms can reduce the difference between calculated and measured observations to nothing and still misestimate the reservoir properties in question. As an example, a reservoir history could be matched using two bottom-hole pressures for observed measurements. The difference between calculated and measured pressures would be reduced to zero albeit unrealistic estimated permeability and other petrophysical properties.

The simplest and most commonly used objective function, F(x), is a sum of squares defined as:

$$F(x) = \frac{1}{2} \Sigma f(x)^2 \tag{2.1}$$

$$f(x) = (\hat{\psi}(x) - \psi)\, w \tag{2.2}$$

where f(x) is the residual or error vector, i.e. the difference between calculated ($\hat{\psi}(x)$) and measured (ψ) observation times a weight (w). Weights emphasize more accurate measurements and allow the use of measurements of different dimensions.

More sophisticated objective functions exist. However, their effective use requires a better knowledge of the interrelationships

between the estimated parameters than what normally exists. Gavalas et al. (1976) used Bayesian estimation to allow for the incorporation of prior information in their automatic history-matching scheme. The inclusion of prior information acts to keep parameter estimates reasonable, but it can force a solution to an ill-posed problem. A composite objective function that includes pressure and permeability comparisons was suggested. This approach assumed that an average reservoir permeability and variance are known. Solutions that departed from the average were penalized.

Cooley (1983) adopted a history-matching scheme similar to Gavalas et al., but incorporated prior information in a non-Bayesian method. The resulting objective function incorporated a wide range of data ranging from well-test derived permeabilities to informed guesses of recharge rates.

Watson et al. (1980) presented another automatic history-matching algorithm which estimate relative permeability exponents in conjunction with porosity and permeability values. This algorithm used a composite objective function that utilized both pressure and production data. Watson's objective function addressed the lack of pressure data instead of trying to constrain parameter estimates.

2.2 History-Matching Parameters

Reservoir properties are adjusted in order to match simulated production to measured production. Porosity, f, permeability, k, aquifer influx characteristics, B,t_D, relative permeability, k_r, capillary pressures, PVT data, fluid properties, and rock compressibilities could be adjusted to obtain a

match. Adjusting only the first four properties in a 200 node model (10 x 10 x 2), it is possible to have more than 1,600 variables [200*($f + k_x + k_y + k_z + B + t_D + K_{ro} + K_{rw}$)], while the reservoir history only justifies adjusting a few independent parameters.

History-matching parameters are used to overcome this difficulty. These parameters are formed by grouping variables with common physical and spatial relationship. The spatial relationship can be defined by zonation, sensitivity vectors, or weight matrices.

Zonation assumes the reservoir can be subdivided into homogenous zones. Each zone is characterized by an independent history-matching parameter. Zonation is preferred when geologic data indicate abrupt, discontinuous boundaries (e.g.: faults, facies changes, etc.). A possible permeability distribution produced by zonation with four independent parameters is shown in Figure 2.1a. Zonation, whether appropriate or not, is used more often than other methods due to the ease of application (Jahn, 1966, Coats, 1970, Veatch and Thomas, 1971, Cooley, 1977, Durbin, 1986, and Carrera and Neuman, 1986).

Sensitivity vectors treat the reservoir property as a continuous spatial function (Chen et al., 1974). For example, let the horizontal permeability, $K(x,y) = c \sin(ax) \sin(by) + d$. The variables a, b, c, and d become the history-matching parameters. Figure 2.1b shows one possible permeability distribution for K(x,y). Other investigators

a.) Zone Multipliers

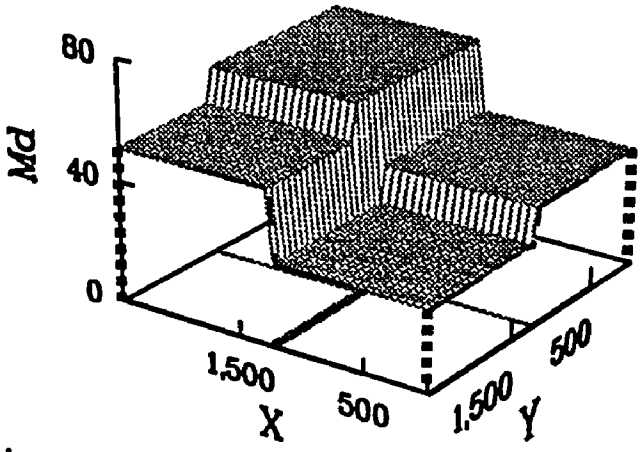

b.) Sensitivity Vector

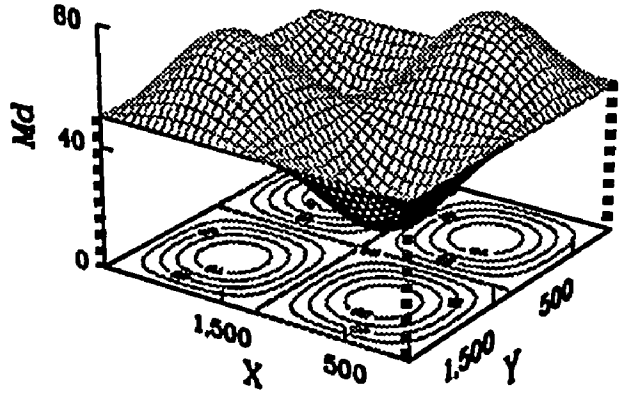

c.) Weight Matrix

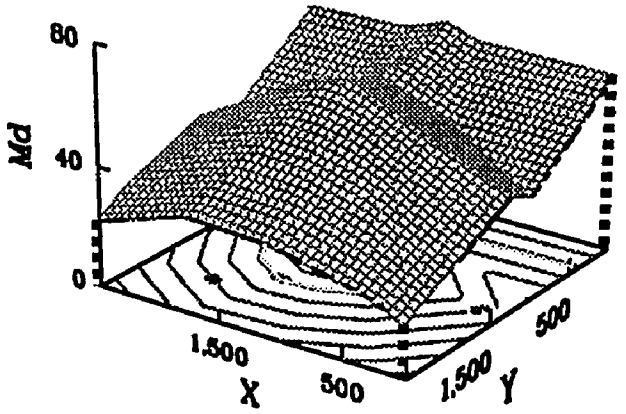

Figure 2.1--Three permeability distributions generated by zone multipliers, a sensitivity vector, and a weight matrix.

(Chavent et al., 1975, Gavalas et al.,1976, and Watson, 1980) have also used this approach to define history-matching parameters.

Weight matrices combine aspects of both zonation and sensitivity vectors. A weight matrix allows for smooth changes within a distribution and for constant relative change from one node to another. The horizontal permeability example of figure 2.1c results from the relationship:

$$K(x,y)_n = a + bw_n \qquad (2.3)$$

where, a = a constant,

b = weight matrix multiplier, and

w_n = nth weight in matrix [W] defining potential permeability distribution.

For larger data sets, weight matrices can be filled by kriging or some other interpolation scheme. For limited data sets, subjective information can help fill these matrices.

The choice of history-matching parameters is a key ingredient since poor choices cannot be compensated by increasing or improving the data of the reservoir history. Carrera and Neuman (1986c) determined the permeability distribution in a small hypothetical model for ten different zonation schemes. A large addition of noise to the reservoir history affected the match only slightly for the versions in which the permeability distribution was ill-defined.

The use of an excessive number of history-matching parameters produces a smaller error between simulated and measured production histories. However, it frequently misestimates reservoir characteristics to a

greater degree than schemes with fewer parameters. As the number of parameters increases, a larger fraction of these parameters is insensitive to model change (Shah, 1978 and Yeh and Yoon, 1981). Freyberg (1988) had nine groups of graduate students history match a hypothetical, 2-D, groundwater model using predevelopment pressure measurements. The groups estimated the permeability distribution, a uniform recharge rate, and the aquifer base. The best permeability estimate and drawdown prediction came from the model made up of only a few homogenous regions.

CHAPTER III
SEARCH ALGORITHMS

History-match improvement is an iterative process due to the non-linearity of the problem. Consequently, automatic history-matching algorithms start with an initial parameter estimate and solve for an incremental parameter change, p. The direction and amount of change is based on minimization of the objective function. These algorithms are referred to as search algorithms since they all seek to find the smallest difference between calculated and measured observations.

Several available search algorithms are discussed in this chapter. A two-parameter, vertical (K_z) and horizontal permeability (K_{xy}), groundwater example will be used to illustrate the workings of each search algorithm. The model is described in appendix A. Model errors were calculated for a wide range of each parameter and an error surface of K_{xy} vs. K_z was mapped. This provides a base map that is used to illustrate parameter change between iterations (Fig. 3.1). The range of K_{xy} and K_z values examined in this illustrative example is much greater than the associated uncertainties, but gives a better perspective on model sensitivity.

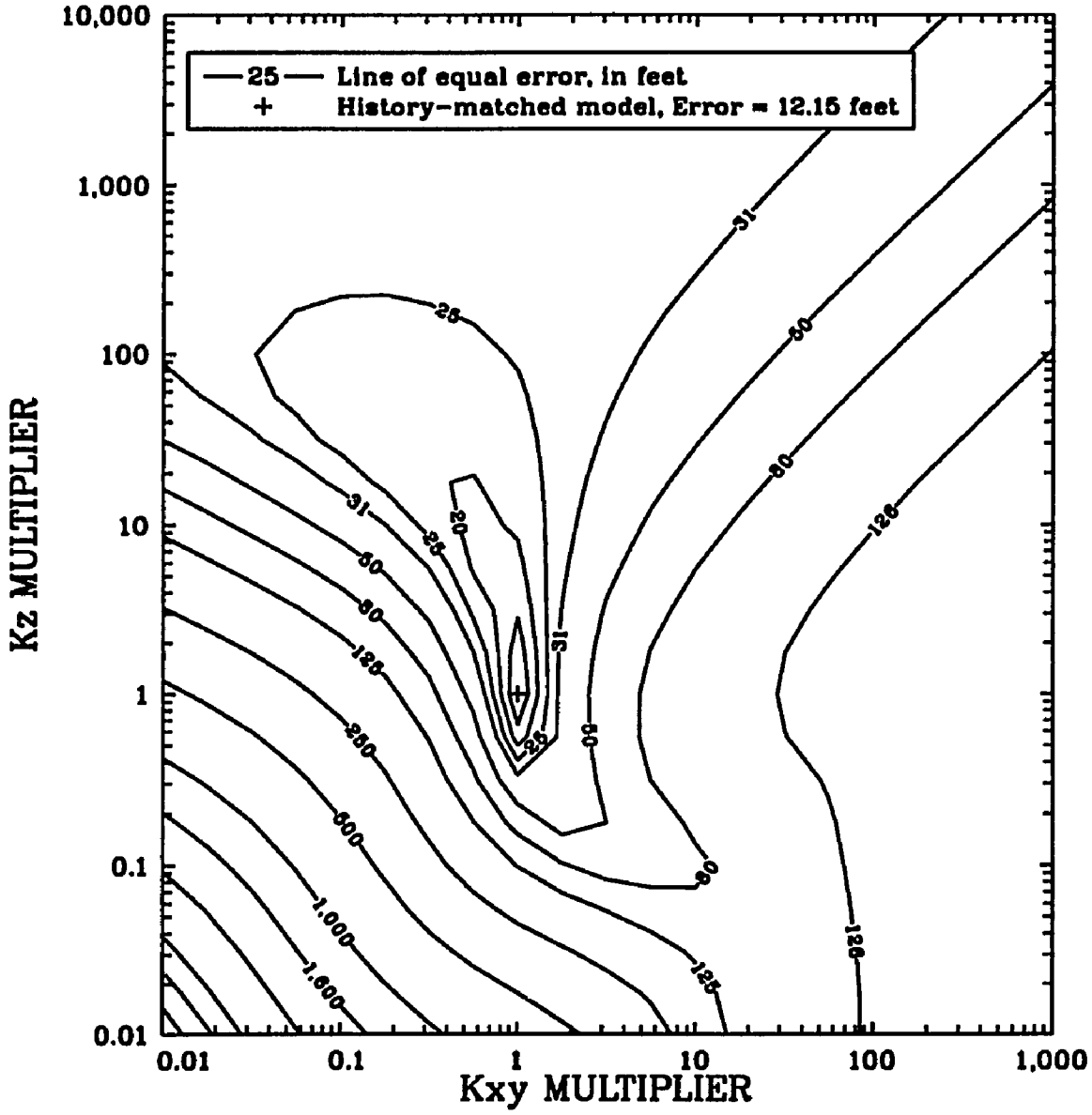

Figure 3.1--"1,200-foot" aquifer model's sensitivity to changes in Kxy and Kz.

3.1 Steepest Descent

A steepest-descent search direction at iteration l is the opposite of the partial derivatives of (Eq. 2.1), or the negative gradient.

$$p_l = -g_l(x) . \tag{3.1}$$

where,

$$g_l(x) = \frac{df_l(x)}{dx}, \text{ the gradient at } x_l.$$

The magnitude of change, step length, is fixed *a priori* or scaled relative to the error change at the previous step. The path travelled along the error surface (Fig. 3.2) is similar to that of a marble rolling down a hillside. The simplicity of the approach and its intuitively obvious search direction has a strong appeal. Both Chen et al. (1974) and Chavent et al. (1975) used steepest-descent search algorithms. Steepest-descent algorithms have guaranteed convergence on a minimum, but the rate of convergence is usually slow (Gill et al., 1981). The penalty imposed by this slow rate of convergence is great enough to warrant the use of other methods.

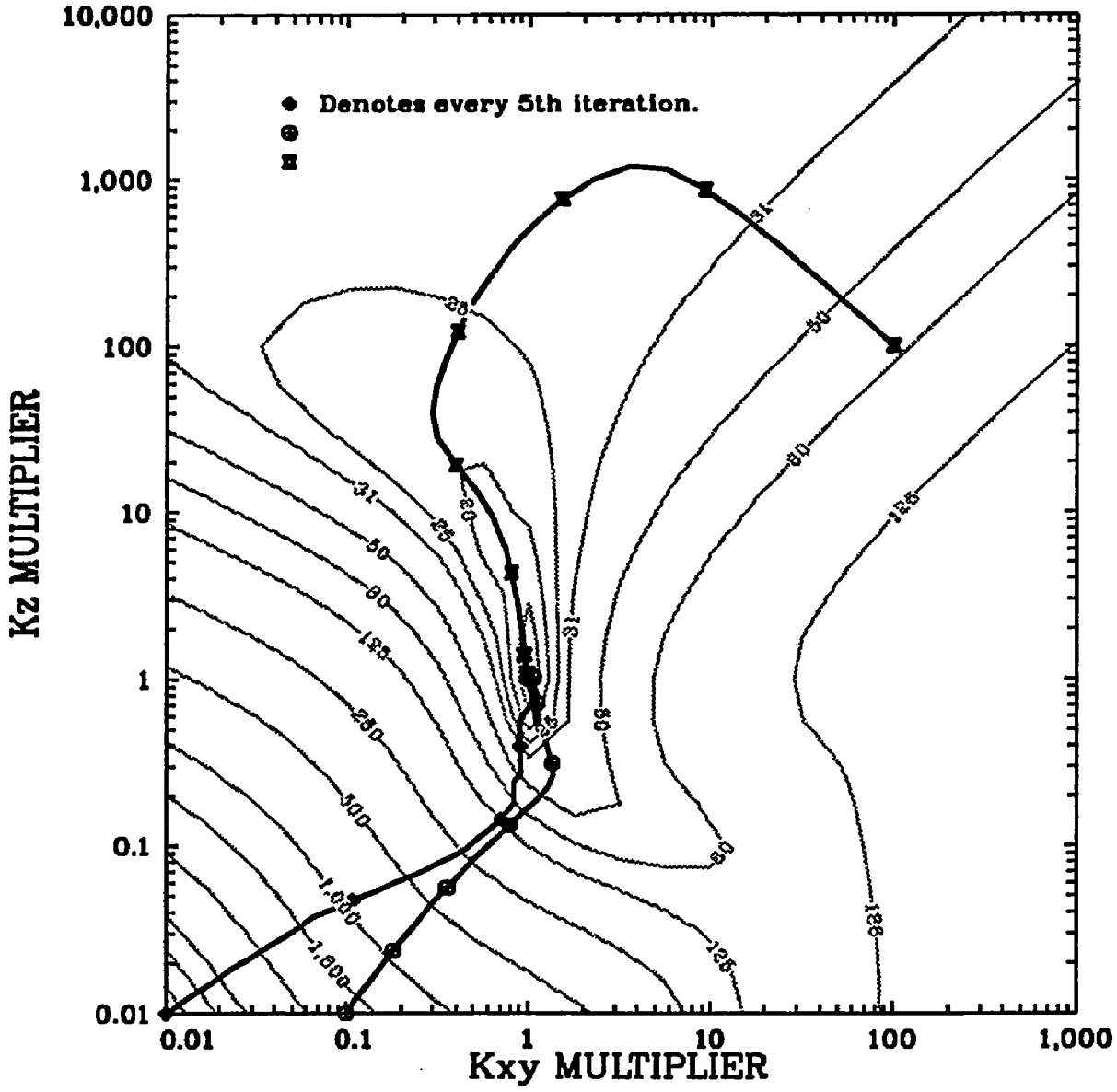

Figure 3.2--Steepest-descent search paths for three cases.

3.2 Newton's Method

Newton's method is the basis for the most practical and prevalent of minimization algorithms. Yet, Newton's method itself is never used since explicit evaluation of the second-derivative terms is too costly. Model improvement is accomplished iteratively by these algorithms as they solve for a search direction, p, based on the first and second derivatives of a quadratic objective function, F (Gill *et al*, 1981). The first three terms of a Taylor-series expansion about the history-matching parameters, at the current iteration, l, form a quadratic model of the objective function in terms of p_l. For simplicity, the one parameter case of Newton's method will be shown first with M comparisons:

$$F(x+p) \simeq F(x) + p \sum_{m=1}^{M} \frac{df}{dx} f(x) + \frac{1}{2} p^2 \sum_{m=1}^{M} \left[\frac{df}{dx}\frac{df}{dx} + \frac{d^2f}{dx^2} f(x) \right] \quad (3.2)$$

where,

$$F(x) = \frac{1}{2} \Sigma f(x)^2 \quad (2.1)$$

The minimization of p in (Eq. 3.2) defines the best search direction. If the first and second derivative terms in (Eq. 3.2) are set equal to some function of p:

$$P(p) = p \sum_{m=1}^{M} \frac{df}{dx} f(x) + \frac{1}{2} p^2 \sum_{m=1}^{M} \left[\frac{df}{dx}\frac{df}{dx} + \frac{d^2f}{dx^2} f(x) \right] \quad (3.3a)$$

or

$$P(p) = pg(x) + \frac{1}{2} p^2 G(x) \quad (3.3b)$$

where,

$$P(p) = F(x+p) - F(x)$$

The first derivative of P(p) when set to 0 gives the appropriate search direction

$$G(x)p = -g(x)\,. \tag{3.4}$$

Equations 3.2, 3.3b, and 3.4 are equivalently represented in their more useful matrix form at a specific iteration, l, by equations 3.5, 3.6, and 3.7.

$$F(x_l+p) \simeq F_l(x) + g_l(x)^T p + \frac{1}{2} p^T G_l(x) p \tag{3.5}$$

$$P(p) = g_l(x)^T p + \frac{1}{2} p^T G_l(x) p \tag{3.6}$$

$$G_l(x)p_l = -g_l(x) \tag{3.7}$$

where:

$$g(x) = J(x)^T f(x) \tag{3.8}$$

$$G(x) = J(x)^T J(x) + Q(x) \tag{3.9}$$

$$Q(x) = \sum_{m=1}^{M} f_m(x) G_m(x) \tag{3.10}$$

J(x) is the Jacobian matrix of F(x), or the partial derivative of F at all comparison points with respect to parameter change, and is an M x N matrix. G(x) is the Hessian matrix of F(x) or set of second partial derivatives. $G_m(x)$ is the Hessian matrix of $f_m(x)$.

3.2.1 Gauss-Newton Algorithm

Variations on Newton's method are much more useful than Newton's method itself, since they all avoid the explicit calculation of $G_m(x)$ in (Eq. 3.10). The Gauss-Newton method negates Q(x) with the argument that $||f(x)||$ tends to zero near the minimum and that Q(x) will also tend to zero. The Gauss-Newton search direction, p_l, is found by solving

$$(J_l^T J_l)\, p_l = -J_l^T f_l \,. \tag{3.11}$$

Four paths produced by the Gauss-Newton method are shown in Figure 3.3. The minimum was obtained much sooner for these cases than for those solved as a steepest-descent problem. Extreme differences between a steepest-descent path and a Gauss-Newton path can occur as shown in Figure 3.4, where the initial search directions are nearly orthogonal to one another. Gauss-Newton has been and still is a popular search algorithm (Jhans, 1966, Thomas et al. 1971, Watson et al. 1980).

3.2.2 Levenberg-Marquardt Algorithm

A variation on the Gauss-Newton method is the Levenberg-Marquardt method in which the search direction is found by solving

$$(J_l^T J_l + \lambda_l I)\, p_l = -J_l^T f_l \,. \tag{3.12}$$

where λ_l is a positive scalar. λ is an arbitrary value that modifies the

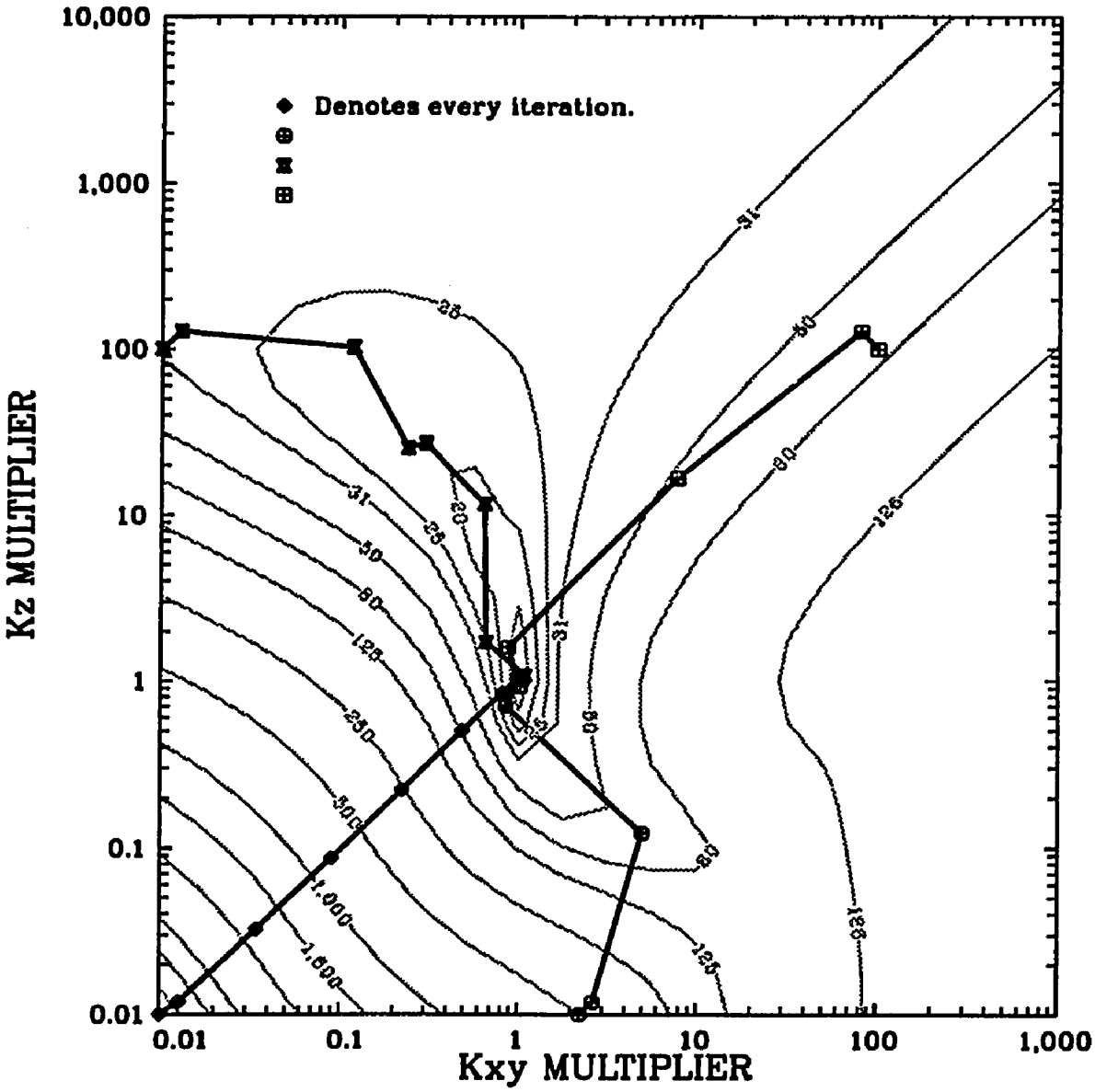

Figure 3.3--Gauss-Newton search paths for four cases.

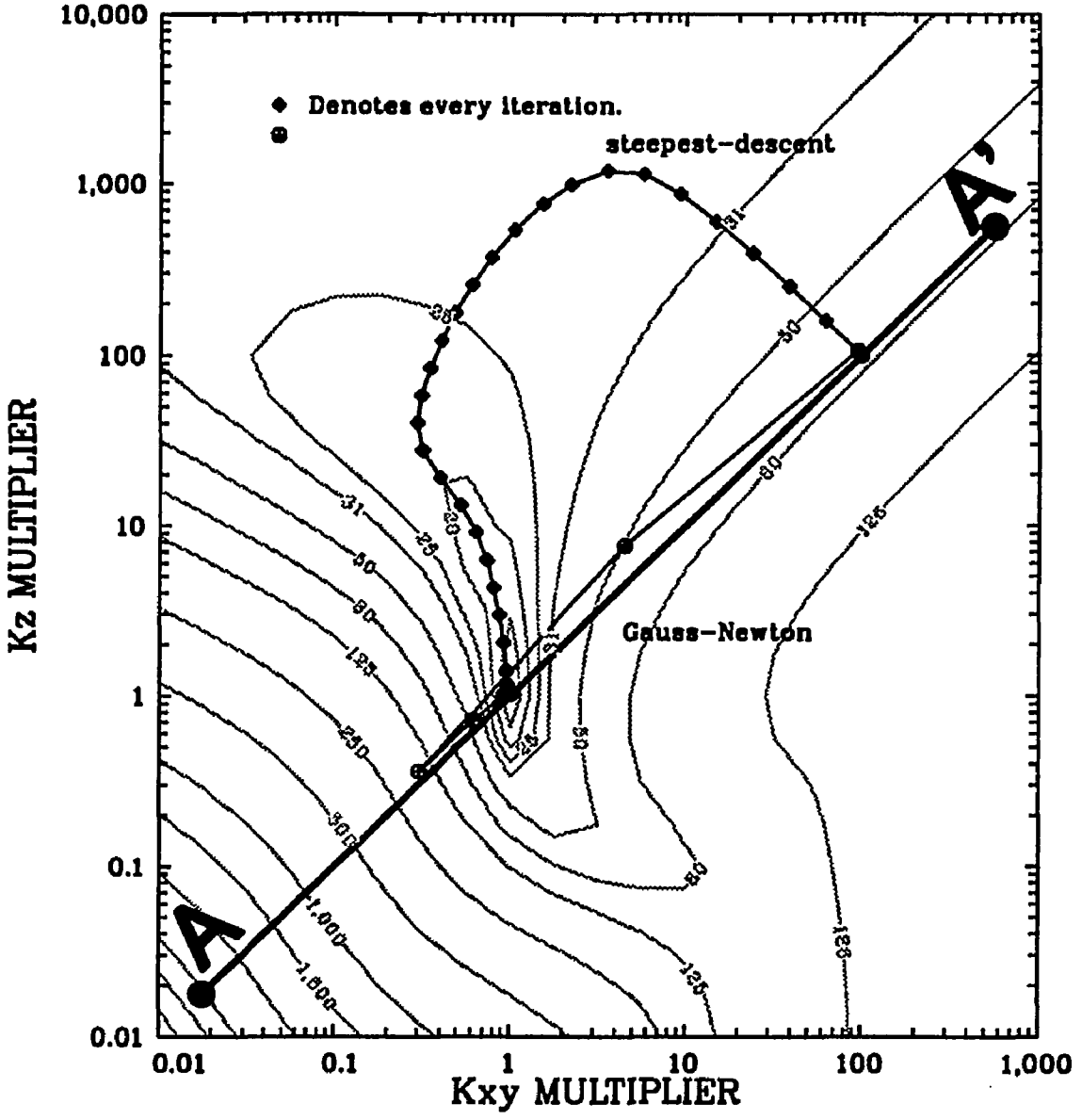

Figure 3.4--The differences between steepest-descent and Gauss-Newton search paths for a case.

search direction and serves as a choke on the step length where the magnitude of λ_l is defined relative to $||J_l||^2$. For λ_l much greater than $||J_l||^2$, the step length becomes small and the search direction becomes a steepest-descent one, i.e. (Eq. 3.1). As λ_l approaches 0 the search direction is a Gauss-Newton one, i.e. (Eq. 3.11). λ_l has been defined in several ways by different authors (Cooley, 1977, Durbin, 1983, Watson and Lee, 1986). Marquardt (1963) defined λ_l as:

$$\lambda_l = \frac{f_l^T J_l J_l^T f_l}{LR}. \tag{3.13}$$

where LR is a constant, termed the Levenberg radius. λ_l is defined inversely proportional to LR so the Levenberg radius would approximate a maximum step length.

The effect of LR on search direction and step length depends greatly on the current error surface position. The selection of Levenberg Radius can have a relatively minor effect (Fig. 3.5, inset A) or a rather pronounced one (Fig. 3.5, inset B). Figure 3.5 also shows that a steepest-descent search direction will result from most reasonable LR values. These extreme solutions are better understood by examining an error cross-section A-A' (Fig. 3.6). When the rate of gradient increase is underestimated, $Q(x) < 0$, $||p||$ is overestimated. Likewise, when the rate of gradient decrease is underestimated, $Q(x) > 0$, $||p||$ is underestimated.

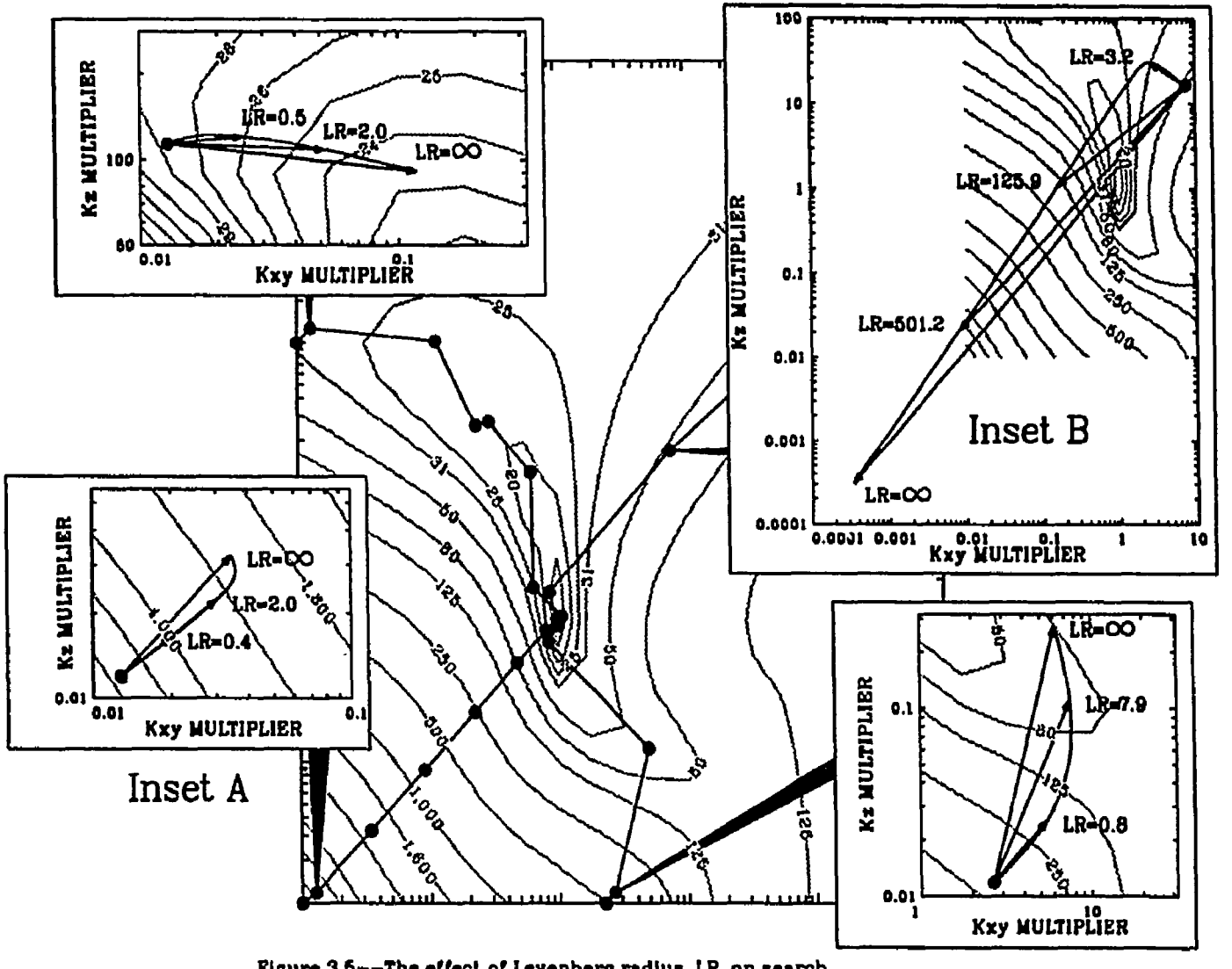

Figure 3.5--The effect of Levenberg radius, LR, on search direction and range.

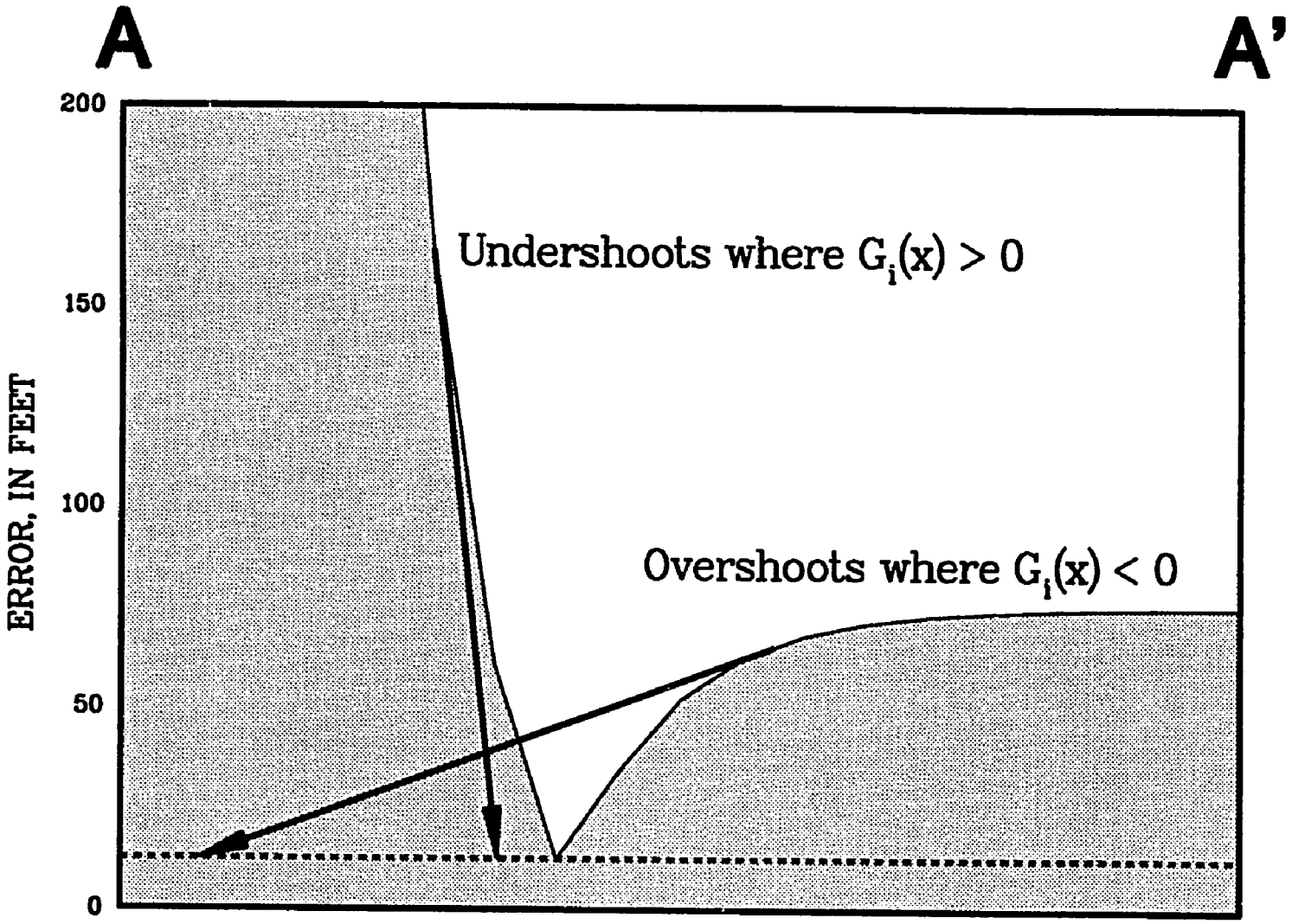

Figure 3.6--Errors in search direction and range, p, from the Gauss-Newton approximation.

3.2.3 Quasi-Newton Algorithm

Quasi-Newton methods attempt a closer approximation of G(x) by approximating Q(x) instead of negating it. This is useful when the combined measurement and model errors, $||f(x)||$, do not tend to zero. Quasi-Newton methods maintain an approximation of Q(x), M(x), by comparing first-order changes between iterations to update M(x). Many different schemes, which are sometimes referred to as variable-metric methods, have been devised to update M(x) (Fletcher, 1970; Goldfarb, 1970; Shanno, 1970). One of the more effective M(x) update algorithms is the Broyden-Fletcher-Goldfarb-Shanno (BFGS) update (Gill et al., 1981) where the search algorithm is:

$$(J_l^T J_l + M_l)p_l = -J_l^T f_l \ . \tag{3.14}$$

and the BFGS update is:

$$M_{l+1} = M_l - \frac{1}{s_l^T W_l s_l} W_l s_l s_l^T W_l + \frac{1}{y_l^T s_l} y_l y_l^T \tag{3.15}$$

where,

$$W_l = J_{l+1}^T J_{l+1} + M_l \tag{3.16}$$

$$s_l = x_{l+1} - x_l \ . \tag{3.17}$$

if no step-length criteria are exceeded, $s_l = p_l$

$$y_l = J_{l+1}^T f_{l+1} - J_l^T f_l \tag{3.18}$$

Yang et al. (1987) were the only group of researchers to use variable-metric methods.

CHAPTER IV

EXPANDED OBJECTIVE FUNCTION

A composite, sum-of-squares, objective function is opted for in this study. Shut-in bottom-hole pressure measurements are usually not the only data type used to decide the adequacy of a history match. Additional data types can help make the problem more unique and constrain estimates to a believable range.

Multiple data types within a composite objective function are usually of dissimilar units and scales. The standard deviation of the measurements within each data type is the only basis of comparison between data types. Dissimilar units and scales are addressed by weighting observations from different data types. The weight function, w, in (Eq. 2.2) becomes:

$$w = \frac{\sigma_1}{\sigma_n} \tag{4.1}$$

where,

σ_1 = the standard deviation of the first data type

σ_n = the standard deviation of the nth data type

Table 4.1 lists an example of 118 observations of 7 data types, the first of which is pressure. The other six data types were made comparable with the first data type by converting them to an equivalent pressure, w.

Table 4.1--An example of 118 observations with 7 data types.

n	Type	M	Average	σ	$w = \frac{\sigma_1}{\sigma_n}$
1	PRES	26	3631.3	195	1.00
2	PF	26	3521.2	252	0.77
3	QW	19	77.7	50.0	3.95
4	SOIL	2	0.5	0.0636	3070
5	KX	7	192.2	88.8	2.19
6	PRDT	19	- 1.2	0.720	271
7	PFDT	19	- 1.7	1.46	134
		118			

4.1 Comparison of Measured Observations

The direct measurement types used in this study are:

(1) shut-in bottom hole pressures, p_{sbh},

(2) flowing bottom hole pressures, p_{fbh},

(3) oil, gas, and water rates, q_o, q_g, and q_w,

(4) GOR and WOR,

(5) oil, gas, and water saturation, s_o, s_g, and s_w, and

(6) permeability and porosity.

Pressure and production data provide the primary measurements for comparison since they are more prevalent and are directly influenced by the properties being estimated. Additional data such as WOR, GOR, and saturation estimates from post-discovery well logs obtained in wells drilled to

or through the reservoir being studied can help match changes in the gas/oil or water/oil contacts.

Permeability and porosity measurements constrain nearby estimates of those properties. The degree of constraint varies with the weight assigned to each measurement. Permeability measurements from well tests would be given a higher weight than those obtained from core data. In addition to well tests and core data, educated guesses can also be used to keep estimates within believable ranges.

4.2 Comparison of synthesized observations

Additional synthesized comparison types are:

(1) averages,

(2) inequalities,

(3) temporal changes, d/dt, and

(4) spatial changes, d/dx, d/dy, and d/dz.

Synthesized data allow an automatic history-matching program to mimic qualitative judgments made during trial-and-error history matching. Additional comparisons are generated by averaging measurements, using measurements as limits, and approximating first-derivative changes.

Average values compare better than point values when a total amount is known but not its distribution. Production measurements are treated best as averages since production commonly comes from multiple zones. A production measurement from each zone is needed for comparison, but only a

total rate is known. If point values are compared, an assumption must be made about the distribution of production from each zone.

For example, a well produced 1200 Bbls/d from 2 zones of equal thickness. Assuming production is proportional to thickness only, 600 Bbls/d would come from each zone. A simulation showed 900 Bbls/d came from zone 1 and 300 Bbls/d from zone 2. Direct comparisons would indicate parameters should be changed to reduce production from zone 1 and increase production from zone 2. Comparing an average of the two zones would produce a result consistent with what is known and would indicate no further changes are necessary.

Inequality comparisons provide useful limits that would otherwise be disregarded by allowing for indefinite data in the objective function. Flowing bottom-hole pressure measurements are not usually known with the greatest of accuracy, but the flowing tubing pressure added to the static fluid column provides a minimum value. Inconclusive well-test data can be incorporated to indicate a minimum and maximum permeability in the objective function.

Change in a type of measurement over time, specifically production rates or pressures, needs to be explicitly incorporated in the objective function to influence the history match. If only the measured values are compared, many results that have the same root-mean-square error are possible (Fig. 4.1). An objective function based only on pressures will report the error for all three cases to be 650 psi, while one that compares pressures and $\frac{dp}{dt}$ will favor the solution that represents the correct reservoir drive mechanism. The degree of bias towards that solution depends on the weights

used to transform $\frac{dp}{dt}$ into equivalent pressures. Direct comparisons of production changes, $\frac{dq}{dt}$, help match relative permeability curves.

Spatial gradient comparisons are more useful for groundwater work where observation wells are common. In areas of relatively little or uniformly distributed stress, the potentiometric surface can be approximated by a plane (Fig. 4.2). Three head measurements can be used to find $\frac{dp}{dx}$ and $\frac{dp}{dy}$. If a head measurement is available in an adjacent aquifer, $\frac{dp}{dz}$ can be approximated also. These comparisons help estimate permeability distributions.

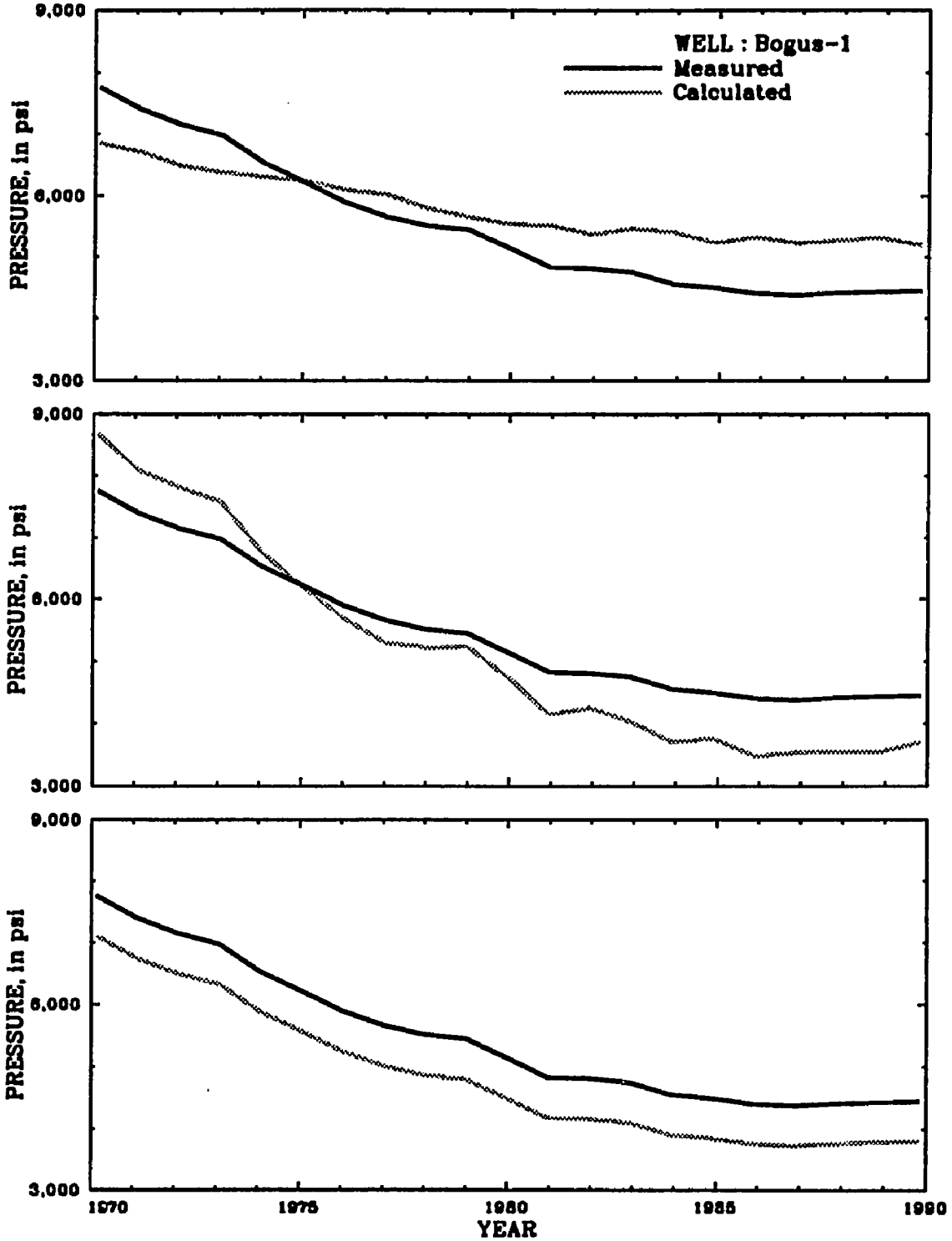

Figure 4.1--Three different matches with a root-mean-square error of 650 psi.

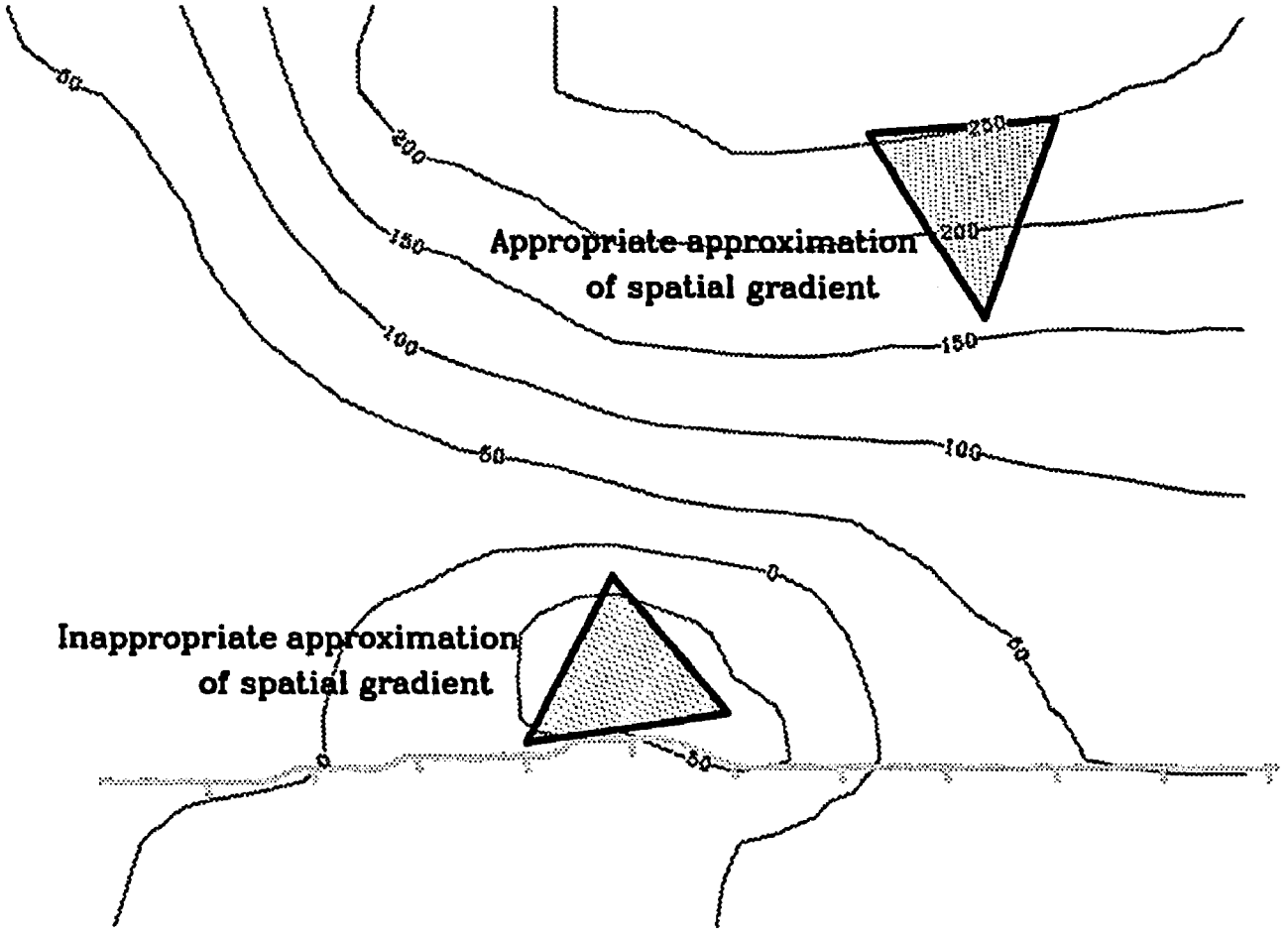

Figure 4.2--An example of appropriately and inappropriately approximating a potential surface with a plane defined by three water-level measurements.

CHAPTER V

INCORPORATING RESERVOIR CHARACTERISTICS IN HISTORY-MATCHING PARAMETERS

Final estimates depend greatly on how spatial relationships are defined within the history-matching parameters. If extensive data is available, kriging or some other interpolation scheme can acceptably define the spatial variability of a property. Unfortunately, most reservoir simulation studies are marred by a lack of data. Geologic knowledge and experience are used to supplement limited data bases. Weight matrices from iso-value lines achieve this function.

The spatial variation of porosity, permeability, and aquifer influx characteristics will be defined with weight matrices generated by iso-value contours. A sparse collection of core and log data coupled with known depositional models will outline parameter distribution within a reservoir. An iso-value contour can be inferred from this limited data set and become the basis for spatial parameter variations within a model. Parameter definition by iso-value contours:

(1) constrains results to geologically plausible solutions,

(2) reduces the uncertainty of a solution, and

(3) generates model matrices easily.

5.1 Iso-Value Contours

An iso-value contour is approximated by a series of line segments. The weight matrix is formed by calculating the distance from each model node to the appropriate iso-value segment. A point must fall within a

segment's influence, and the distance from the point to the line must be the minimum of all possible distances.

A two-dimensional example will be used for defining and demonstrating a segment's "zone of influence." In this example, all segments lie in the same plane so that the plane that separates any two segments can be illustrated as a line (Fig. 5.1a). The iso-value contour begins at point 1 and extends right to point N. The final scheme works equally well if the numbering is reversed. Segments are referred to by their end points (e.g.: seg 2).

The zone of influence for segment *n* is defined by the planes that:

(1) pass through the points *n* and *n-1*,

(2) bisect the angle between -seg *n* and seg *n+1* and -seg *n-1* and seg *n*, and

(3) are perpendicular to the plane defined by -seg *n* and seg *n+1* and -seg *n-1* and seg *n*.

The dividing planes are referred to by the point they pass through (e.g.: plane *n* passes through point *n*.). Any points between planes *n* and *n-1* can be influenced by segment *n* (Fig. 5.1b).

The dividing plane *n* is found by:

(1) Determining the angle, α, between segments *n* and *n+1* (fig. 5.2a),

$$\alpha = \cos^{-1}\left[\frac{-\text{seg } n \quad * \quad \text{seg } n+1}{|\text{seg } n| \ |\text{seg } n+1|}\right] \tag{5.1}$$

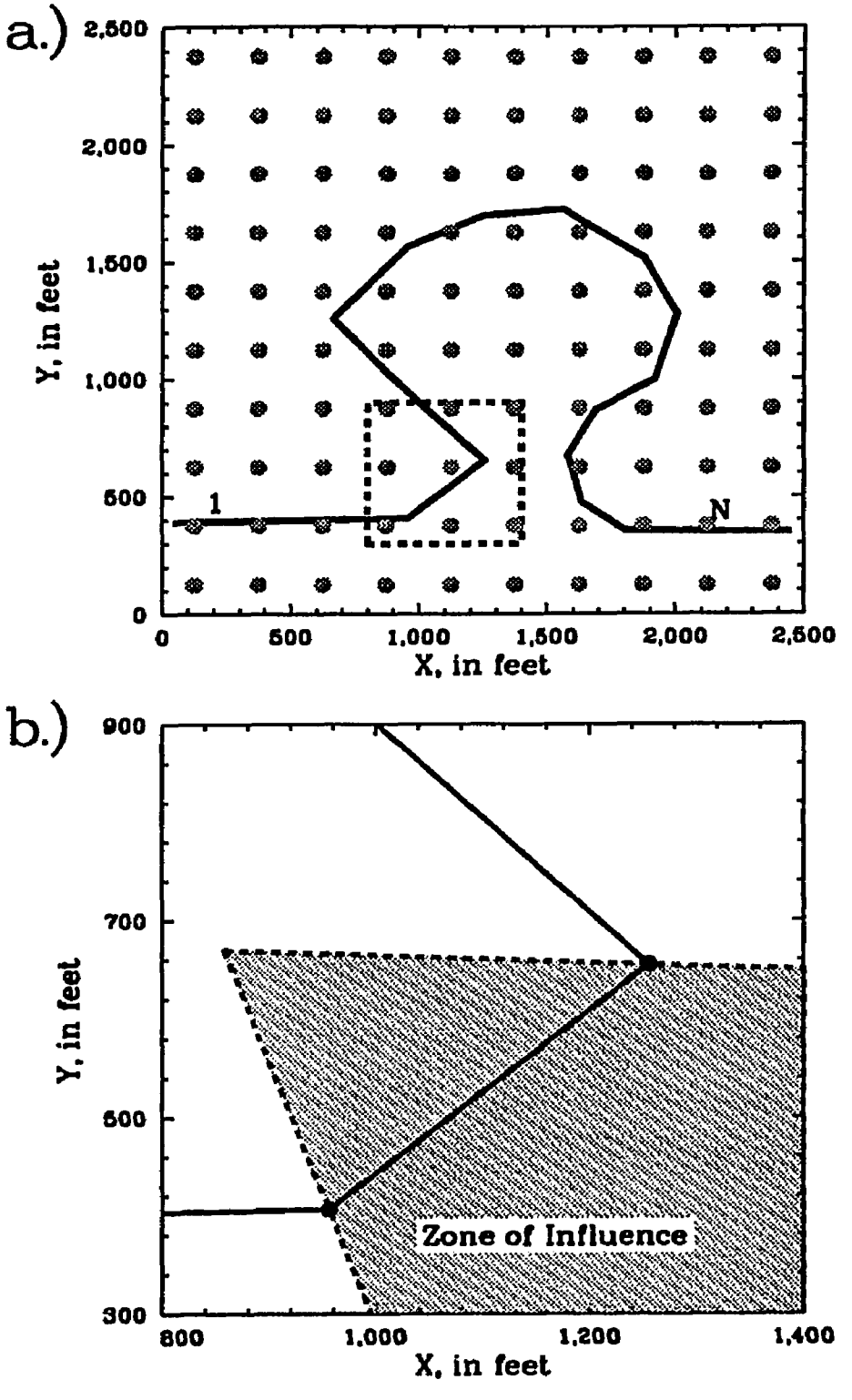

Figure 5.1--An example iso-value contour and zone of influence. associated with seg 3.

where:

$$\text{seg } n = \langle x_n - x_{n-1},\ y_n - y_{n-1},\ z_n - z_{n-1} \rangle$$

$$|\text{seg } n| = \sqrt{(x_n - x_{n-1})^2 + (y_n - y_{n-1})^2 + (z_n - z_{n-1})^2}$$

(2) Taking the cross product of the two vectors originating from n and extending to *n-1* and *n+1* to define a vector, V_N, perpendicular to segments *n* and *n+1* (Fig. 5.2b) ,

$$V_N = -\text{seg } n \ \text{X} \ \text{seg } n+1 \quad . \tag{5.2}$$

(3) Solving simultaneously for the unit vector V_{Pn}, the vector that defines plane *n*, (Fig. 5.2c) and:

$$-\text{seg } n * V_{Pn} = \cos(90^0 \pm \frac{\alpha}{2}) |\text{seg } n| \ |V_{Pn}| \ , \text{a constant.} \tag{5.3}$$

$$\text{seg } n+1 * V_{Pn} = \cos(90^0 - \frac{\alpha}{2}) |\text{seg } n+1| \ |V_{Pn}|, \text{a constant.} \tag{5.4}$$

$$V_N * V_{Pn} = \cos(90^0) |V_N| \ |V_{Pn}| \quad , 0 \, . \tag{5.5}$$

where,

$$V_{Pn} = \langle a, b, c \rangle$$

(4) The intercept between plane n and point n is:

$$d = a\,x_n + b\,y_n + c\,z_n \tag{5.6}$$

The shortest distance between the line-defined segment *n* and value to be extrapolated at point *q* (Fig. 5.3a) is:

a.)

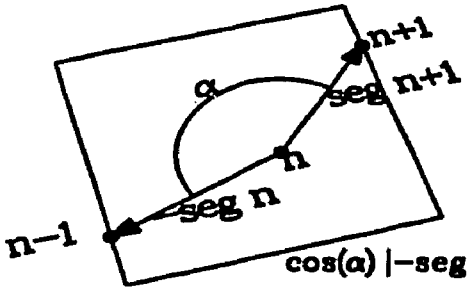

$\cos(\alpha)\,|-\text{seg n}||\text{seg n+1}| = -\text{seg n} \cdot \text{seg n+1}$

b.)

Plane defined by −seg n and seg n+1

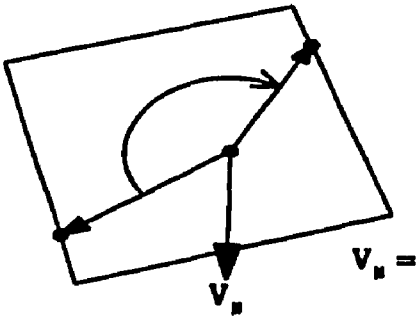

$V_n = -\text{seg n} \times \text{seg n+1}$

c.)

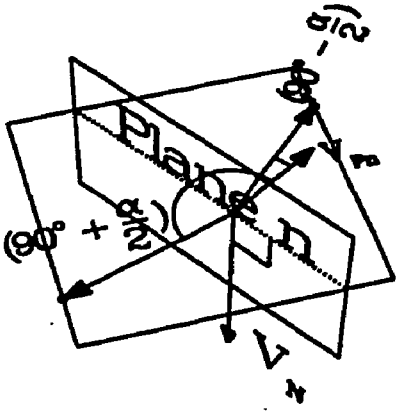

$-\text{seg n} \cdot V_{Pn} = \cos(90° + \frac{\alpha}{2})|-\text{seg n}||V_{Pn}|$

$\text{seg n+1} \cdot V_{Pn} = \cos(90° - \frac{\alpha}{2})|\text{seg n+1}||V_{Pn}|$

$V_n \cdot V_{Pn} = 0$

Figure 5.2--Defining dividing planes.

$$r = |V_q| \sin(\beta). \tag{5.7}$$

where,

$$\beta = \cos^{-1}\left[\frac{V_q * \text{seg } n}{|V_q| \ |\text{seg } n|}\right]. \tag{5.8}$$

$$V_q = \langle x_q - x_{n-1}, y_q - y_{n-1}, z_q - z_{n-1} \rangle$$

After determining which segment is appropriate and what the minimum distance is, there remains the dilemma of what side of the segment does the point lie? Another plane is needed to delineate the positive side from the negative side within the "zone of influence" (Fig. 5.3b) that:

(1) contains seg *n*, and

(2) is perpendicular to the plane defined by -seg *n* and seg *n+1*.

This plane is defined by the vector:

$$V_s = -\text{seg } n \ X \ V_N. \tag{5.9}$$

where,

$$V_s = \langle A,B,C \rangle$$

and the intercept between the plane and point n is:

$$D = A x_n + B y_n + C z_n = A x_{n-1} + B y_{n-1} + C z_{n-1}. \tag{5.10}$$

The resulting vector will always pass through the obtuse angle generated by seg *n* and seg *n+1* (fig. 5.3b). This will produce a polarity reversal each time the curve turns back on itself (fig. 5.3c). For contouring, all of the V_s vectors must point to the same side of the curve. An external reference is used to calculate polarity, an integer value of 1 or -1, determined by:

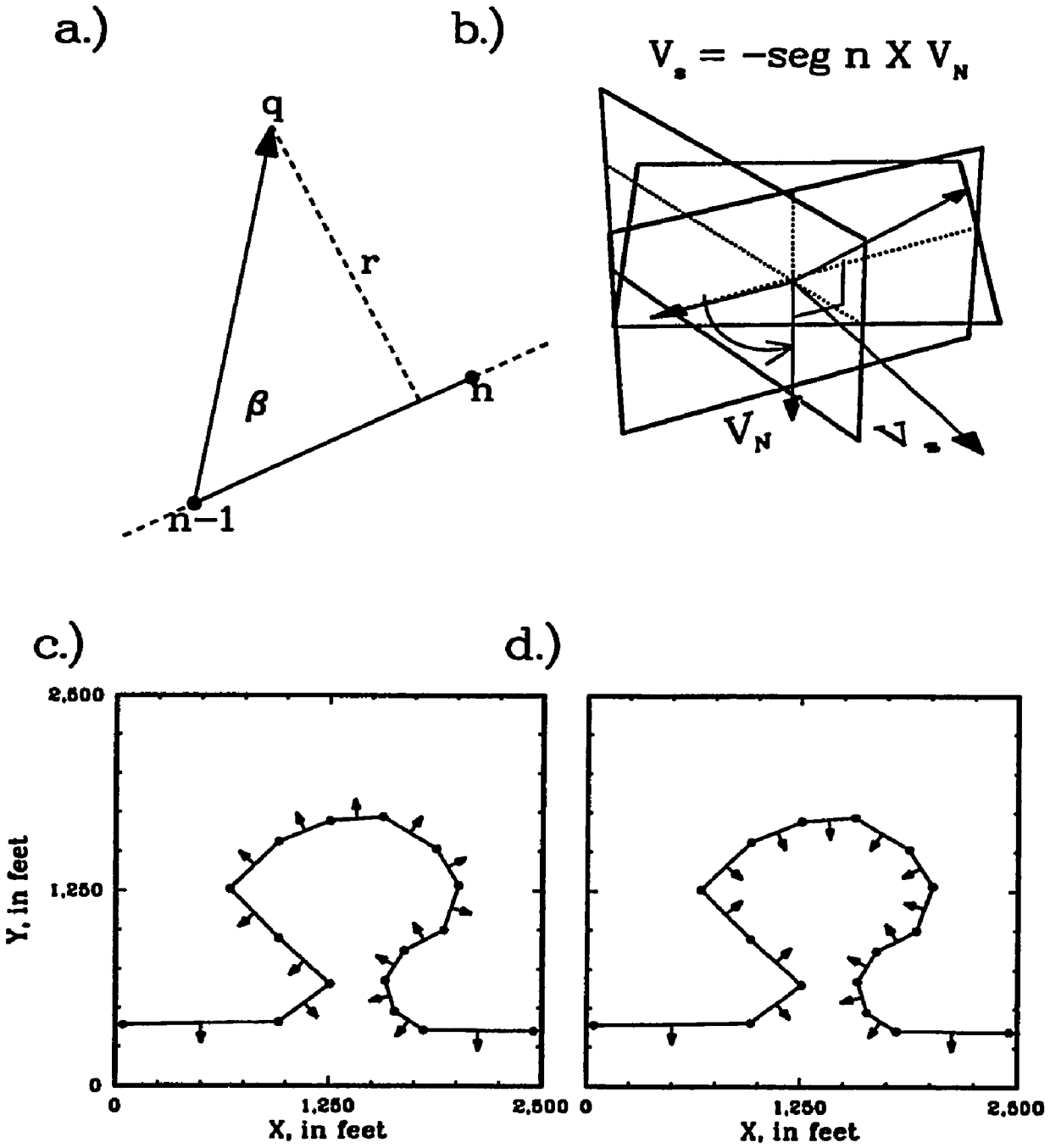

Figure 5.3--Determinig distance to a segment and polarity of segments within an iso-line.

$$ANG = \cos^{-1}\left[\frac{V_{ref} * seg\ n}{|V_{ref}|\ |seg\ n|}\right]\frac{y_n - y_{n-1}}{|y_n - y_{n-1}|}\frac{z_n - z_{n-1}}{|z_n - z_{n-1}|} \qquad (5.11)$$

$$V_{ref} = \langle 1,0,0 \rangle$$

where,

ANG = angle between seg n and the reference vector, V_{ref}

If ANG_n is greater than or equal to ANG_{n-1}, then the polarity is 1 otherwise; it is -1. This maintains all vectors pointing to the same side of the curve (Fig. 5.3d).

Repeating this procedure for all points within a matrix [W] generates a set of distances between simulator nodes and the iso-value contour. An example [W] matrix looks like:

-1160	-978	-875	-774	-687	-667	-647	-719	-856	-993
-988	-806	-646	-545	-444	-418	-398	-510	-647	-784
-816	-634	-453	-317	-216	-169	-164	-301	-438	-612
-644	-462	-281	-100	17	81	47	-92	-271	-489
-472	-290	-109	73	242	330	255	70	-148	-366
-488	-304	-121	64	247	401	255	81	-158	-397
-484	-474	-290	-107	69	242	60	-86	-233	-471
-234	-229	-225	-220	-61	100	-32	-261	-273	-275
19	23	27	31	132	278	89	-23	-25	-26
267	271	275	280	324	437	291	230	228	226

which came from superimposing a 10 X 10 X 1 matrix of regularly spaced points on the same plane that the iso-value in Figure 5.1a occupies. The distances shown in matrix [W] were calculated from segments:

6	6	7	7	8	8	8	9	9	9
6	6	7	7	7	8	8	9	9	9
6	6	6	7	7	8	9	9	9	10
6	6	6	6	7	8	9	9	10	10
6	6	6	6	7	8	9	10	10	10
5	5	5	5	5	13	12	11	11	11
2	5	5	5	4	4	13	12	11	11
2	2	2	3	3	3	14	15	16	16
2	2	2	2	3	14	15	16	16	16
2	2	2	2	3	15	15	16	16	16

Two hypothetical permeability distributions are produced by multiplying [W] by two arbitrary values, 0.025 and -0.025, and adding 50 md in each case. The resulting surfaces are shown in Figure 5.4.

Determination of zones of influence and polarity works equally well if the iso-value line is a three-dimensional series of segments. The polarities calculated might be of questionable value if the angular change between the planes defined by seg *n-1* and seg *n* and seg *n* and seg *n+1* is greater than 30^{o}. The following is a three-dimensional example where the angular change between successive planes is small. The iso-value is defined by:

n	Segment	Dividing Plane	X	Y	Z
1	-	-	0.0	0.0	1.0
2	2	2	3.0	1.0	1.5
3	3	3	1.5	4.5	2.0
4	4	4	3.5	8.5	2.5
5	5	5	6.5	9.0	3.5
6	6	6	7.5	5.0	4.0
7	7	7	5.8	2.5	4.5
8	8	8	8.2	1.0	6.0
9	9	-	10.0	3.0	8.0

a.) $Kxy_n = +0.025\ W_n + 50$

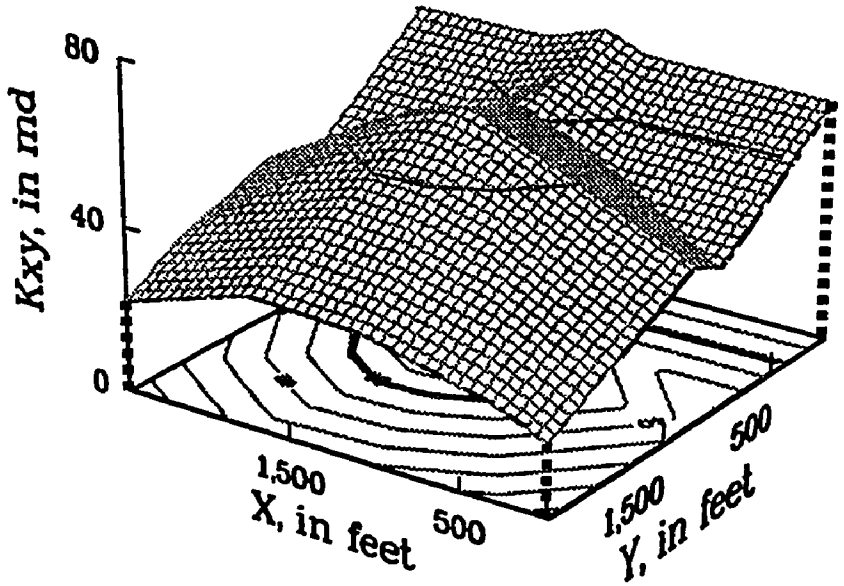

b.) $Kxy_n = -0.025\ W_n + 50$

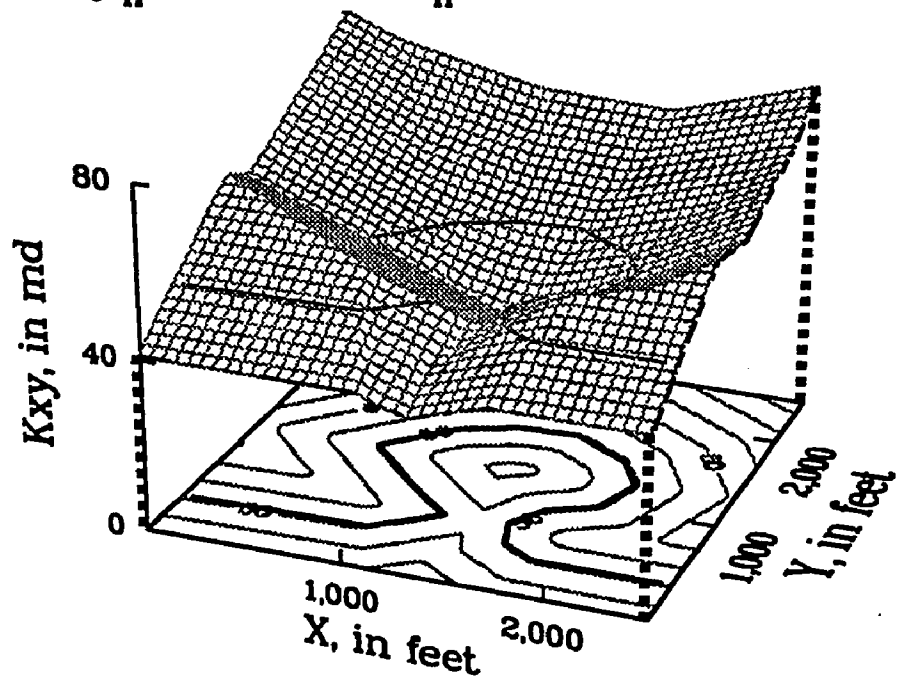

Figure 5.4--Two permeability distributions generated with the iso-value line of figure 5.1.

The planes that delineate the boundaries between segments are illustrated as 2 by 2 squares (fig. 5.5). Any distortion is due to perspective. The vector shown in each square indicates the final polarity of V_s but not its exact direction since V_s is perpendicular to the segment. For all cases, the first and last segments in the curve are unbound at points 1 and N. The first segment's positive and negative sides are based on its position in the plane defined by seg 2 and seg 3.

5.2 Weight Matrix Application

Weight matrices can alter property estimates as either an exponent, a multiplier, or an additive term, depending on the property being estimated. In all cases, the modifier at a given node, n, is:

$$\text{Modifier}_n = a + bw_n \tag{5.12}$$

where, a = a constant,

b = weight matrix multiplier, and

w_n = nth weight in matrix [W].

The additive modifier is of greater use in estimating groundwater recharge rates than in any petroleum application.

5.2.1 Exponential Modifier

The exponential modifier is best suited to most petroleum applications because it estimates log transformed values of a property. This is particularly relevant for permeability estimation since it is log-normally distributed (Neuman, 1980). The exponential update is:

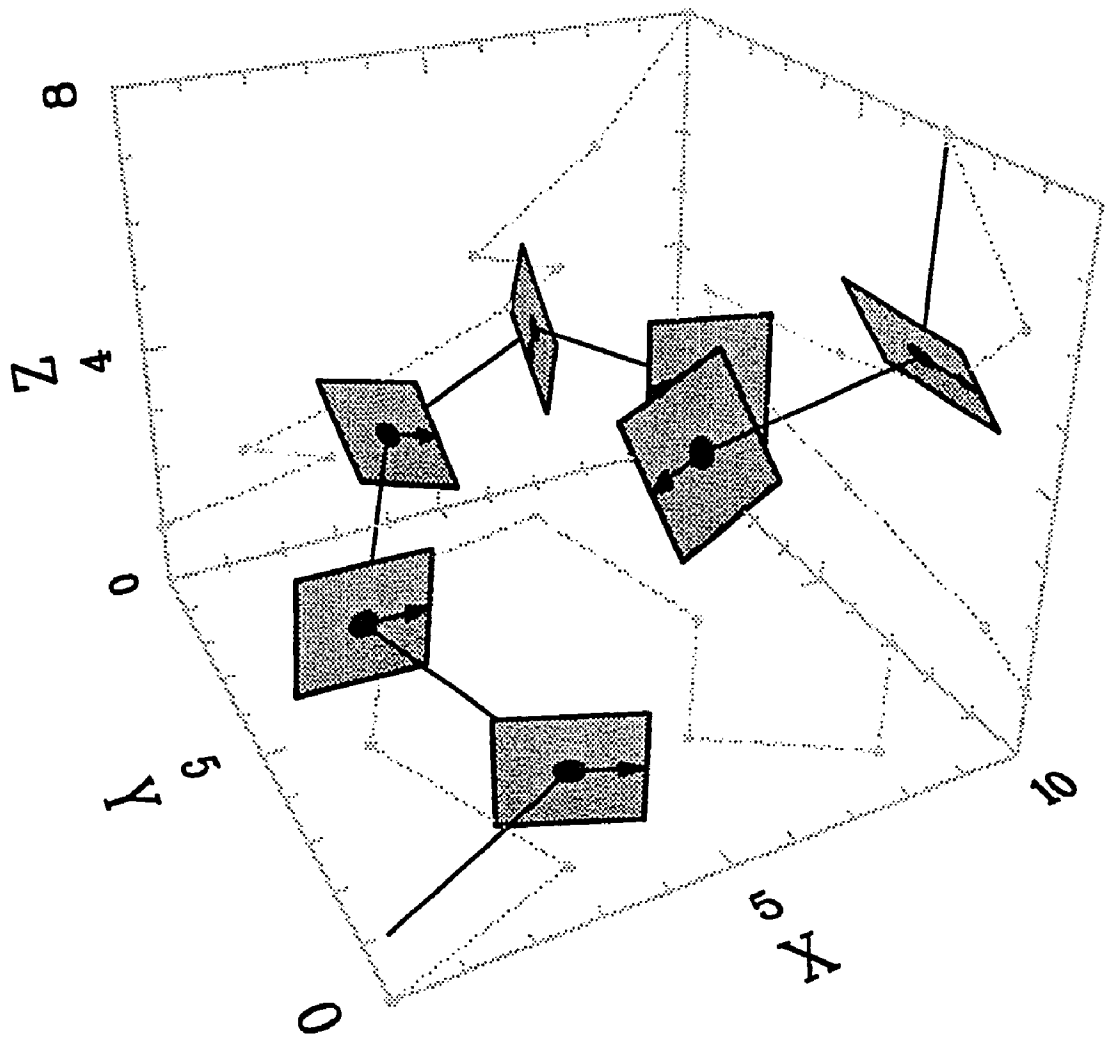

Figure 5.5--A three-dimensional example of dividing planes on an iso-line.

$$k_n = k_n * 10^{\text{Modifier}_n} \tag{5.13}$$

Exponential modifiers also thwart two potential problems by:

(1) reducing scaling problems between parameters that are of different orders of magnitude, and

(2) preventing negative estimates.

Aquifer influx and porosity estimates are also well served by these safeguards.

5.2.2 Average Values

If an average value is known, the properties distribution, based on an appropriate weight matrix, can be determined. The average value, $\overline{P}$, is maintained by defining a as function of b. The definition of $\overline{P}$ and a depends on how the weight matrix modifies the reservoir properties being estimated. For the exponential modifier:

$$\overline{P} = \frac{\Sigma\ Vol_n P_n 10^{(a + bw_n)}}{\Sigma\ Vol_n} \tag{5.14}$$

and

$$a = f(b) = \log\left[\frac{\overline{P}\ \Sigma\ Vol_n}{\Sigma\ Vol_n P_n 10^{(bw_n)}}\right] \tag{5.15}$$

For the multiplicative modifier:

$$\bar{P} = \frac{\Sigma\ P_n\ Vol_n (a + bw_n)}{\Sigma\ Vol_n} \tag{5.16}$$

and

$$a = f(b) = \frac{(\bar{P}\ \Sigma\ Vol_n - b\ \Sigma\ Vol_n P_n w_n)}{\Sigma\ Vol_n P_n} \tag{5.17}$$

In both cases, Vol_n is the gross reservoir volume associated with the nth node.

Porosity distribution is an appropriate application in the case of a volumetric reservoir. A more useful application in south Louisiana is determination of aquifer influx distribution. Both applications require pressure and production data sufficient for a material balance estimate of the average of either property.

5.3 Relative Permeability

The relative permeability of a given phase is a function of both saturation and location. Considering the large degree of uncertainty associated with any set of relative permeability curves, it is more prudent to assume that they are a function of saturation alone. For automatic history matching, relative permeability needs to be defined as a function of only one or two variables.

The hyperbolic tangent function will be used to define relative permeability curves since it increases monotonically and provides a wider range of appropriate curves than exponential or power descriptions. Relative

permeabilities, K_r, will be defined with two fitting parameters, a and b, in the form:

$$K_r = c \{ \tanh[a(S_w^* + b)] - \tanh(ab) \} \quad (5.18)$$

where,

a = fitting parameter that alters shape of K_r curve,

b = fitting parameter that positions K_r on tanh curve,

$$c = \frac{K_r (S_{max})}{\tanh [a(S_w^* + b)] - \tanh(ab)} \quad (5.19),$$

$$S_w^* = \frac{S - S_{min}}{S_{max} - S_{min}} \quad (5.20), \quad \text{and}$$

S is the saturation.

The parameter b controls what portion of the hyperbolic tangent curve will be used to model K_r (Fig. 5.6a). As an independent variable, b is only useful from -1 to 0. Beyond this range, the same results can be obtained using a alone. The curvature of K_r is controlled by a as shown in Figure 5.6b,c. As a approaches 0, K_r becomes a straight line. Conversely, as a grows larger, K_r becomes less linear (Fig. 5.6b,c).

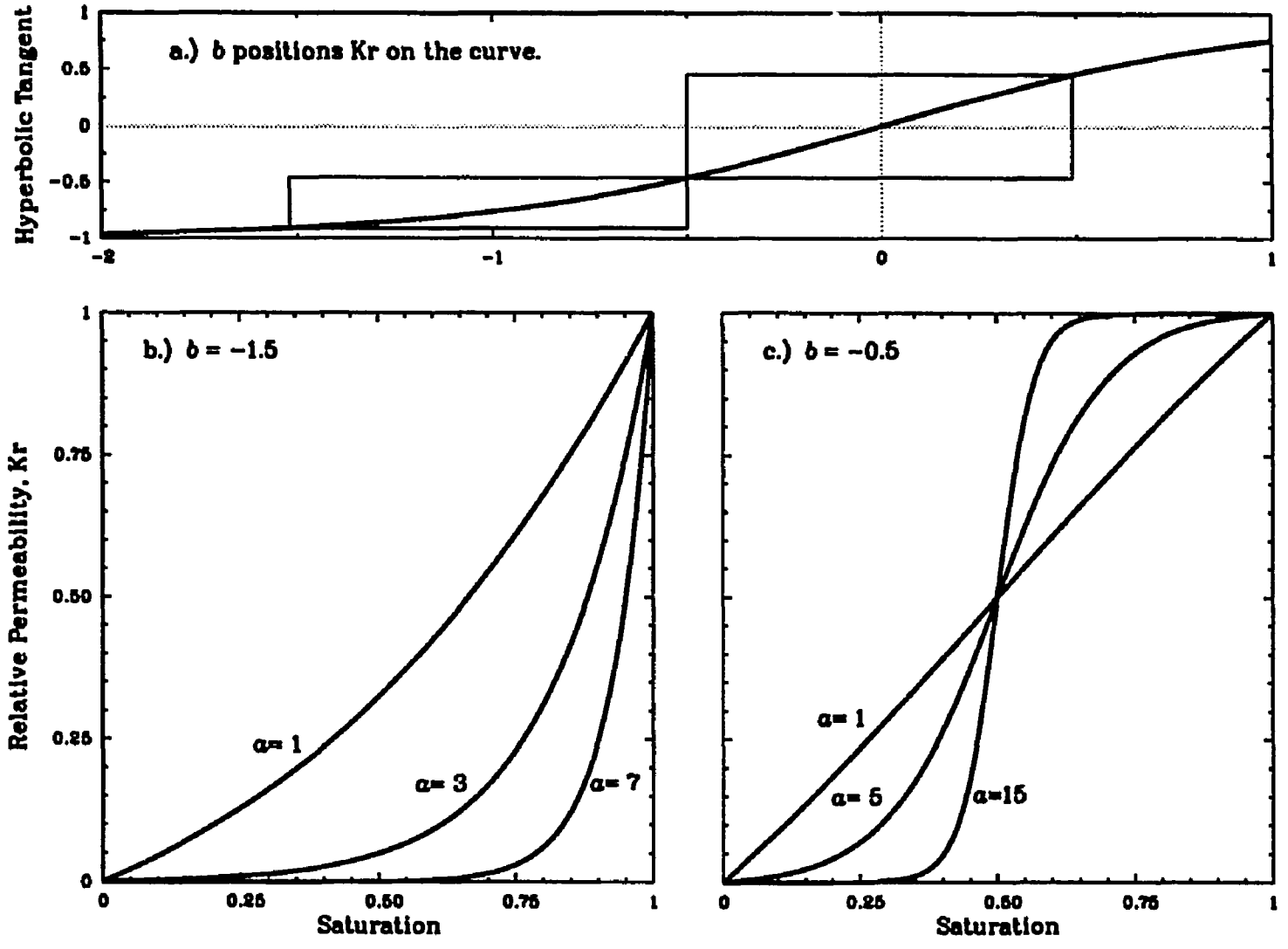

Figure 5.6--Defining relative permeability curves with a hyperbolic tangent function and the effect of varying fitting parameters α and b.

CHAPTER VI
AUTOMATIC HISTORY-MATCHING ALGORITHM

An automatic history matching algorithm, OPTIM, has been coded with an expanded objective function and improved parameter formation tools. OPTIM has been coupled as a subroutine with BOAST II, a 3-D oil and gas simulator, (Fanchi, J.R. *et al*, 1987) and MODFLOW, a 3-D groundwater-flow simulator, (McDonald and Harbaugh, 1988).

6.1 Coordinate Systems

Both reservoir and groundwater simulation require carving the system into a series of discrete elements. The elements in both BOAST II and MODFLOW are cubes since both are finite-difference models. This produces the common model reference system of column (x), row (y), and layer (z) (Fig. 6.1). Using BOAST II nomenclature, the eastern most column is II, the southern most row is JJ, and the deepest layer is KK. Node locations are denoted by three indices, $<i,j,k>$ or a single index, n, where

$$n = (k\text{-}1)\ \text{II}\ \text{JJ} + (j\text{-}1)\ \text{II} + i \qquad (6.1)$$

for solving pressure distributions and bookkeeping purposes.

Well locations, producing intervals, reservoir boundaries, oil/water contacts, and any other features are usually mapped in Cartesian coordinates <x,y,z>. All measured values are located with a coordinate system that differs from the system used to locate calculated values. Consequently, measured values rarely coincide with node locations.

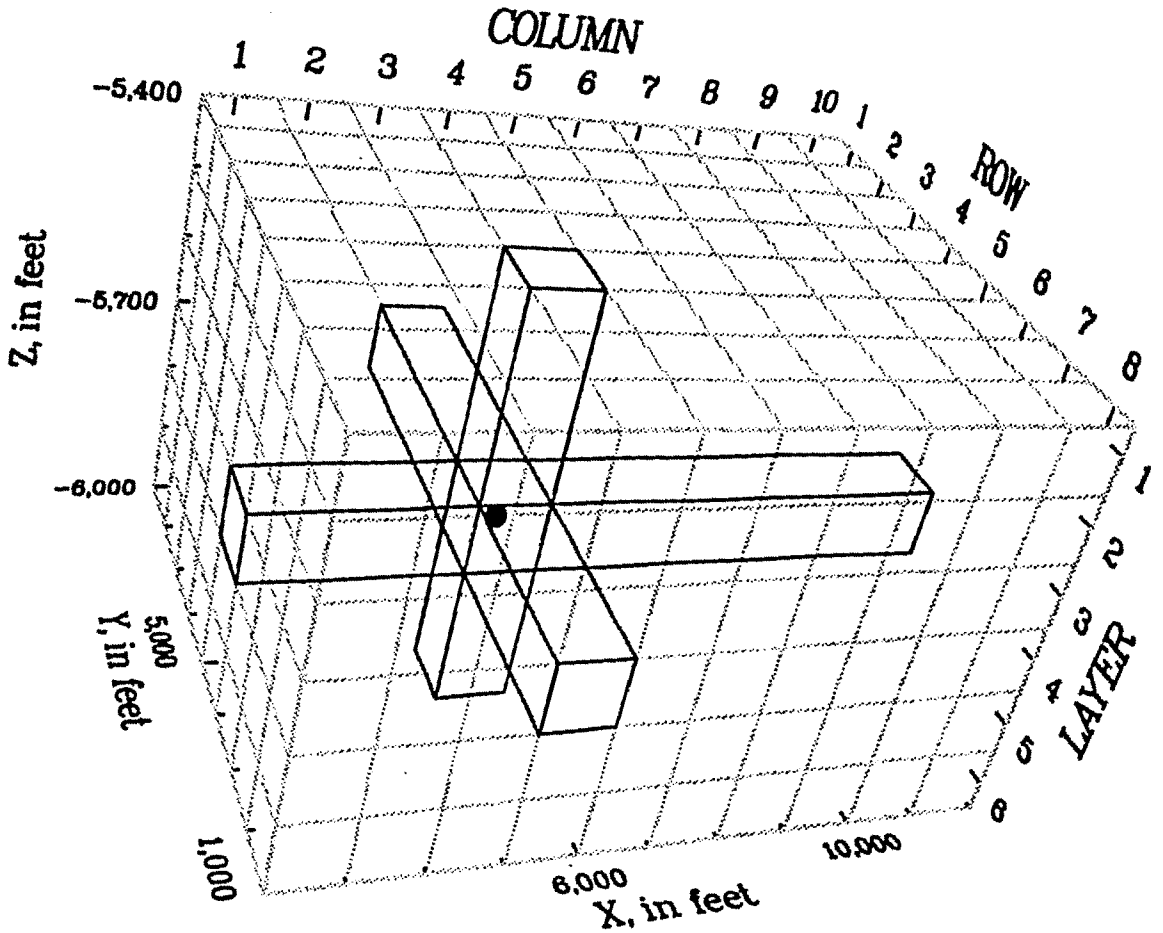

Figure 6.1--Cartesian coordinate system superimposed on a column, row, and layer system.

Model indices and Cartesian coordinates are linked by setting a reference node $<i_r,j_r,k_r>$ equivalent to $<x_r,y_r,z_r>$ (Fig. 6.1). The horizontal locations of the remaining nodes are defined by two one-dimensional matrices of II and JJ locations, x = f(i) and y = f(j). Both BOAST II and MODFLOW allow vertical deformation of the model grid to better match stratigraphic changes. Consequently vertical locations are defined by a three-dimensional matrix of II x JJ x KK locations, z = f(i,j,k).

Calculated shut-in bottom-hole pressure, saturation, permeability, and porosity values are interpolated within a layer for comparison with measured values. An observation is calculated by:

$$\hat{\psi} = \sum_{l=1}^{4} f_l \psi_l \qquad (6.2)$$

where,

f_l = fraction of observation$_l$ in the comparison.

The locations of l and fraction assignments are shown in Figure 6.2. Vertical interpolation is usually inappropriate since model layers correspond to stratigraphic changes and the properties are discontinuous across layers. Flowing bottom-hole pressure, production, GOR and WOR measurements are not interpolated and are compared to the nearest node since these are point values. All calculated observations are interpolated in time for comparison with measured values excepting permeability observations.

$$\hat{\psi} = \sum_{l=1}^{4} f_l \psi_l$$

$$f_1 = \frac{(\Delta X - \Delta x)(\Delta Y - \Delta y)}{\Delta X \, \Delta Y}$$

$$f_2 = \frac{\Delta x \, (\Delta Y - \Delta y)}{\Delta X \, \Delta Y}$$

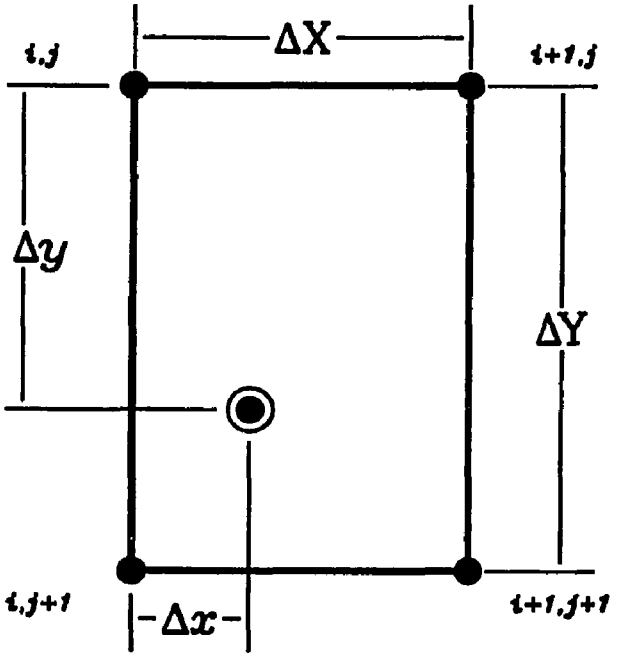

$$f_4 = \frac{(\Delta X - \Delta x) \, \Delta y}{\Delta X \, \Delta Y}$$

$$f_3 = \frac{\Delta x \, \Delta y}{\Delta X \Delta Y}$$

● Model nodes

◉ Interpolated value

Figure 6.2--Obtaining calculated observation by interpolation.

6.2 Zonation

Zonation delineates both the reservoir and regions within the reservoir such as faults, facies changes, shale-outs, *etc.* OPTIM maps zones in an integer array, IZONE. Zones are elemental building blocks that can either be used individually or be combined to form effective history-matching parameters. The IZONE matrix is filled by direct entry or by using closed contours to map zones within a layer. When closed contours are used, the subroutine INOUT determines if a node falls within the loop. Those nodes falling within the contour are marked as part of that zone (Fig. 6.3).

Using a structure map to delineate zones, an example, 8 by 5 by 1 model is broken into three zones (Fig. 6.4). The resulting IZONE matrix is:

0	0	0	1	1	1	1	0
0	1	1	7	7	7	7	1
0	1	7	7	7	7	7	1
1	7	7	7	7	7	7	1
1	7	7	0	0	7	7	1

where the reservoir is not present in zone 0, the initial oil/water contact is in zone 1, and the remainder is in zone 7.

Model grid superimposed on reservoir outline.

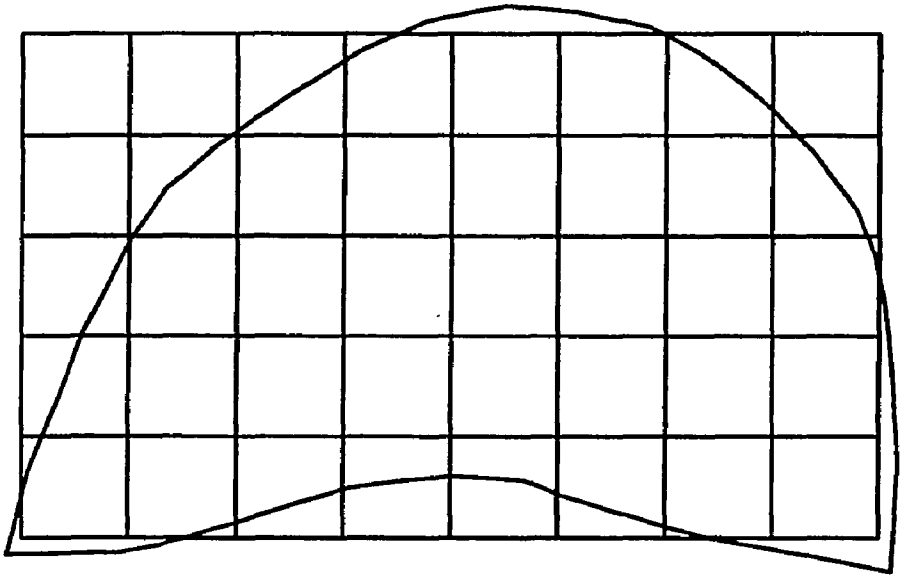

Zone defined by reservoir outline.

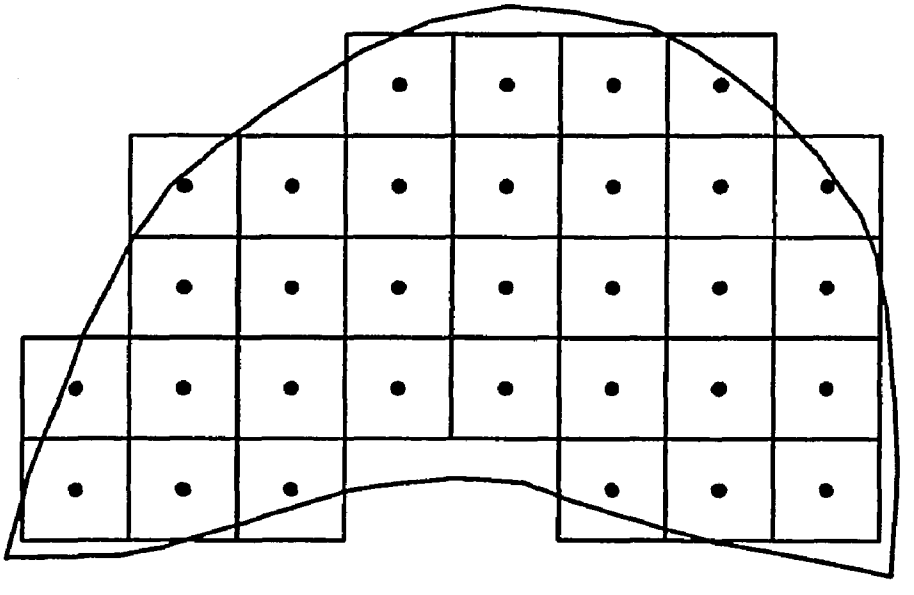

Figure 6.3--Defining model zones with a closed contour.

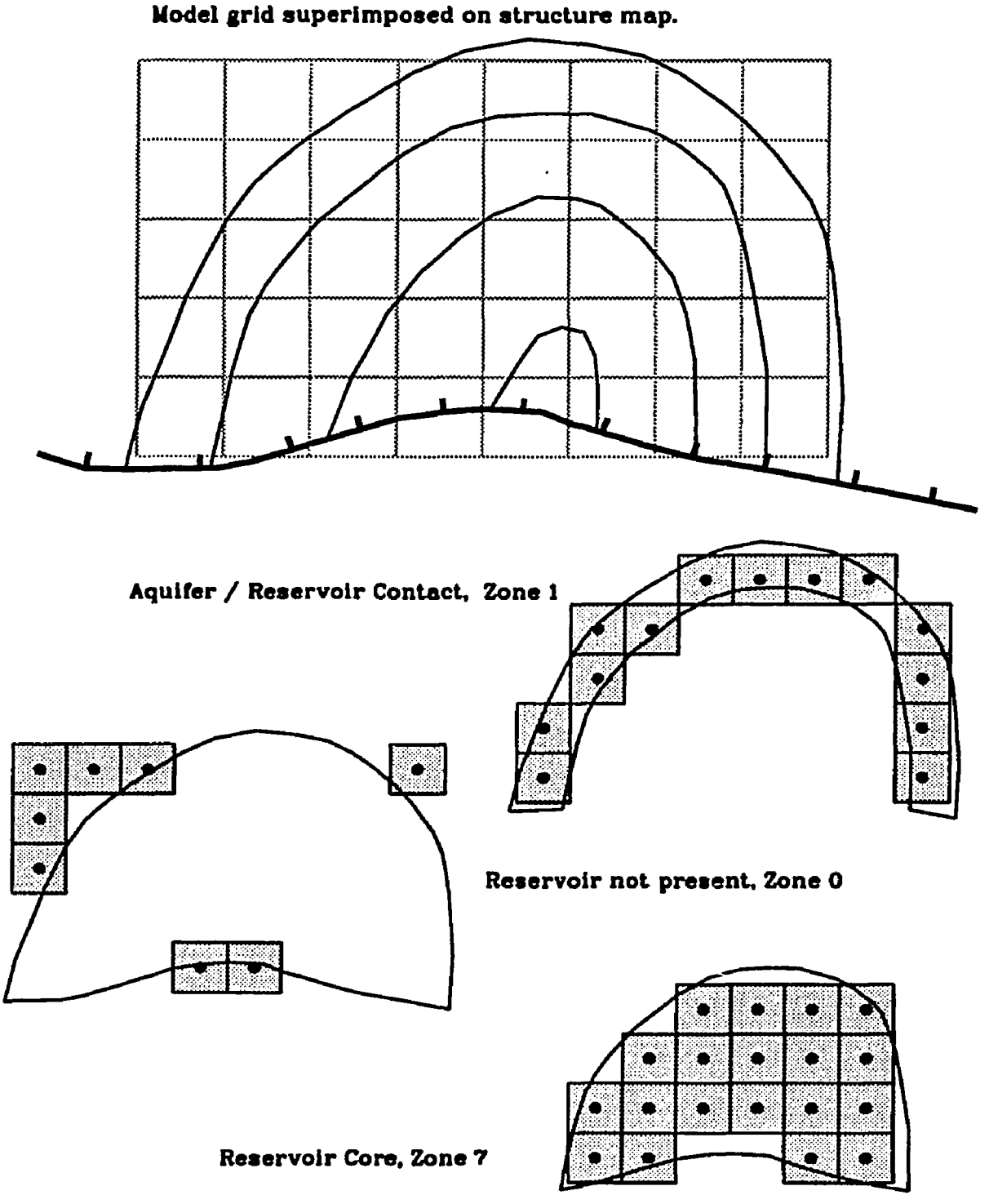

Figure 6.4--Dividing a model into zones with a structure map.

6.3 Weight Matrices

Weight matrices define the spatial variation of porosity, permeability, and aquifer influx characteristics. OPTIM acquires weight matrices directly or as an iso-value line. If an iso-value line is used, the matrix is filled with distances from the nodes to the iso-value line. The polarity of the distances is retained if the weight matrix approximates a smooth surface.

A special weight matrix can be requested for aquifer influx characteristics. The weights are equal to the area of the oil/water contact along the model periphery. The edge water-drive model only considers lateral cell faces while the bottom water-drive model also considers lower cell faces. All interior weights are equal to zero.

Parameter sensitivity problems arise when weight matrices of different magnitudes are used. e.g. Using matrix [W1], the horizontal permeability at a node, Kxy_n, ranges from 25 to 50 md when parameter b ranges from 0 to 1. Using matrix [W2], where [W2] is equal to 10 times [W1], the same range of permeability change is obtained while b only ranges from 0 to 0.1. This becomes a problem when it artificially makes one parameter much more sensitive than another.

To reduce parameter sensitivity problems, all weight matrices are scaled so that their magnitudes are similar. The initial magnitude is defined by the standard deviation of all values in the matrix. Scaled matrices are produced by dividing the initial matrix by its standard deviation.

6.4 History-Matching Parameters

Reservoir properties are modified by history-matching parameters a and b of Equations 5.12 and 5.18. For absolute permeability, aquifer influx, and porosity, Equation 5.12 defines how the parameters modify the reservoir properties. Equation 5.18 governs the modification of relative permeability curves. The history-matching parameters modify reservoir properties as either an exponent, a multiplier, or an additive term. The reservoir properties which OPTIM estimates and the property identifiers used in OPTIM are listed in Table 6.1. OPTIM stores parameter options as an alphanumeric tag, PINFO. The available options are summarized in Table 6.2. OPTIM echoes back the choices as seen in Table 6.3.

The reservoir properties are linked to the history-matching parameters through the zones delineated in IZONE. Using the example reservoir of Figure 6.4, the permeability parameters are linked to zones 1 and 7 while the aquifer influx parameters are only linked to zone 1.

Reservoir property estimates are restricted by limiting the history-matching parameter's range. If a parameter exceeds its lower or upper limit, it is made inactive in future iterations. The last parameter estimate is not forced to the limit it exceeded since the limits are usually arbitrary.

Table 6.1--Reservoir properties that can be modified by OPTIM and their associated identifiers.

Identifiers	Reservoir Properties
KX	absolute permeability in X
KY	absolute permeability in Y
KZ	absolute permeability in Z
PHI	porosity
AQTD	dimensionless time factor for aquifer influx
AQFR	degree of connection between reservoir and aquifer
KXY	absolute permeability in X and Y
KXZ	absolute permeability in X and Z
KYZ	absolute permeability in Y and Z
KXYZ	absolute permeability in X, Y, and Z
KRO	relative permeability of oil
KRW	relative permeability of water
KRG	relative permeability of gas
KROG	relative permeability of gas to oil

Table 6.2--History-matching parameter options.

Terms used from Eqs. 5.12 & 5.18	Identifier in OPTIM	Weighting used when $a = f(b)$	Parameter Modifier Used	Parameter Scaling
a	Constant	Volume	Exponential	*
b	Weight	Area	Multiplier	Scaling
a,b	Both	Unweighted	Additive	No Scaling
$a=f(b)$	Average			

The first letter of each option as added to make an information tag, PINFO, that identifies a parameters characteristics. e.g. A parameter using b, a volumetric weight, an exponential modifier, and no scaling is tagged as WVEN.

* Parameter is scaled to vary between -1 and 1 based on the lower and upper bounds given.

Table 6.3--An example of history-matching parameter report from OPTIM.

Entry	PINFO	Tag	Type	Lower Limit	Initial Value	Upper Limit	Weight Matrix Index
	Zone : Multiplier,	Zone : Multiplier,					
1	AAMN	Aqui	AQFR	0.5000	1.0000	5.000	2
	1: 1.000 ,						
2	BVES	Perm	KXY	2.199	0.2041	0.5000	1
	1: 1.000 ,	7: 1.000 ,					
3	BVES	Per2	KXY	0.000	0.0000	0.3010	1
	1: 1.000 ,	7: 1.000 ,					
4	CVAN	Kro	KRO	-1.500	0.0000	1.000	0*
	3: 2.057 ,	9:-1.353 ,	1: ,				

*For relative permeability curves a weight matrix index = 0 marks a as the parameter and a weight matrix index < 0 marks b as the parameter. The Zone : Multiplier pairs identify:

$Index_{Smin}$: $a_{initial}$,	$Index_{Smax}$: $b_{initial}$,	Rock region: ,

For some problems, the inverse solution can be better posed by scaling the history-matching parameters. Parameters are scaled by:

$$x_{scl} = 2\left[\frac{x - \frac{1}{2}(x_u + x_l)}{x_u - x_l}\right] \qquad (6.3)$$

where,

x_u = upper limit of parameter x

x_l = lower limit of parameter x

The scaled lower and upper parameter limits are -1 and 1, respectively. Scaling solves problems that arise when the properties estimated have disparate magnitudes or sensitivities.

Solving for permeability and porosity distributions is an example of two properties with disparate magnitudes. A change of 0.10 is a very large change in porosity, but the same change is insignificant for most permeability values expressed in millidarcies. If a scaled parameter is used and the expected porosity values range from 0.15 to 0.25, a parameter change of 0.2 produces a porosity change of 0.01, using Equation 6.3. If permeability is also modified with a scaled parameter and the expected values range from 100 md to 500 md, a change of 0.2 produces a permeability change of 40 md, also using Equation 6.3. After scaling, the algorithm perceives the two parameters as similar in magnitude.

Large disparities in parameter sensitivity occur both within the estimation range of an individual parameter and between different parameters. Figure 6.5a shows a hypothetical model's error mapped in the Kxy-Kz plane. Both Kxy and Kz are more sensitive to change for values less

than the history-matched value of <63,10>, the coordinate of zero error. Log-transforming the permeability distribution (Fig. 6.5b) acts as a type of scaling. It makes a parameter's sensitivity less variable within its estimation range. The model sensitivities for both Log(Kxy) and Log(Kz), $\frac{\partial\hat{\psi}}{\partial \text{Log(Kxy)}}$ and $\frac{\partial\hat{\psi}}{\partial \text{Log(Kz)}}$, are constants over the entire region mapped in Figure 6.5b. The model is still twice as sensitive to changes in Log(Kxy) than Log(Kz). The apparent sensitivity of Log(Kxy) is made similar to Log(Kz) by scaling Log(Kz) from Log(1), 0, to Log(100), 2, and scaling Log(Kz) from Log(20), 1.3, to Log(200), 2.3, (Fig. 6.5c).

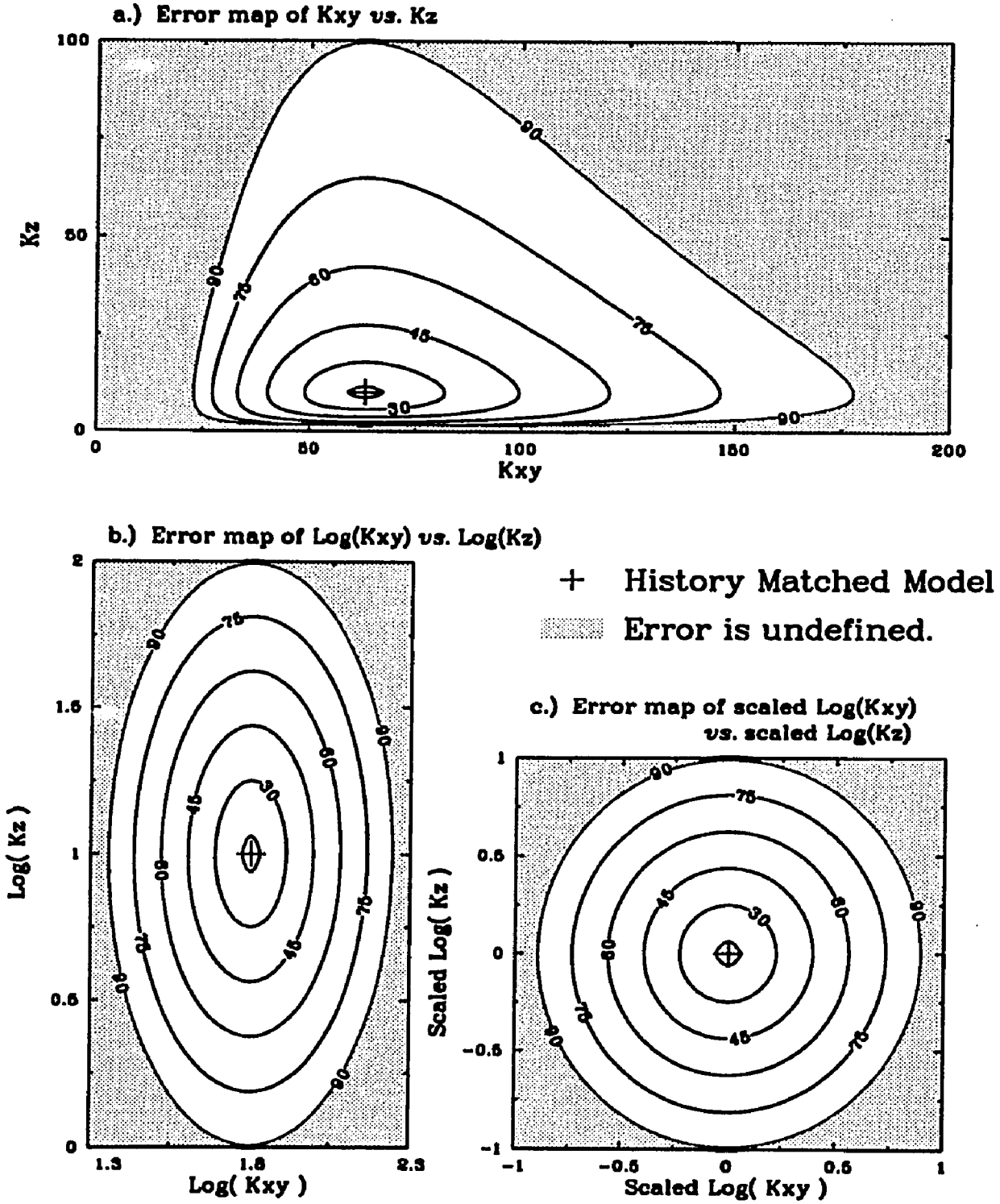

Figure 6.5--Effect of log transforms and scaling on parameter sensitivity.

6.5 History Aquisition

OPTIM acquires the reservoir history as a series of discrete observations. A type identifier, group identifier, time, location, weight, and well identifier are read with each observation. OPTIM recognizes the observation types listed in table 6.4. OPTIM calculates any spatial or temporal gradients requested after reading all observations.

The group identifier is used for comparing average values. For example, if three observations have the same group identifier, OPTIM replaces those three measurements with their average. All calculated observations from that group are averaged prior to comparison.

After all observations have been read or synthesized, OPTIM finds how many different observation types exist, the number of observations within each type, and the standard deviation of each type. The weight associated with each observation is adjusted by Eq. 4.1 so that all observations have consistent units.

Inequality observations are recognized by a "<" or ">" sign as the first character of the well identifier. Observations marked with a "<" sign are not used unless the calculated value is less than the measured one. Reciprocally, observations marked with a ">" sign are not used unless the calculated value is greater than the measured one.

Table 6.4--Observation types OPTIM compares to calculated values and their associated identifiers.

Identifiers	Observation Types
PRES	Shut-in bottom hole pressure[1,2]
PORO	Porosity[1,2]
SOIL	Oil saturation[1,2]
SGAS	Gas saturation[1,2]
SWAT	Water saturation[1,2]
PF	Flowing bottom hole pressures[1]
QO	Oil production rate[1]
QG	Gas production rate[1]
QW	Water production rate[1]
GOR	Gas/oil ratio[1]
WOR	Water/oil ratio[1]
KX	$Permeability_x$
KXLG	$Log(Permeability_x)$
KY	$Permeability_y$
KYLG	$Log(Permeability_y)$

1 Derivatives of this observation type in time can be approximated.

2 Derivatives of this observation type in space can be approximated.

6.6 Search Algorithm

The parameter estimation process begins by calling BOAST once and establishing

$$f(x) = (\hat{\psi}(x) - \psi)\, w \qquad (2.1)$$

the initial, weighted differences between calculated and measured observations. These differences, or residuals, are what the algorithm seeks to minimize. The algorithm uses sum of squares to gauge how well a model is history matched. Root-mean-square, standard deviation, and average errors are also reported.

Using the base run, the Jacobian, J(x), is calculated by the influence coefficient method (Yeh, 1986). The sensitivity coefficients, the derivatives of observation change with respect to parameter change, that compose the Jacobian are approximated by

$$\frac{\partial \hat{\psi}_m(x)}{\partial x_n} \simeq \frac{w_m(\hat{\psi}_m(x+\Delta x_n) - \hat{\psi}_m(x))}{\Delta x_n}, \; m = 1,M, \; n = 1,N \qquad (6.4)$$

where,

Δx_n = perturbation of the nth parameter

$\hat{\psi}_m(x+\Delta x_n)$ = mth observation calculated with the nth parameter perturbed

$\hat{\psi}_m(x)$ = mth observation calculated in the base run

w_m = mth observation weight

This requires perturbing each parameter by Δx_n and calling BOAST II N times, once for each parameter being estimated. The covariance matrix, FIR(x), and the gradient, g(x), are calculated where

$$FIR(x) = J(x)^T J(x) \tag{6.5}$$

and

$$g(x) = J(x)^T f(x) \tag{6.6}$$

The parameters and all associated matrices are ranked in importance based on the main diagonal of FIR(x), e.g.

$$FIR(x)=\begin{vmatrix}1&1&0\\1&5&3\\0&3&2\end{vmatrix}, g(x)=\begin{vmatrix}3\\1\\2\end{vmatrix} \xrightarrow[\text{ranking}]{\text{After}} FIR(x)=\begin{vmatrix}5&3&1\\3&2&0\\1&0&1\end{vmatrix}, g(x)=\begin{vmatrix}1\\2\\3\end{vmatrix}$$

The parameter associated with the greatest sum-of-squared, sensitivity coefficients is ranked highest.

Ranking is used to avoid solving ill-posed problems that lead to excessive parameter change and little change in the objective function. If the model is a good deal less sensitive to x_n than x_1, it is best to make x_n inactive. The sensitivity of the model to changes in x_n relative to changes in x_1, RS, is approximated by

$$RS_n^2 = \frac{FIR(x)_{n,n}}{FIR(x)_{1,1}}. \tag{6.7}$$

RS_n^2 greater than 0.01 is a good threshold.

The search direction and amount of change are found by solving

$$G(x)p = -g(x) \tag{3.4}$$

for parameter change, p, where the Hessian, G(x), is formed by a Quasi-Newton method (17). In this algorithm, the Hessian is

$$G(x) = FIR(x) + SECD(x) \tag{6.8}$$

where,

$$SECD(x) = M(x), \text{ using the BFGS update} \tag{3.15}$$

SECD(x) is updated with each iteration as long as SECD(x) is a positive definite. If the BFGS update fails or there is no prior parameter change information, FIR(x) is altered in Levenberg-Marquardt (3.12) fashion

$$SECD(x) = \lambda I \,. \tag{6.9}$$

where,

$$\lambda = ff * FIR(x)_{1,1}$$

ff= user defined fraction

SECD(x) now serves as a choke that limits parameter change and forces the solution closer to a steepest-descent path. If parameter change exceeds a user defined limit, p is scaled to that limit. Any parameter that exceeds its bounds is made inactive for the next iteration.

BOAST is updated to reflect the latest parameter estimates and a new set of residuals is calculated. Model statistics, parameter changes, current parameter values, and residual values are reported for the last iteration.

Before starting a new iteration, the algorithm tests for convergence or failure. Convergence is assumed if error reduction or the net parameter change is less than a set minimum. If the iteration counter exceeds the given maximum, the algorithm is assumed to have failed. If the algorithm has not failed or converged, a new error level is set and a new iteration begins. A summary of OPTIM's logic is given in Figure 6.6.

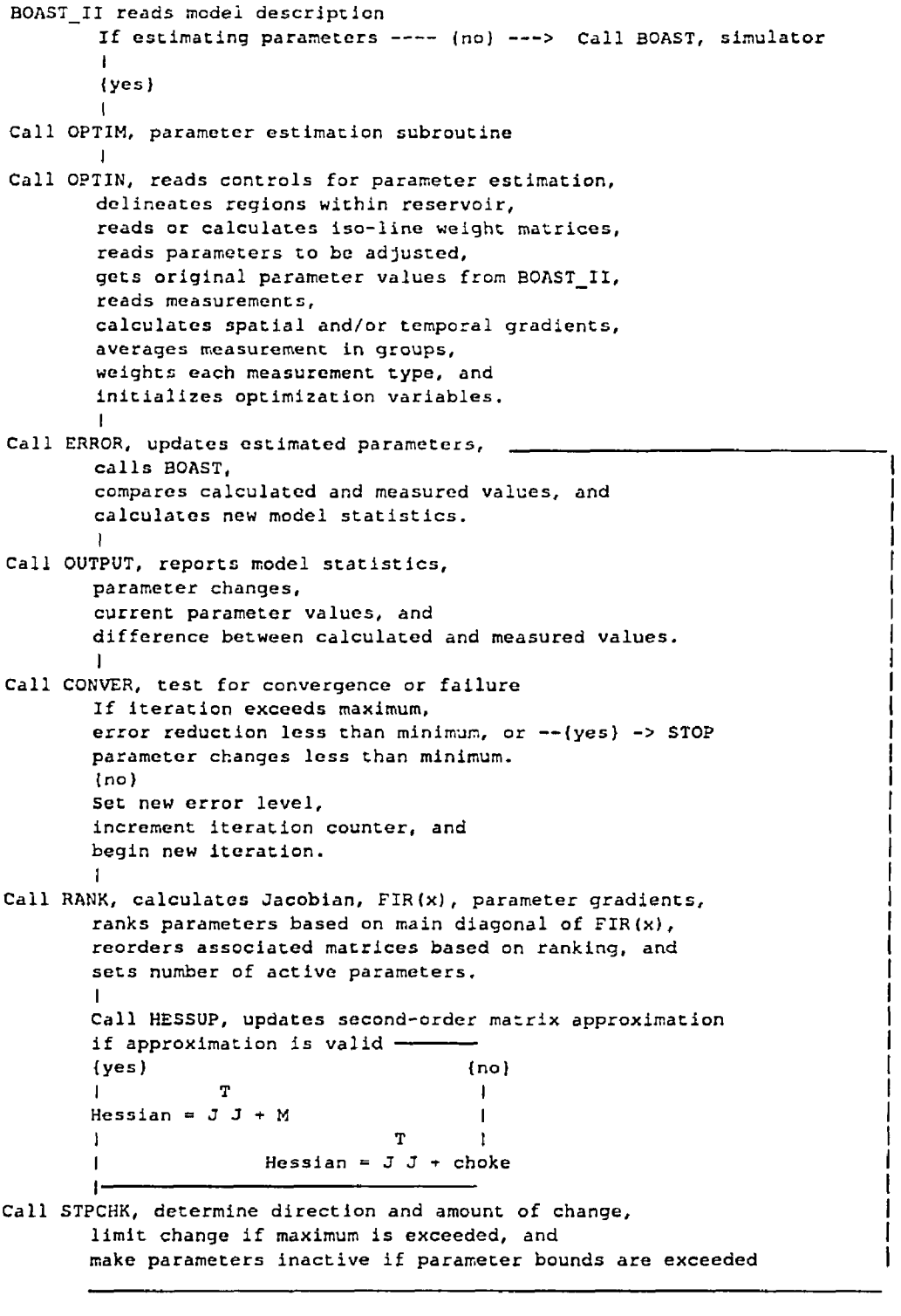

Figure 6.6--Flow chart of OPTIM coupled with BOAST II.

CHAPTER VII
HISTORY MATCH OF BERYL RESERVOIR -- A HYPOTHETICAL CASE

A hypothetical case representing a reservoir of known geometry and properties is used to demonstrate the effectiveness of the proposed history-matching approach. A water-drive reservoir, typical of south Louisiana reservoirs, was synthesized. Structure maps, borehole information, porosity and permeability distributions, and aquifer influx characteristics were created. A model was constructed around this data and simulated for 10 years with specified-voidage rates to generate the production and pressure history of the Beryl reservoir.

7.1 The Beryl Reservoir

The Beryl reservoir is formed by a structural trap (Fig. 7.1). Recoverable oil is present in two distinct, laterally continuous sands, the upper and lower Beryl, both thickened towards the south (Fig. 7.2). The initial oil in place is 13.9 MMBbls and the average pay, porosity, and water saturation is 21 ft, 0.24, and 0.20 respectively. No free gas was initially in place and no gas came out of solution during production since the initial reservoir pressure is 3,990 psia and flowing-well pressures are maintained above the bubble point, 2,000 psia.

Porosity and permeability distributions varied horizontally and are identical in both the upper and lower Beryl. Generally, porosity and horizontal permeability increasing away from the fault (Fig. 7.3a,b). Vertical permeability decreased from the crest to the oil/water contact

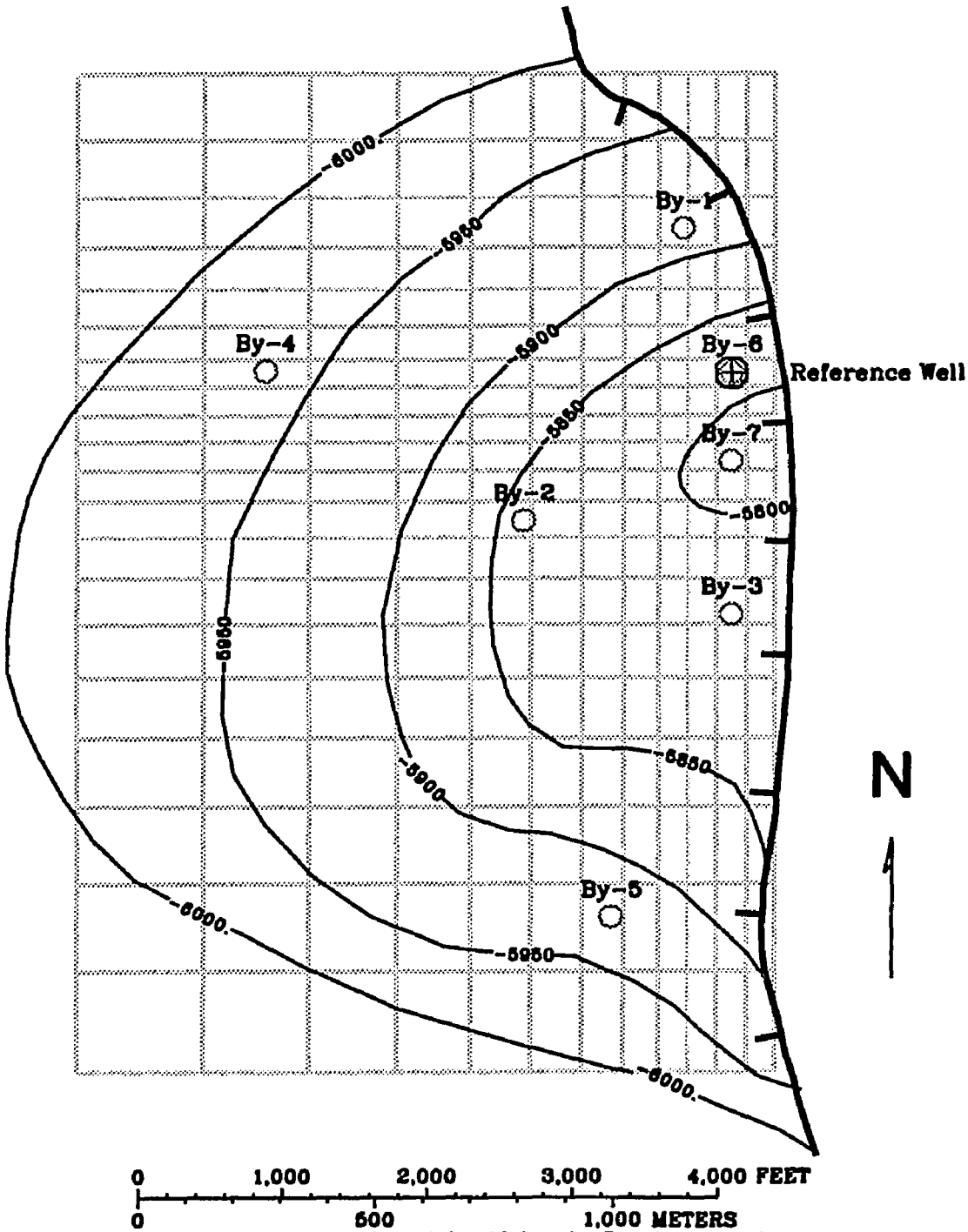

Figure 7.1--Structure map and model grid for the Beryl reservoir, a hypothetical field.

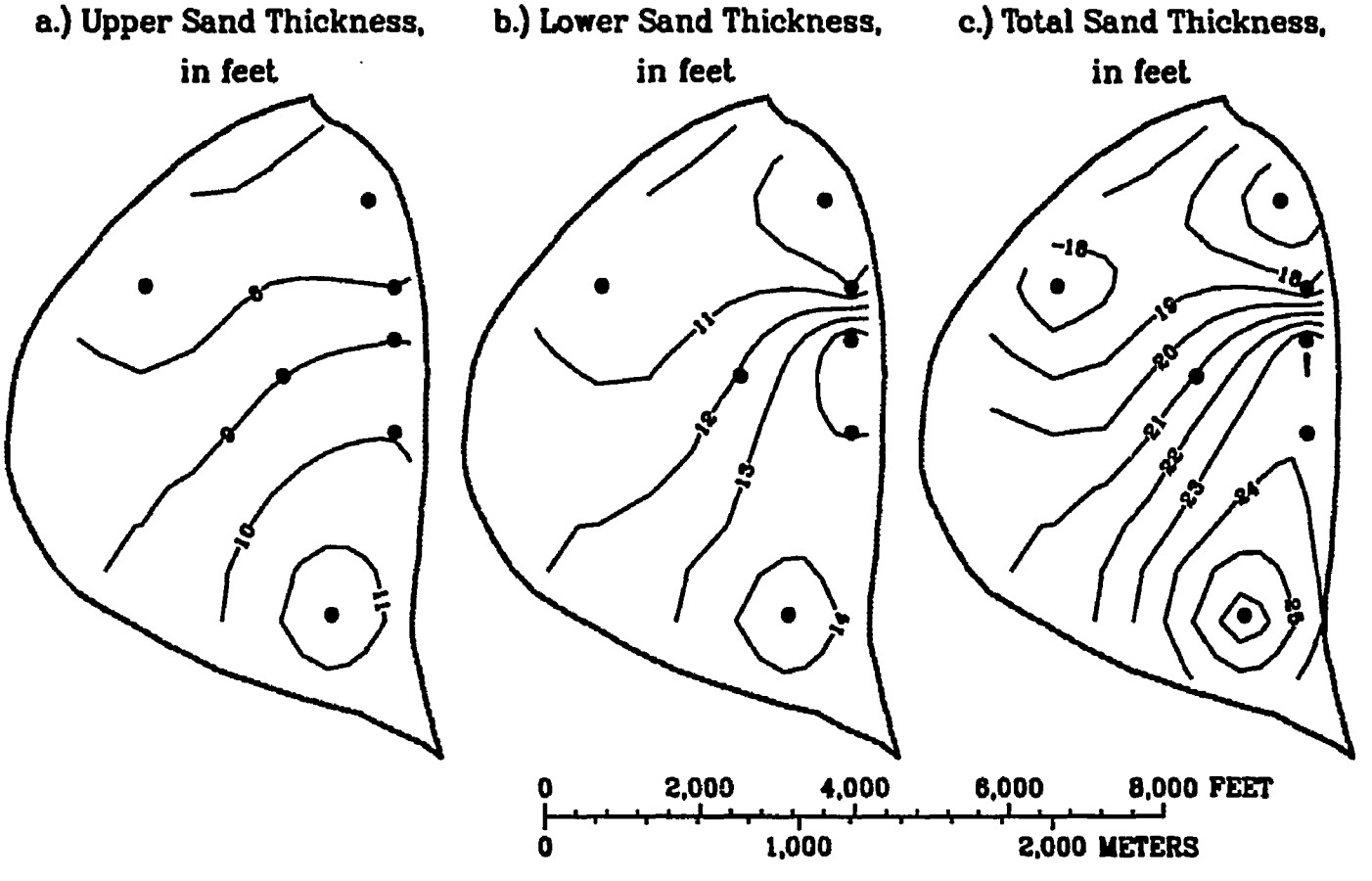

Figure 7.2--Isopach maps of the upper Beryl, lower Beryl, and total sand.

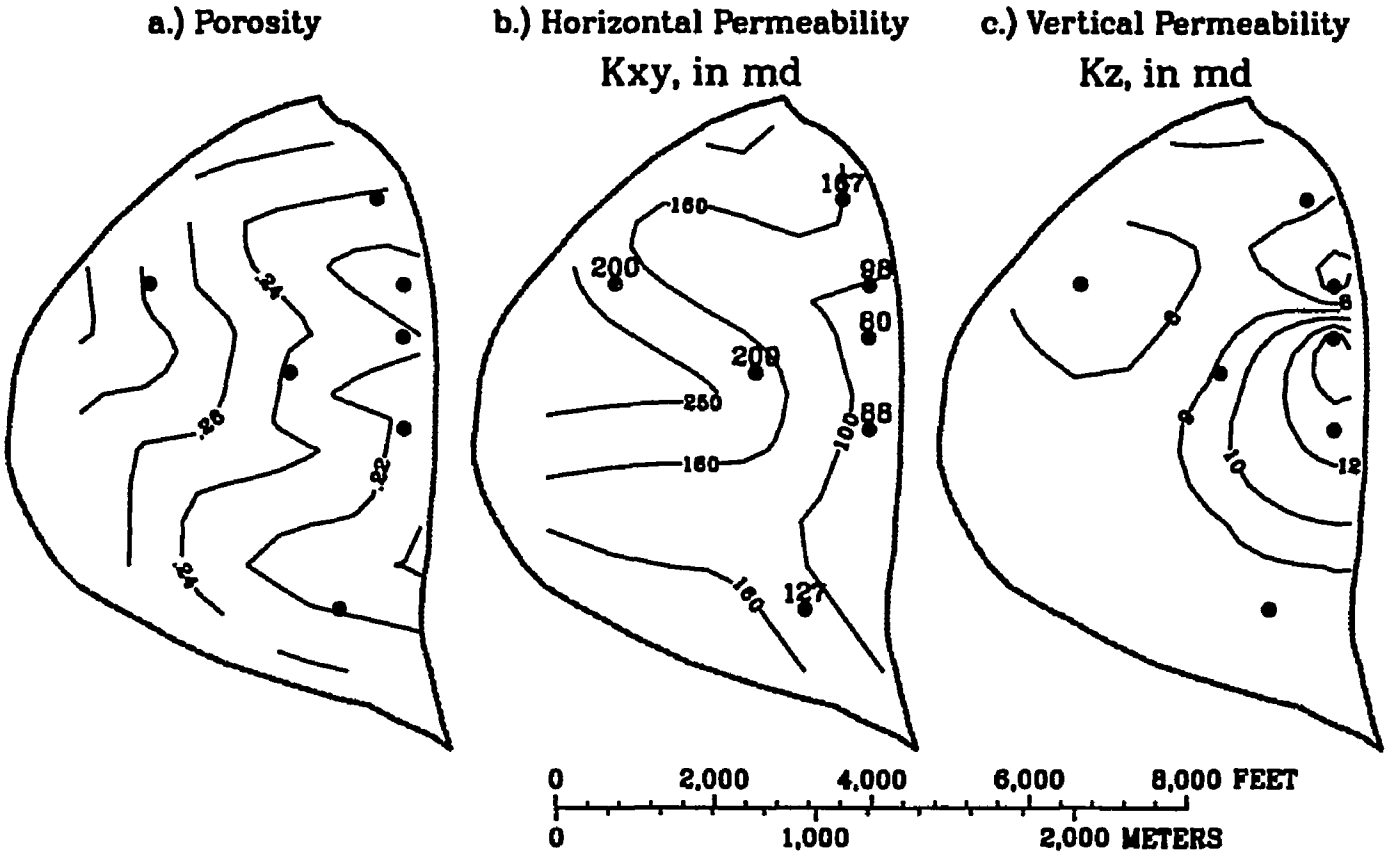

Figure 7.3--Porosity and permeability distributions in the Beryl reservoir.

Table 7.1--Summary of Beryl reservoir, fluid properties, and aquifer characteristics.

Discovery well	Beryl-1	
Initial oil in place	13.9 MMbls	
Initial gas in place	5.0 BCF	
Average net sand thickness	20 ft	
Average permeability	174 md,	volumetrically weighted
Average porosity	0.24	
Irreducible water saturation	0.20,	Residual oil saturation 0.20
Reservoir temperature	150 ^{0}F	
Initial reservoir pressure	3,990 psia	
Bubble point pressure	2,000 psia	
Initial oil/water contact	6,000 ft subsea	
Formation compressibility	15 µsips	

Fluid properties @ 3990 psia and 150 ^{0}F

	Oil	Gas	Water
FVF	1.36	0.0039	1.03
Viscosity, cp	0.29	0.024	0.41
Gas in Solution SCF/BBl	650	---	18
Density, lb/ft^3	51.7	0.05	62.7

Radial aquifer characteristics*

t_D = 0.01 t, from:		Aquifer contact, B, = 7100 ft^2, from:	
Compressibility	8 µsips	Oil/water interface**	364,000 ft^2
Viscosity	0.40 cp	Fraction connected	0.0195
Permeability	80 md		
Porosity	0.25		
Reservoir radius	8,000 ft		
re/rw	∞		

* Modified Van Everdingen and Hurst radial aquifer model where,

$$\text{Aquifer influx} = B \sum_{0}^{t} (p_{t_0} - p_t)\, Q(t_D)$$

** The oil/water interface is the vertical area open to flow along the oil/water contact.

(Fig. 7.3c). The gross reservoir characteristics and fluid properties are summarized in Table 7.1.

The discovery well, By-1 was completed in January, 1975. Six additional wells, By-2 through By-7, were drilled and began producing in early 1976. All wells were completed in both the upper and lower Beryl, except for wells By-4 and By-5, that were completed in the upper Beryl only. Production by well is detailed in Table 7.2.

Table 7.2--Reservoir production summary for the Beryl reservoir.

Well: By-	1	2	3	4	5	6	7	
Production from Layers	1,2	1,2	1,2	1	1	1,2	1,2	
During the years:								
1975	800	0	0	0	0	0	0	
1976 - 1980	800	600	600	600	600	600	600	
1981 - 1985	0	900	900	0	0	600	900	Res. Bbls/d

The Beryl reservoir is simulated as a 12 column, 20 row, 2 layer model (Fig. 7.1). By-6 is the reference well where node <11, 20> is defined as x,y location <10,000, 10,000>. The eastern boundary is treated as impermeable to simulate the fault. The western boundary along the oil/water contact is modelled as an infinite radial aquifer with the properties listed in table 7.1. The total oil, gas, and water production rates and average reservoir pressure are shown by the black, solid curves in Figure 7.4. These results are the supposedly measured reservoir history.

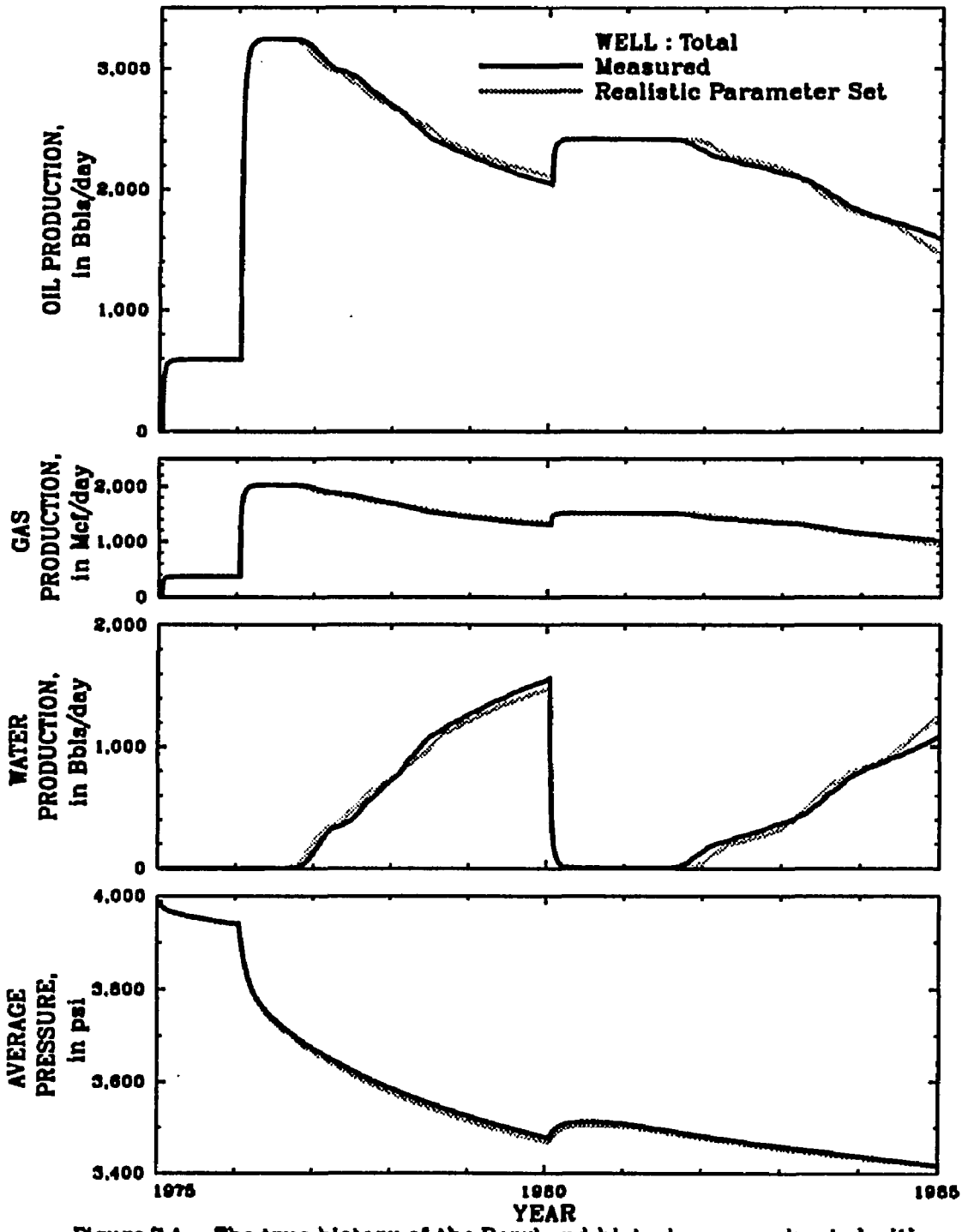

Figure 7.4--The true history of the Beryl and histories approximated with an ideal parameter set and a realistic parameter set.

7.2 History Matching with Ideal Parameters

OPTIM was initially tested by history-matching the Beryl with four ideal parameters. If ideal parameters are used, the true reservoir description can be duplicated. This exercise is only useful for testing the search algorithm since it is very unlikely one would infer the ideal parameters that characterize a reservoir.

Aquifer contact, horizontal permeability, and oil and water relative-permeability curves were the four reservoir properties modified and estimated. The aquifer contact, B, and horizontal permeability, K_{xy}, were modified as constant, exponential, scaled parameters, PINFO = CVES. Both the oil and water relative permeability curves were modified as constant, multiplicative, scaled parameters, PINFO = CVMS. If the parameter multiplier for each of these properties is initially set to one, the reservoir history would be duplicated exactly. The unmatched model was generated by changing the ideal parameter multipliers from one to the values shown in Figure 7.5a at iteration zero.

The objective function incorporated oil, gas, and water production, cell pressure, and flowing pressure data. Temporal gradients were approximated for all data types, bringing the total number of observation types to ten. More emphasis was placed on production rates than pressure data since pressure measurements are usually scanter than the number used here. All model residuals were made comparable by converting them to an equivalent oil production rate. The statistics for each observation type used are listed in Table 7.3.

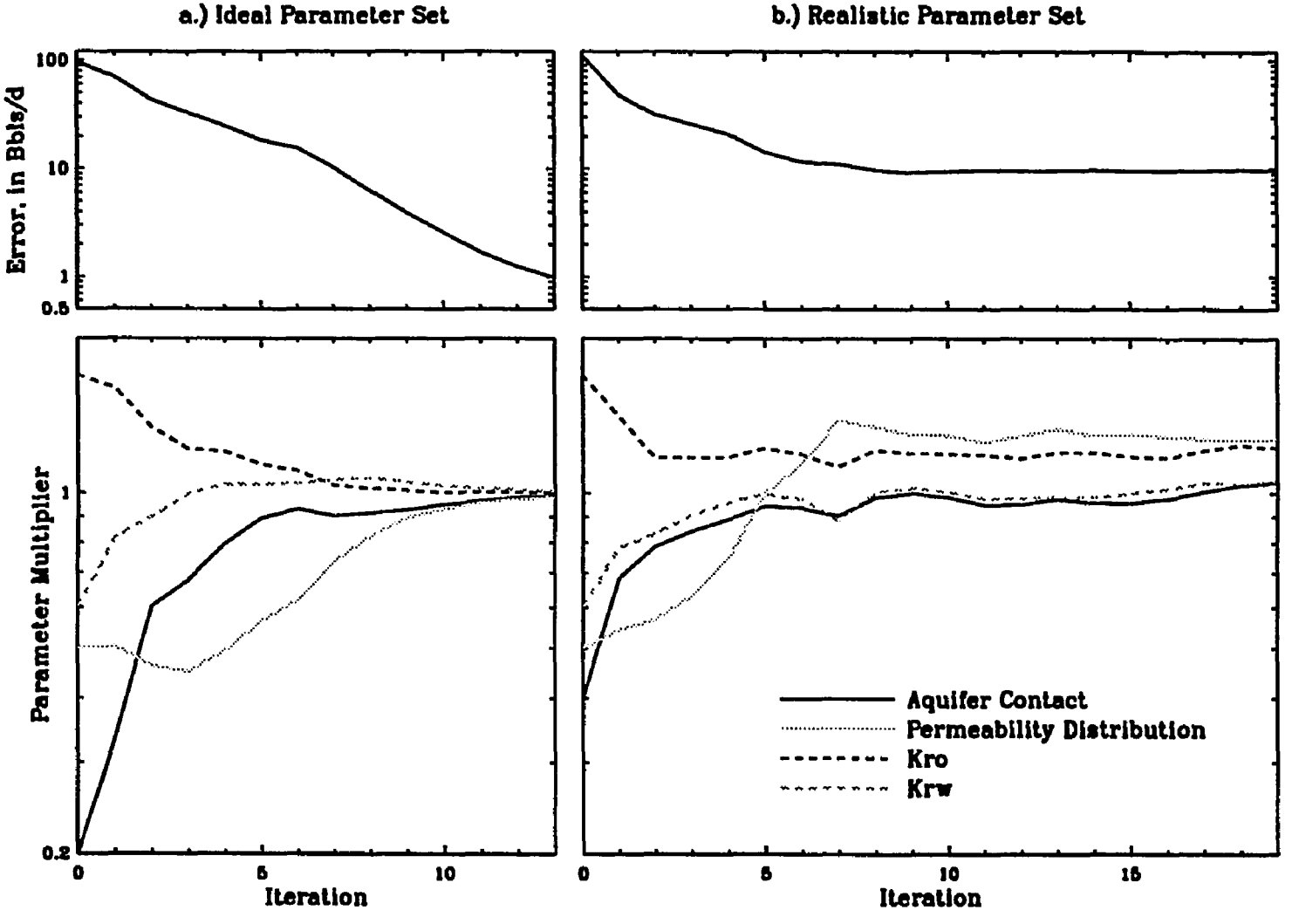

Figure 7.5--Change in model error and parameter multipliers for an ideal and a realistic parameter set.

Table 7.3--Observation types used to history-match the Beryl reservoir.

Type	Number	Average	σ	Ratio	% of weight
Qo	184	40	93.1	1.00	5.4
Qg	184	51	57.3	1.63	1.3
Qw	184	51.1	114	0.82	7.8
Pcell	140	90	279	0.33	9.3
Pflowing	128	60	316	0.29	0.9
Qo/dt	32	-0.066	0.111	837	13.3
Qg/dt	32	-0.047	0.068	370	0.7
Qw/dt	32	0.083	0.139	670	9.3
Pcell/dt	28	-0.105	0.059	590	11.6
Pflow/dt	28	-0.139	0.151	615	0.6

972 observations are used.

Root-mean-square error at iteration zero was 98 Bbls/d and the sum-of-squares was $3.4 \times 10^{6}(\text{Bbls/d})^{2}$. Although the search algorithm minimizes the sum-of-squares, root-mean-square error is discussed since it is physically more meaningful. Root-mean-square error, just error from hereafter, is related to sum-of-squares, SS, by:

$$\text{Error} = \sqrt{\frac{SS}{\Sigma\ w}} \tag{7.1}$$

OPTIM reduced the error from 98 to 0.99 Bbls/d in 13 iterations and reduced the difference between parameter multipliers and their true values to less than a percent (Fig. 7.5a). OPTIM stopped because parameter change had dropped below the assigned minimum of 0.01. Although the error could have been reduced further, it would have been pointless. Both the calculated observations and estimated parameters were practically identical to the measured observations and true parameters. The initial and history-matched relative-permeability curves (Fig. 7.6a) illustrate how the parameters are modifying reservoir properties.

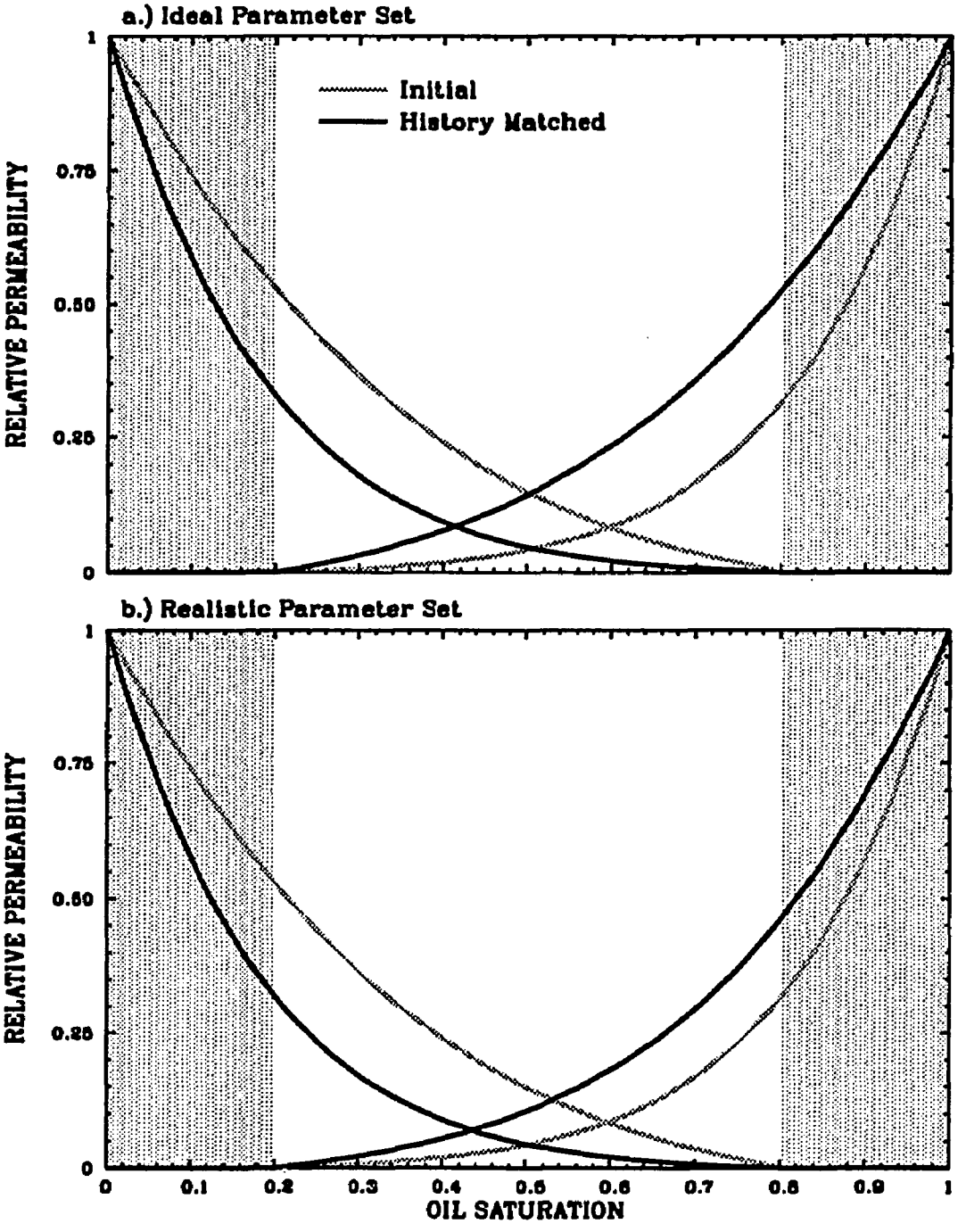

Figure 7.6--Relative permeability curves from models produced with an ideal parameter set and with a realistic parameter set.

7.3 History Matching with Realistic Parameters

The same four reservoir properties modified and estimated in the ideal case were used again. Except, the true horizontal permeability distribution was replaced with a constant value of 180 md at all nodes and was modified as a weight, exponential, scaled parameter, PINFO = WVES. An iso-value contour that agreed with the core permeabilities from each well (Fig. 7.7) was the basis for the weight matrix. Since a realistic parameter set was used, the final parameter estimates need not converge on one. The same objective function was used again so the errors could be compared.

For the first six iterations, error reduction occurred more rapidly than in the ideal case (Fig. 7.5b and Table 7.4). Error reduction slowed until a minimum of 9.3 Bbls/d was reached at the 9th iteration which was the history-matched model. Both error and parameter estimates did not change significantly during the last 10 iterations (Fig. 7.5b). The error is not a reflection of the inability of the search algorithm, but of the imperfect approximation of the horizontal permeability distribution.

The volumetrically-weighted average of the history-matched permeability estimates (Fig. 7.7) was 205 md, which was 18% greater than the true value. The greater permeabilities were compensated by lowering the relative permeability to oil. Comparing history-matched curves in Figure 7.6, the relative permeability to oil at So=0.80 was 14% less than the true value.

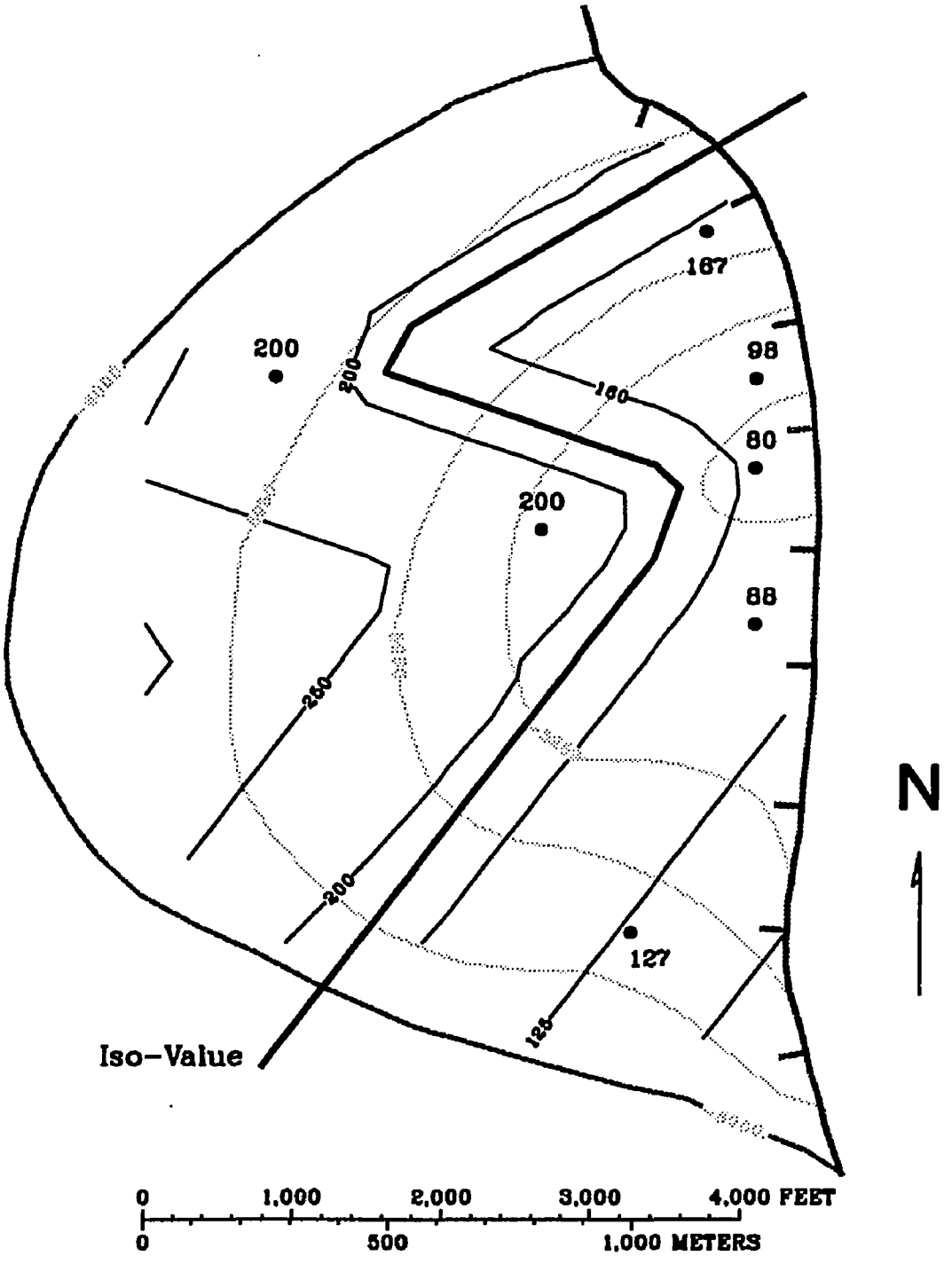

Figure 7.7--History-matched horizontal permeability, Kxy, distribution based on realistic parameter set.

Table 7.4--Error statistics for the Beryl reservoir simulated with an ideal and a realistic parameter set at selected iterations.

	Ideal Parameter Set				Realistic Parameter Set			
Iter.	SS	Error	σ	Average	SS	Error	σ	Average
0	3,387,000	97.9	96.1	19.2	4,403,000	111.7	92.1	-63.3
6	84,900	15.5	15.5	-0.755	47,680	11.6	11.6	-.388
9	5,450	3.93	3.92	-.330	30,370	9.27	9.27	0.404
13	346	0.990	0.999	-.231	33,440	9.73	9.73	-.177

Total production and average pressure differences between the history-matched model and reality are shown in Figure 7.4. For individual wells, By-2 is the best matched (Fig. 7.8) and By-5 matched the worst (Fig. 7.9). By-2 matched well since the nearby estimated permeability distribution was close to the true distribution and it produced mostly oil. The estimated permeability distribution was poorest near By-5 and By-5 had a WOR of 3 prior to being shut-in. The effect of these errors is most evident in the difference between matched and true flowing pressures (Fig. 7.9).

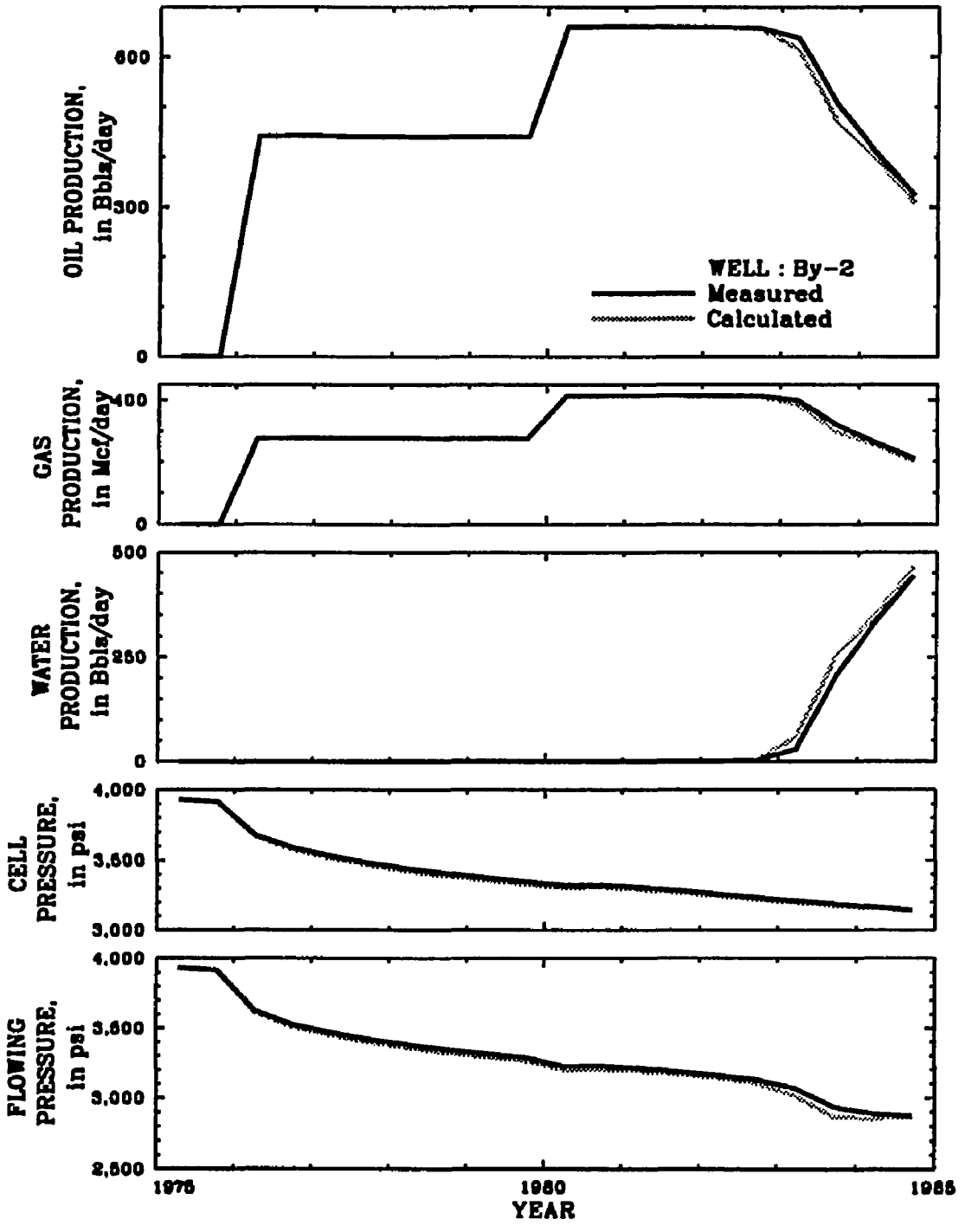

Figure 7.8--Production and pressure history from well By-2, the well fitted best with realistic parameter set.

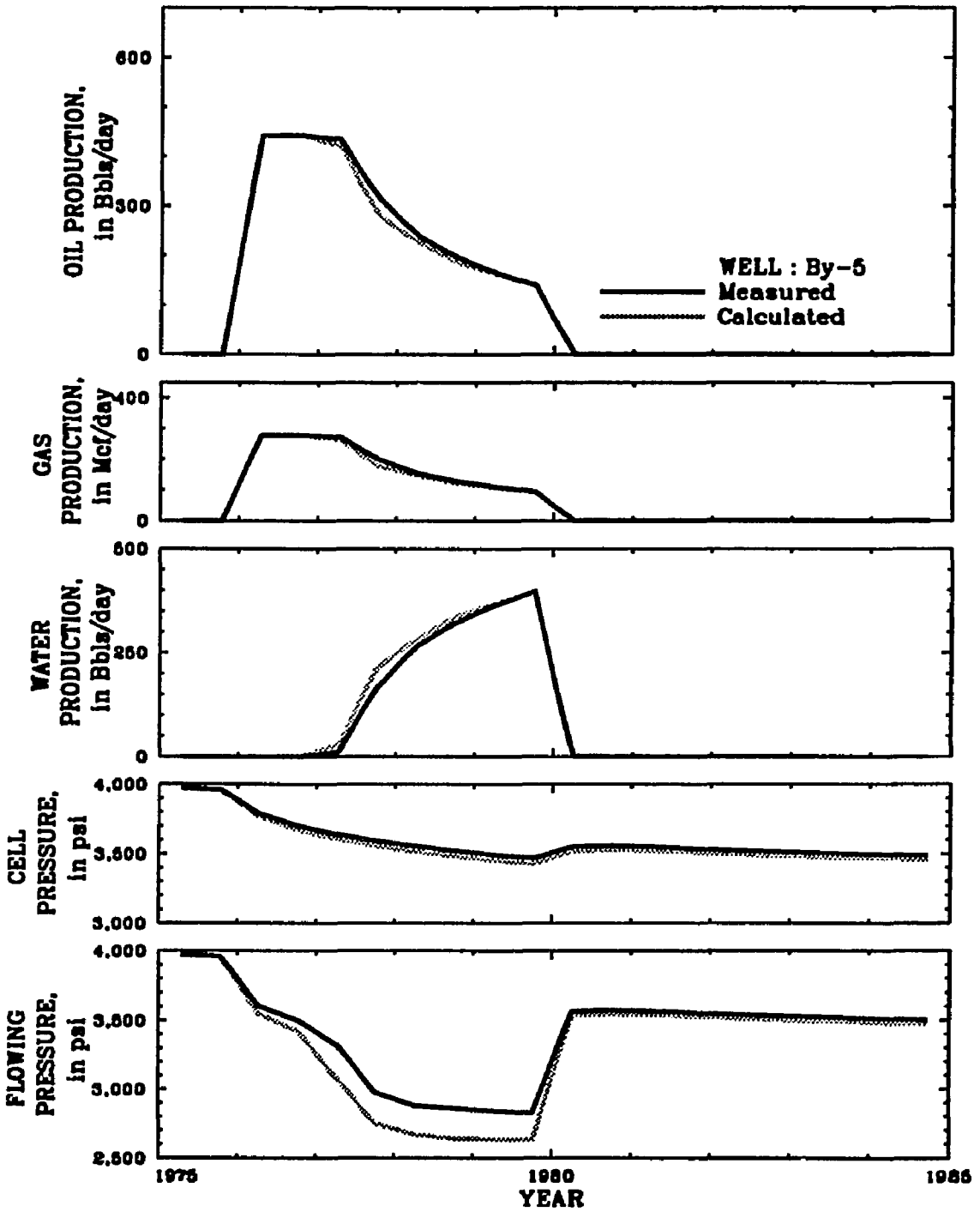

Figure 7.9--Production and pressure history from well By-5, the well fitted worst with realistic parameter set.

CHAPTER VIII

HISTORY MATCH OF SPARTA "B" RESERVOIR -- FORDOCHE FIELD

8.1 The Sparta "B"

The Sparta "B" reservoir is formed by an anticline (Fig. 8.1) and is composed of two laterally continuous sands separated by a thin shale. The thickness of the upper sand varied very little (Figs. 8.2 and 8.3) and averaged 12 ft. The intermediate shale is thickest near well Sm-7, and thins toward the oil/water contact, and averages 5 ft. The lower sand thickens from north to south (Fig. 8.2) and averages 22 ft. Porosity varies more in the lower sand than in the upper sand (Fig. 8.4), but overall, porosity did not vary greatly.

Using the isopach and porosity maps, an initial oil/water contact at 11,588 ft subsea (Fig. 8.3), and an irreducible water saturation of 0.48, the initial oil in place is 3.36 MMSTB. Most of the oil, 2.92 MMSTB, was trapped in the upper sand. No free gas was initially in place and no gas came out of solution during production since the initial reservoir pressure was 7,800 psia and no flowing-well pressures dropped below the bubble point, 2,075 psia.

The horizontal permeability distributions, estimated from core data, for each sand were similar to the porosity distributions (Fig. 8.5). The vertical permeability, K_z, distribution is assumed to be inversely proportional to the intermediate shale thickness (McDonald and Harbaugh, 1988). The gross reservoir characteristics and fluid properties are summarized in Table 8.1.

Table 8.1--Summary of Sparta "B" reservoir, fluid properties, and aquifer characteristics.

Discovery well	N. Smith Jr. #7D, Sm-7
Initial oil in place	3.36 MMSTB
Initial solution gas in place	2.6 BCF
Average net sand thickness	16 ft
Average permeability: Initial	135 md, overall 160 md, near wells
Average permeability: Matched	600 md, overall 235 md, near wells
Average porosity	0.24
Irreducible water saturation	0.48, Residual oil saturation 0.24
Reservoir temperature	228 ^{o}F
Initial reservoir pressure	7,800 psia
Bubble point pressure	2,075 psia
Initial oil/water contact	11,588 ft subsea
Formation compressibility	15 μsips

Fluid properties @ 7,800 and psia 228 ^{o}F

	Oil	Gas	Water
FVF	1.28	0.0034	1.03
Viscosity, cp	0.36	0.012	0.41
Gas in Solution SCF/BBl	650	---	18
Density, lb/ft^3	51.7	0.05	62.7

Radial aquifer characteristics*

t_D = 0.01 t, from:		Aquifer contact, B, = 7130 ft^2, from:	
Compressibility	8 μsips	Oil/water interface**	404,000 ft^2
Viscosity	0.40 cp	Fraction connected	0.0177
Permeability	80 md		
Porosity	0.25		
Reservoir radius	8,000 ft		
re/rw	∞		

* Modified Van Everdingen and Hurst radial aquifer model where,

$$\text{Aquifer influx} = B \sum_{0}^{t} (p_{t_0} - p_t)\, Q(t_D)$$

** The oil/water interface is the vertical area open to flow along the oil/water contact.

The Sparta "B" is simulated as a three layer model (Fig. 8.3). Stratigraphy requires at least two layers to simulate the upper and lower sands. The upper sand is subdivided into two layers to allow for water coning near the wells. A 19 column by 12 row grid is used to define the model laterally (Fig. 8.1). Sm-7 is the reference well where node <7,8> is defined as x,y location <10,000, 10,000>. The oil/water contact defines the model's external boundary in all layers. The boundary is simulated as an infinite, radial aquifer characterized by the properties listed in table 8.1. The initial aquifer contact, B, for each node was proportional to the area of the vertical, external block faces.

8.2 Production and Pressure History

Production started in March of 1973 with the Bl-4 which was completed in the upper sand. The discovery well, Sm-7, was tested in 1970 but was not completed in the Sparta "B" until January, 1974. Sm-4 and Sm-9 were also completed in January 1974. Sm-4 is isolated from the other wells by a shale-out (Fig. 8.1) and is draining a separate reservoir, the Sparta "B-RB". Sm-10 only produced 400 STB for two months in 1985 (Table 8.2). It is not included in the simulation. Production is simulated by specifying the total rate of all three phases, i.e. oil, gas, and water, in reservoir barrels, RBbls.

Table 8.2--Production from the Sparta "B" by well from March 1973 to September 1989.

	Well Comp.	Date Shut-In	Oil MSTB	Gas MMCF	Water MSTB	Sand
Sm-4	1/74	1/86	75.1	53.0	368.7	Upper
Sm-7	1/74	10/84	291.3	163.6	457.3	Upper & Lower
Sm-9	1/74	9/89	378.5	265.6	1,047.7	Upper
Sm-10	3/85	5/85	0.4	0.0	3.0	Upper
Bl-4	3/73	5/89	341.0	273.1	908.7	Upper
Total			1,086.	755.3	2,785.3	

It is not practical to simulate all rate changes a reservoir undergoes while being produced. Consequently, the reservoir history is approximated by a step profile resulting in the same cumulative volumes. As an example, the measured and approximated history of Sm-9 are shown in Figure 8.6. The error introduced by this approximation is offset by using the approximated history as the base for comparison purposes. The approximated total oil, gas, and water production rates of the Sparta "B" are shown in Figure 8.7.

Flowing-surface-tubing pressure, P_{fst}, is the only type of pressure data available. The flowing-surface-tubing pressures ranged from 25 psig to 1,600 psig and averaged 350 psig. Flowing bottom-hole pressures were approximated by adding 4,500 psi representing the hydrostatic pressure of an 11,600 ft column of oil and water, to the flowing-surface-tubing pressure. It is conveniently assumed that frictional pressure losses are offset by neglecting the effect of the gas phase. Considering the crude nature of these estimates, they were only used as a lower limit.

The objective function incorporated oil, gas, and water production, and flowing pressure data. All model residuals were made comparable by converting them to an equivalent oil production rate. The statistics for each observation type used are listed in Table 8.3.

Table 8.3--Observation types used to history-match the Sparta "B".

Observation Type	Number of Observations	Average	Standard Deviation	Ratio of Deviations	Observation Emphasis, %
Qo, STB/d	220	26.8	25.6	1.00	54.2
Qg, MCF/d	220	18.2	13.1	1.97	2.8
Qw, STB/d	220	68.1	57.2	0.45	37.2
Pf, psig	23	4740	505	0.05	5.9
	683 observations used.				

8.3 Automatic History Matching

Differences between calculated and measured observations provide the only quantitative assessment of the model's worth because the true reservoir properties are not known. The first eight years of production, 1973-1981 are used in the automatic history match (Fig. 8.7). The data available for the 1982-1990 period is used to test the predictive ability of the history-matched model.

Aquifer contact, horizontal permeability, vertical permeability, and oil and water relative-permeability curves are the five reservoir properties modified and estimated. The horizontal permeability, K_{xy}, is modified with a weight matrix as an exponential, scaled parameter, PINFO = WVES. The weight matrix allows the permeability to vary from east to west and pivots

about the shale-out. The aquifer contact, B, is modified with a constant and the same weight matrix used to modify K_{xy}. It is also treated as an exponential, scaled parameter, PINFO = BVES. Vertical permeability, K_z, is modified with a constant and a weight matrix based on the intermediate shale thickness. It is also treated as an exponential, scaled parameter, PINFO = BVES. Both the oil and water relative permeability curves are modified as constant, additive, scaled parameters, PINFO = CVAS.

Initial parameter estimates produced a model with an error of 30 Bbls/d (Fig. 8.8 and Table 8.4). Parameter change is included to show the lack of parameter change as OPTIM converges on a minimum, 6.9 Bbls/d at iteration 18. Since no true values are known, exponential parameters are divided by their history-matched values so they converged on one. The oil and water relative permeability coefficients, a, were reported without modification.

Table 8.4-Error statistics, in Bbls/d, for the Sparta "B" initial model, history-match, prediction, and overall.

Period:	RMS	σ	Average	SS	Σw	M
Initial model, 1973-1981	29.65	27.68	-10.67	134,400	153	366
History-match, 1973-1981	6.92	6.93	0.26	7,328	153	366
Prediction, 1982-1990	6.28	6.18	1.18	5,594	142	319
Overall, 1973-1990	6.62	6.59	0.70	12,922	295	685

The reservoir characteristics taken from core data and incorporated in the K_{xy} weight matrix force the horizontal permeability distribution to vary along an east-west trend. The history-matched distribution reflects this bias and increases from west to east (Fig. 8.9). Qualitatively, this agrees with the

shale-out that separates the Sparta "B" from the Sparta "B-RB". The fitted relative permeability coefficients produced the curves shown in Figure 8.10.

Total production differences between the history-matched model and reality are shown in Figure 8.7. The calculated and measured production from Sm-4, Sm-7, Sm-9, and Bl-4 is shown in Figures 8.11-14. The difference between calculated and measured cumulative oil production is 2% in 1981 at the end of the history-match (Table 8.5).

Table 8.5--Cumulative calculated and measured production from the Sparta "B".

	Oil, MSTB		Gas, MMCF		Water, MSTB	
From 1973 to:	$\hat{\psi}$	ψ	$\hat{\psi}$	ψ	$\hat{\psi}$	ψ
1978	590	640	330	330	220	220
1981	870	890	510	470	780	830
1982	930	930	540	500	1,000	1,000
1990	1,140	1,090	720	760	2,670	2,780

The predictive RMS error, 6.3 Bbls/d, is less than the history-matched RMS error, 6.9 Bbls/d, but the predictive average error, 1.2 Bbls/d. was greater than the history-matched average error, 0.3 Bbls/d, (Table 8.4). These consistently high estimates are most evident in production from the Smith-9 (Fig. 8.13). The difference between calculated and measured cumulative oil production from 1982 to 1990 is 25% but as a whole the cumulative calculated oil production is only 5% greater than the cumulative measured oil production (Table 8.5). Most of the oil migration is from east to west (Figs.

8.15-16). Most of the by-passed oil is located in a low permeability region near the shale-out (Fig. 8.16).

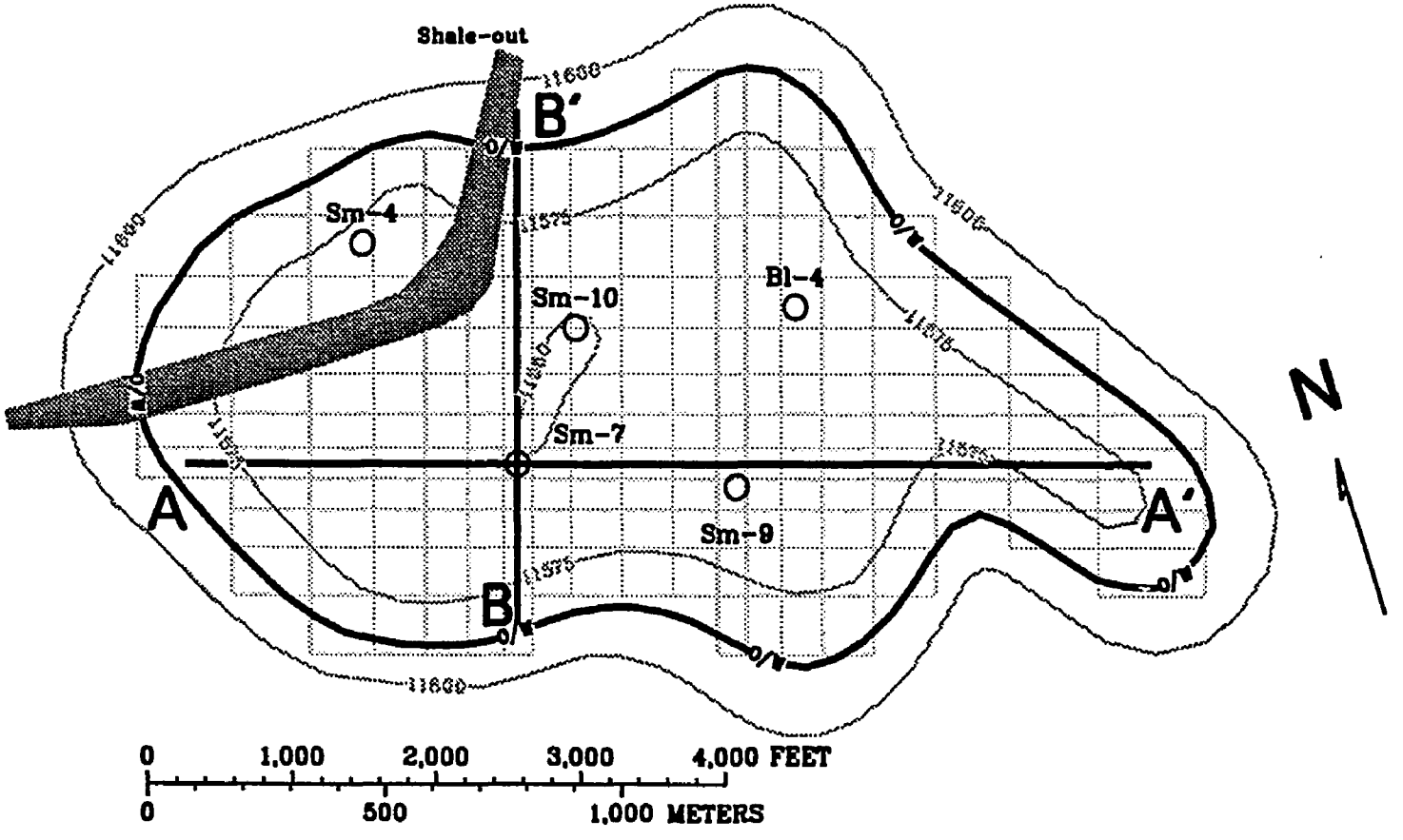

Figure 8.1--Structure map and model grid for the Sparta "B".

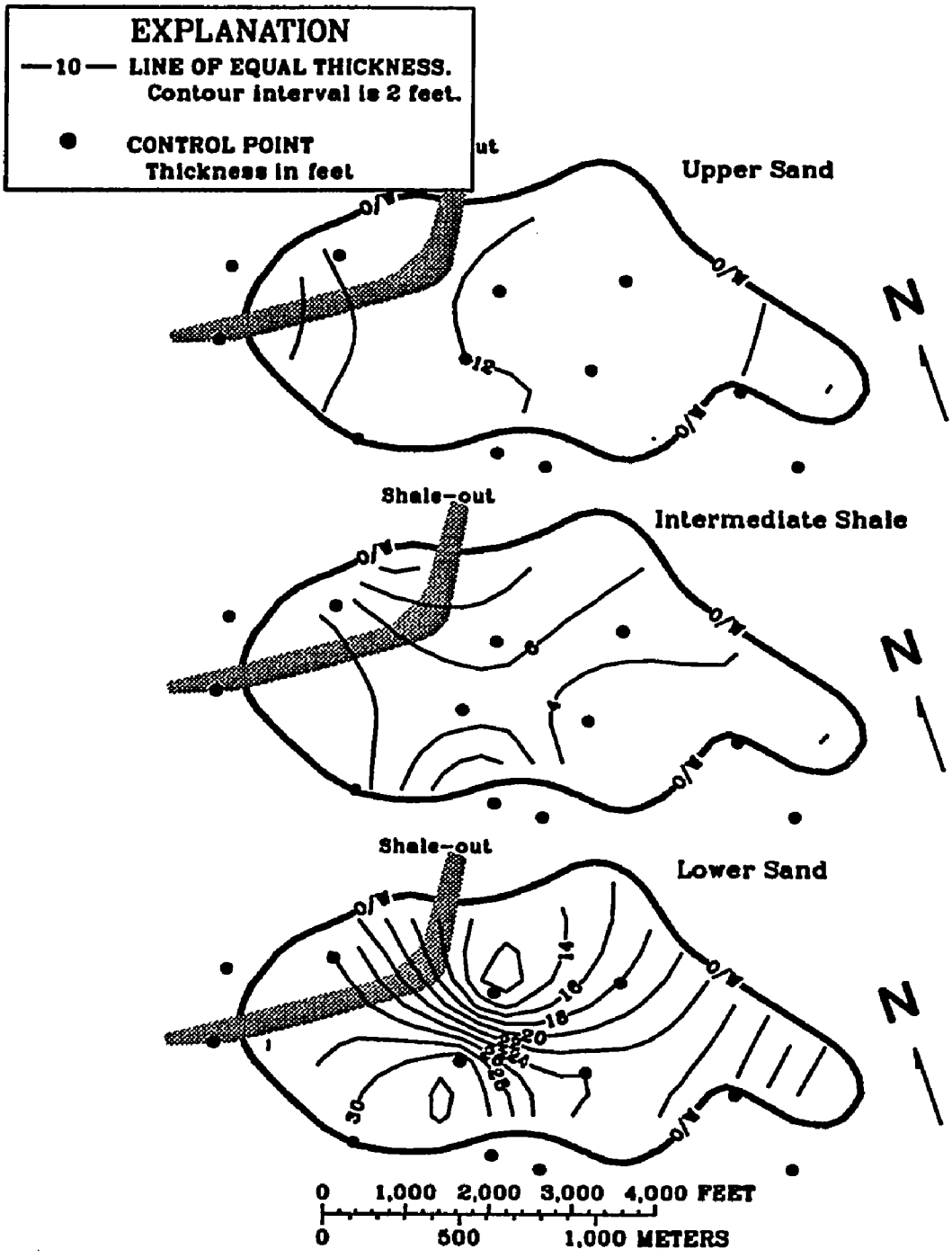

Figure 8.2--Isopach maps of Sparta "B" upper sand, intermediate shale, and lower sand.

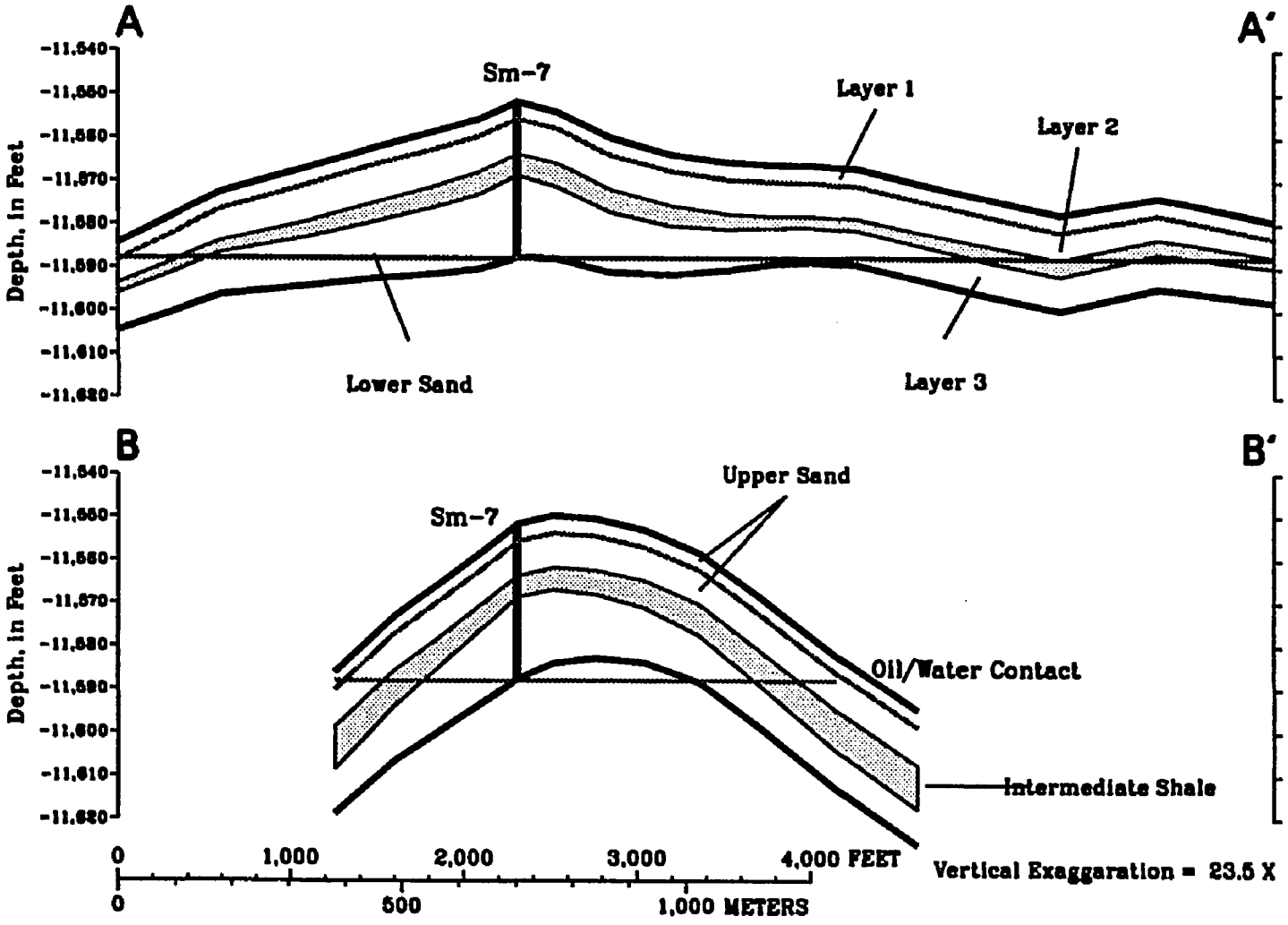

Figure 8.3--Cross-sections A-A' and B-B' through the Sparta "B". See figure 8.1 for sections traces.

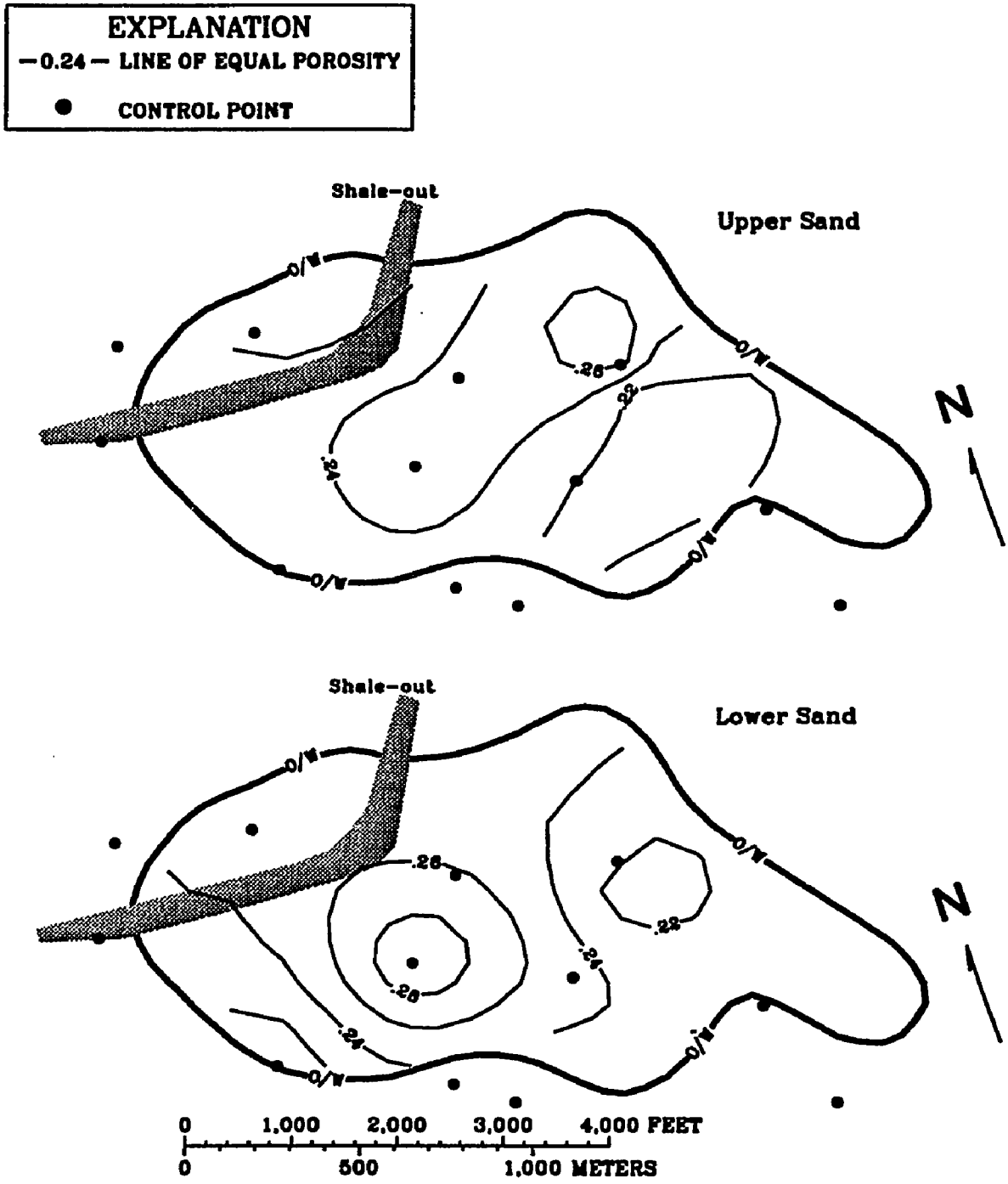

Figure 8.4--Porosity maps of Sparta "B" upper and lower sands.

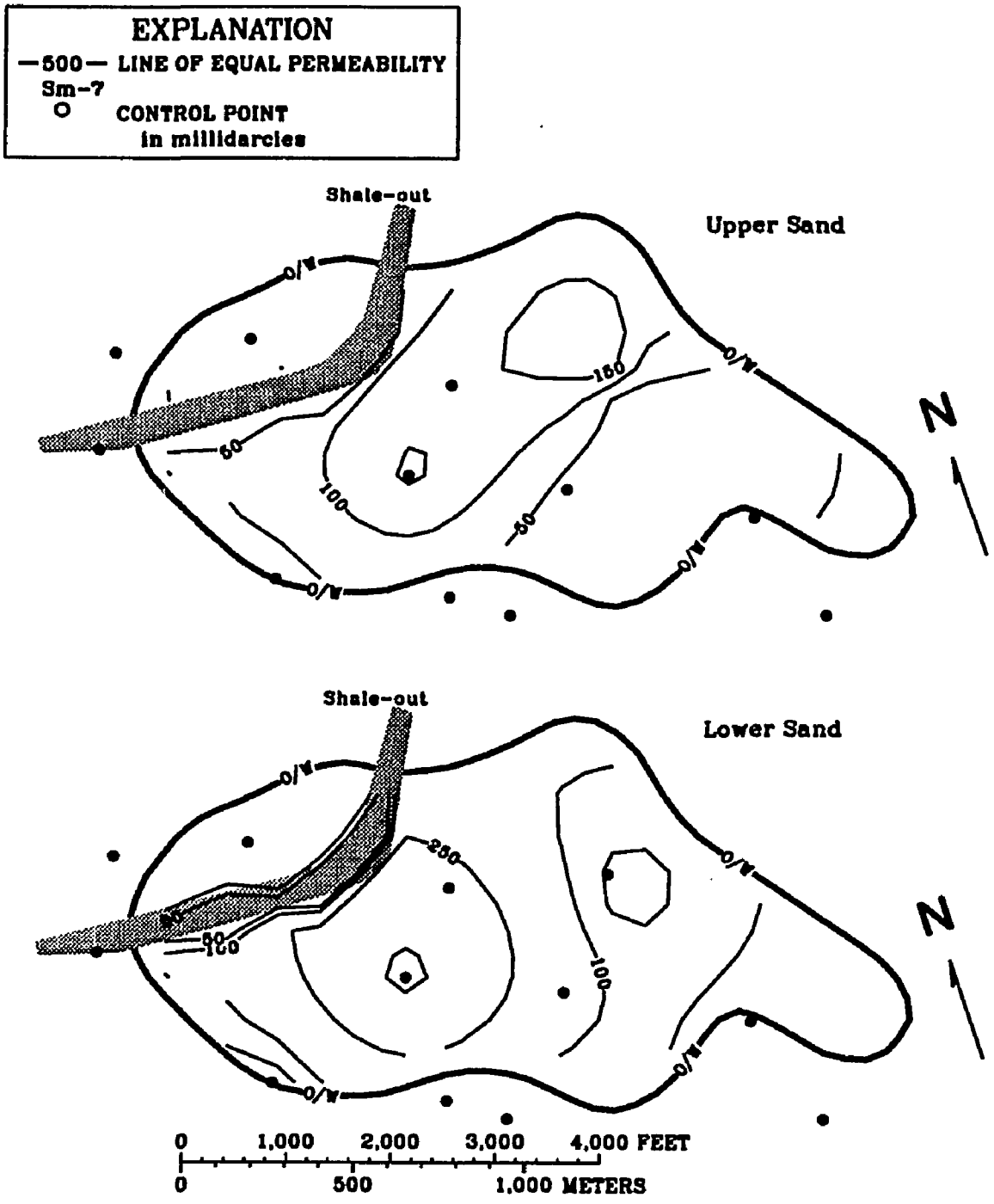

Figure 8.5--Initial permeability maps of Sparta "B" upper and lower sands.

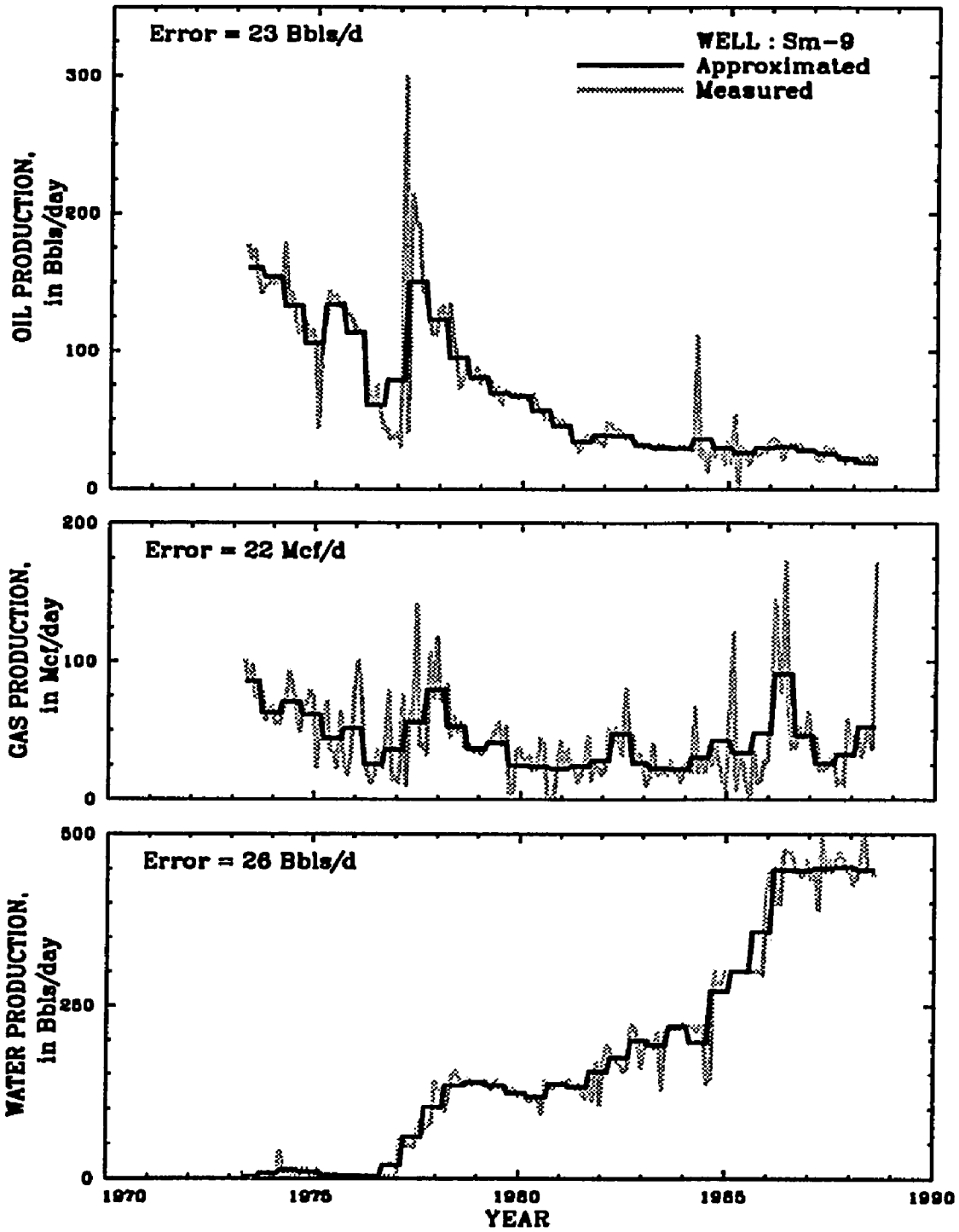

Figure 8.6--Observation error introduced by step-wise approximation of production rates.

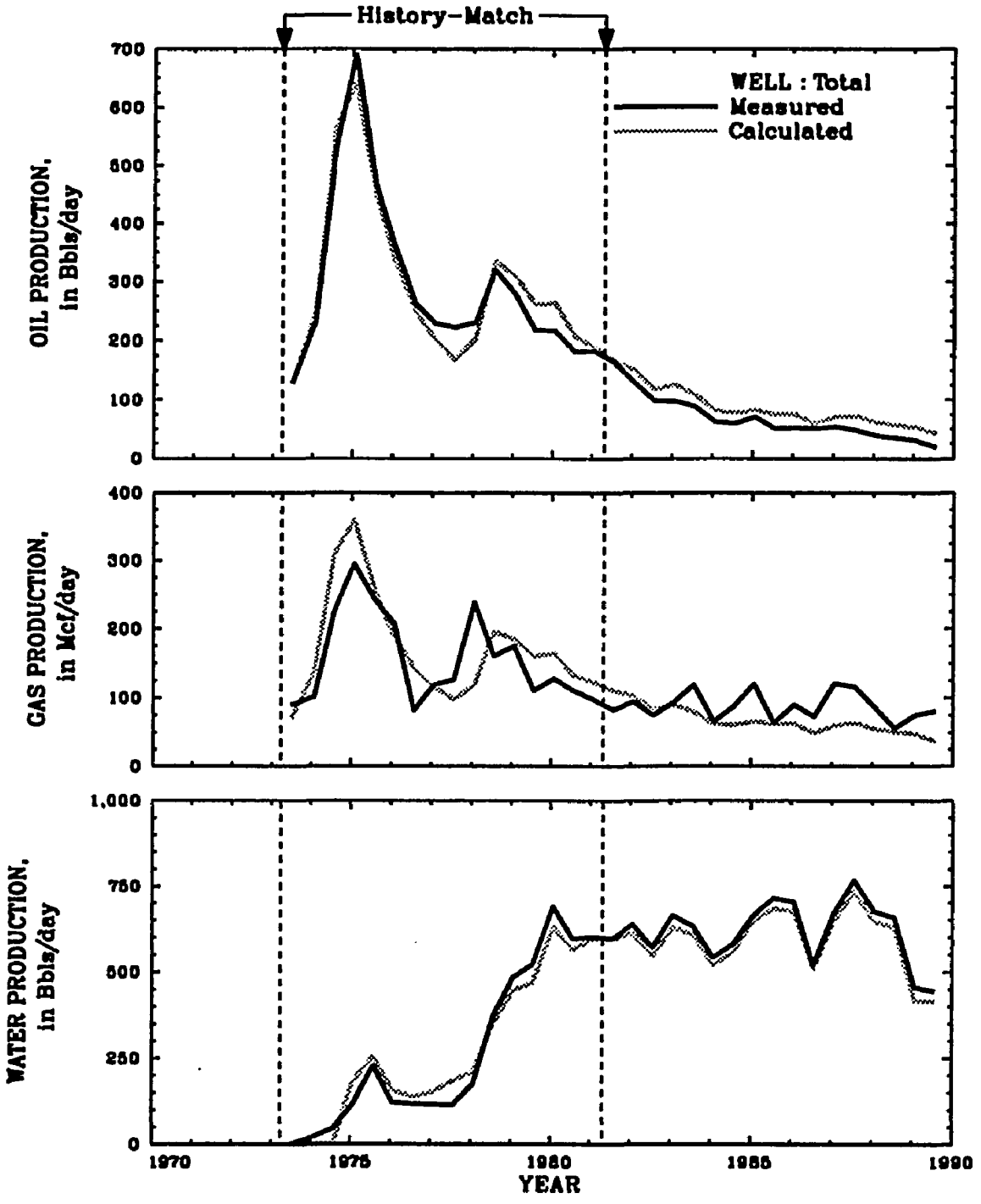

Figure 8.7--Total production from the Sparta "B".

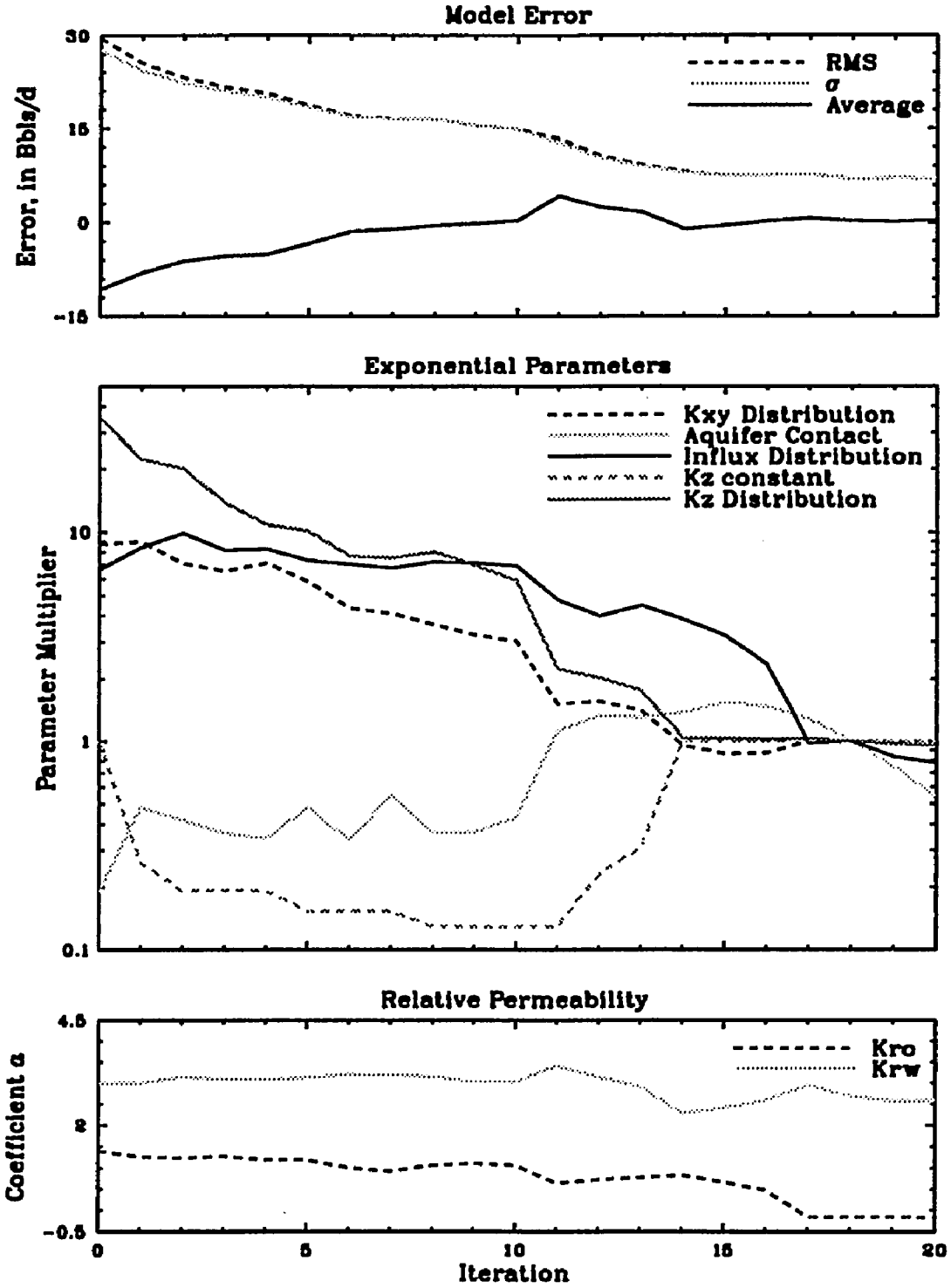

Figure 8.8--Change in model error and parameter multipliers for the Sparta "B".

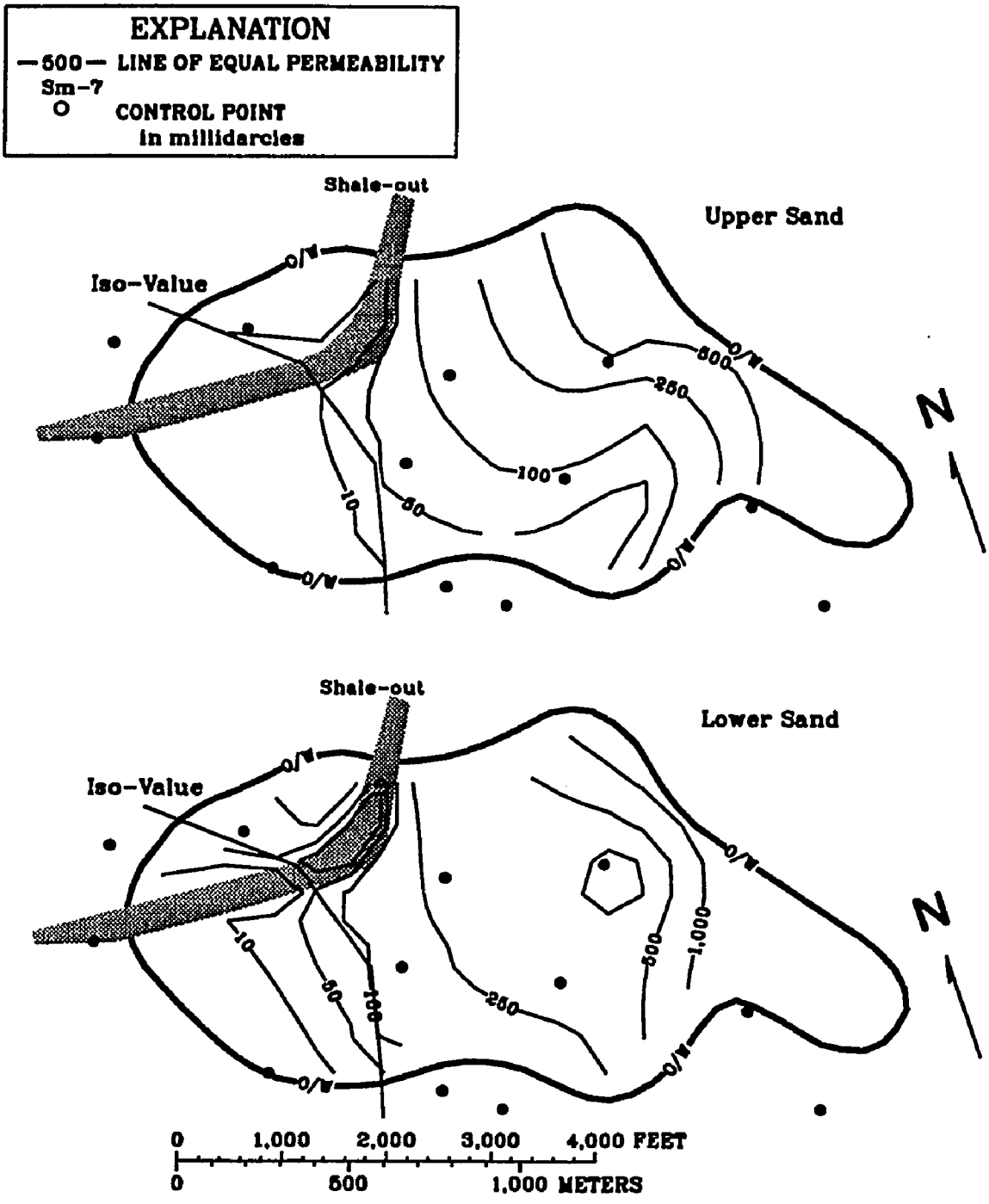

Figure 8.9--History-matched permeability maps of Sparta "B" upper and lower sands.

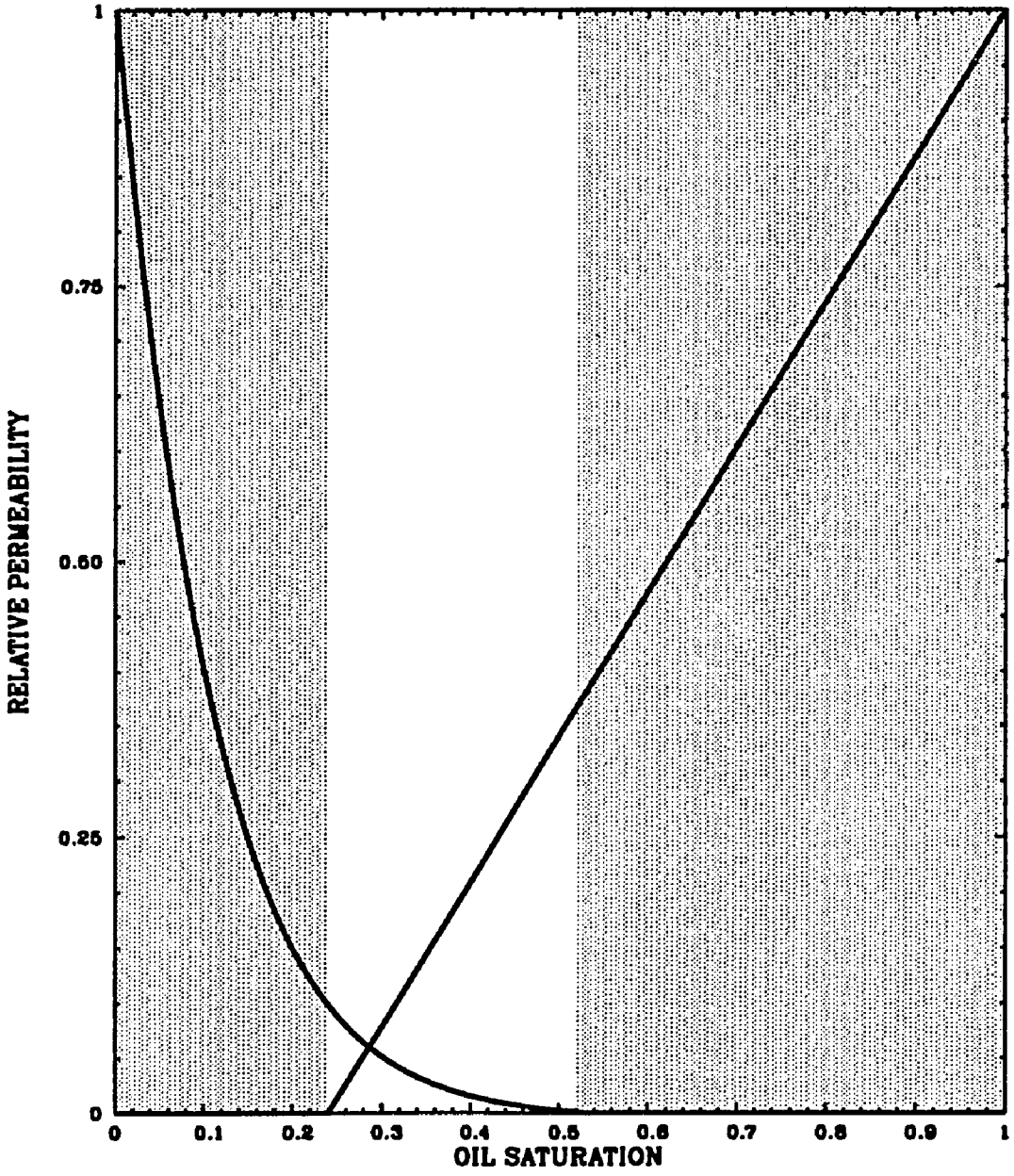

Figure 8.10--Relative permeability curves for the Sparta "B".

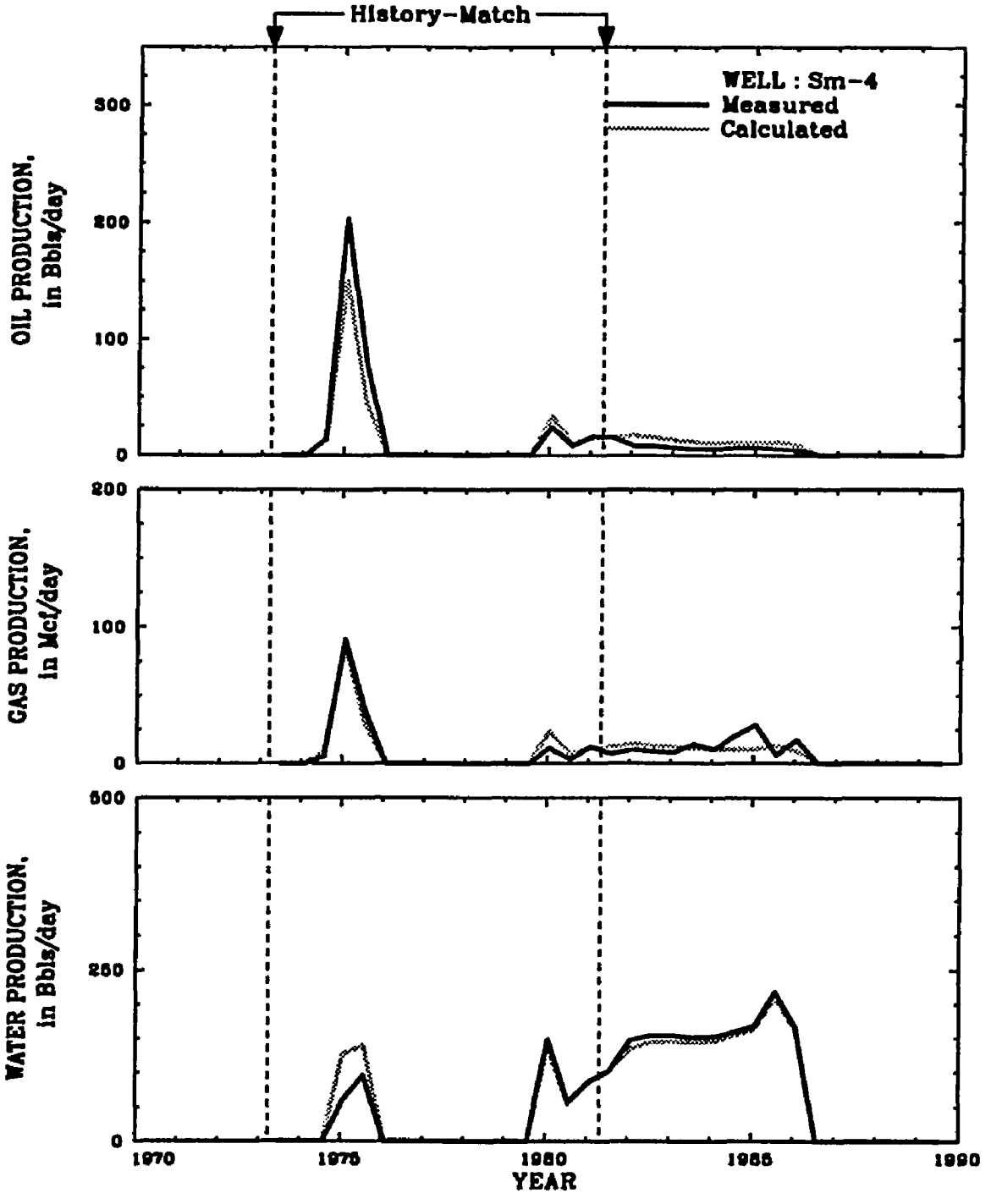

Figure 8.11--Production from well Sm-4 in the Sparta "B".

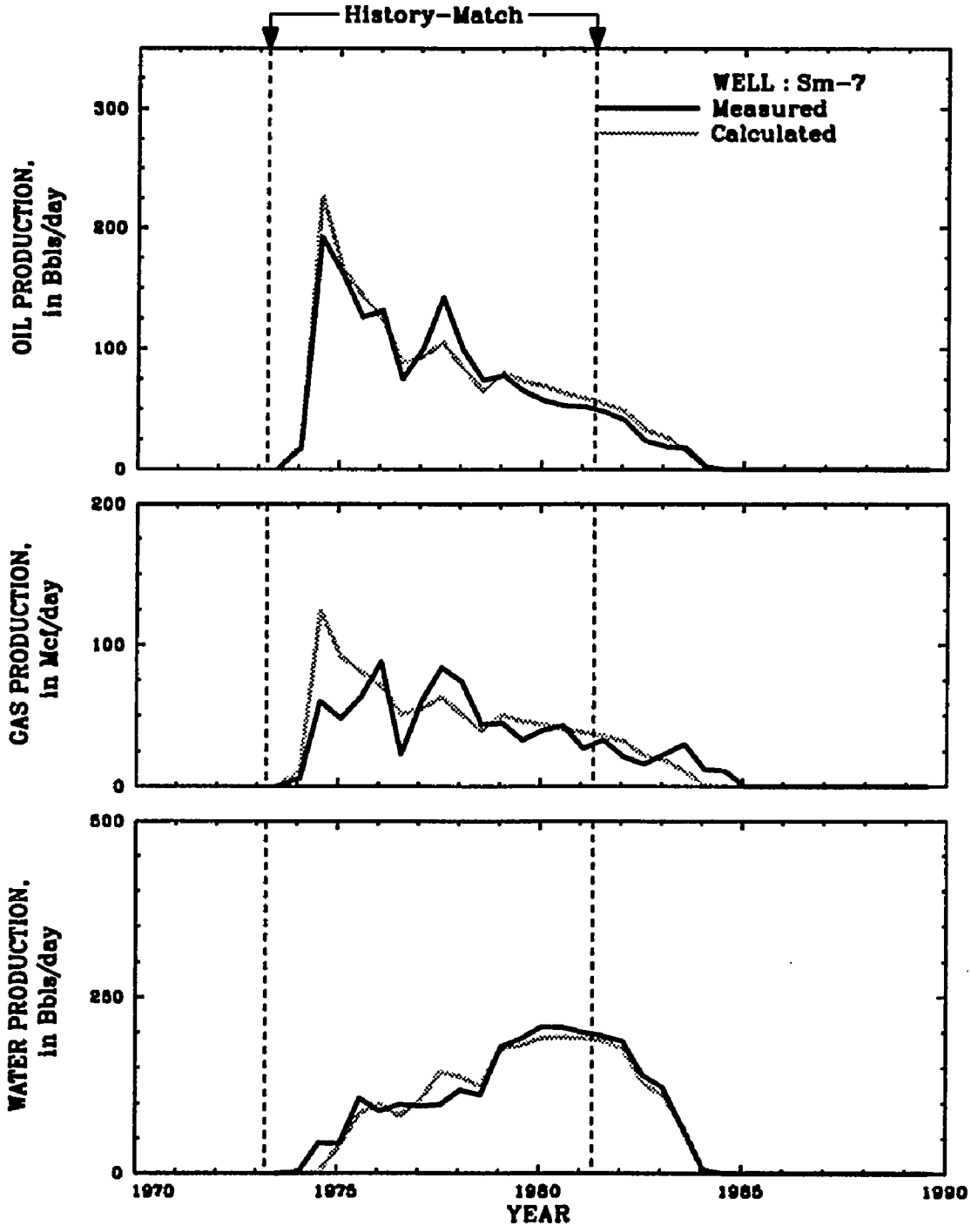

Figure 6.12--Production from well Sm-7 in the Sparta "B".

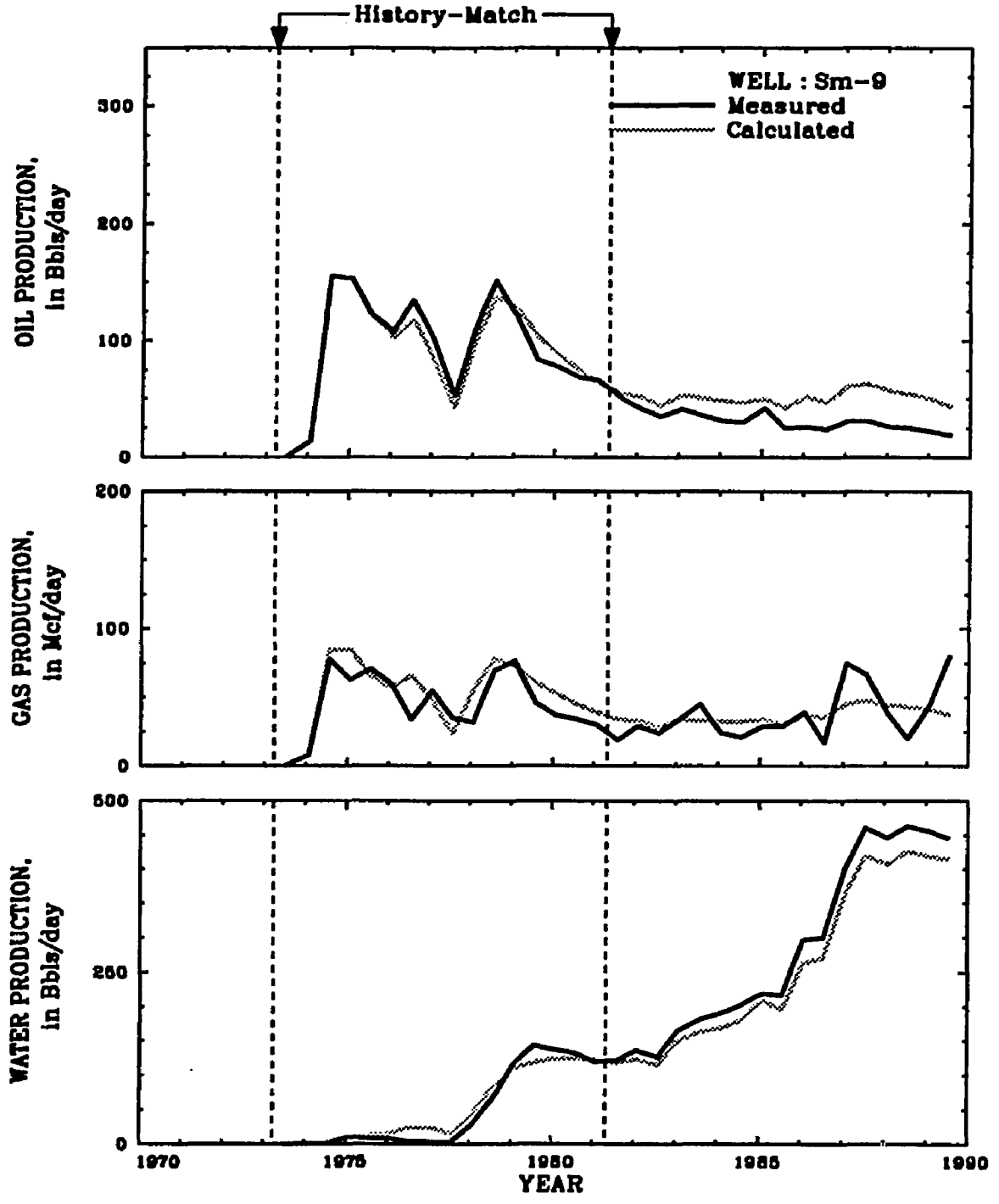

Figure 8.13--Production from well Sm-9 in the Sparta "B".

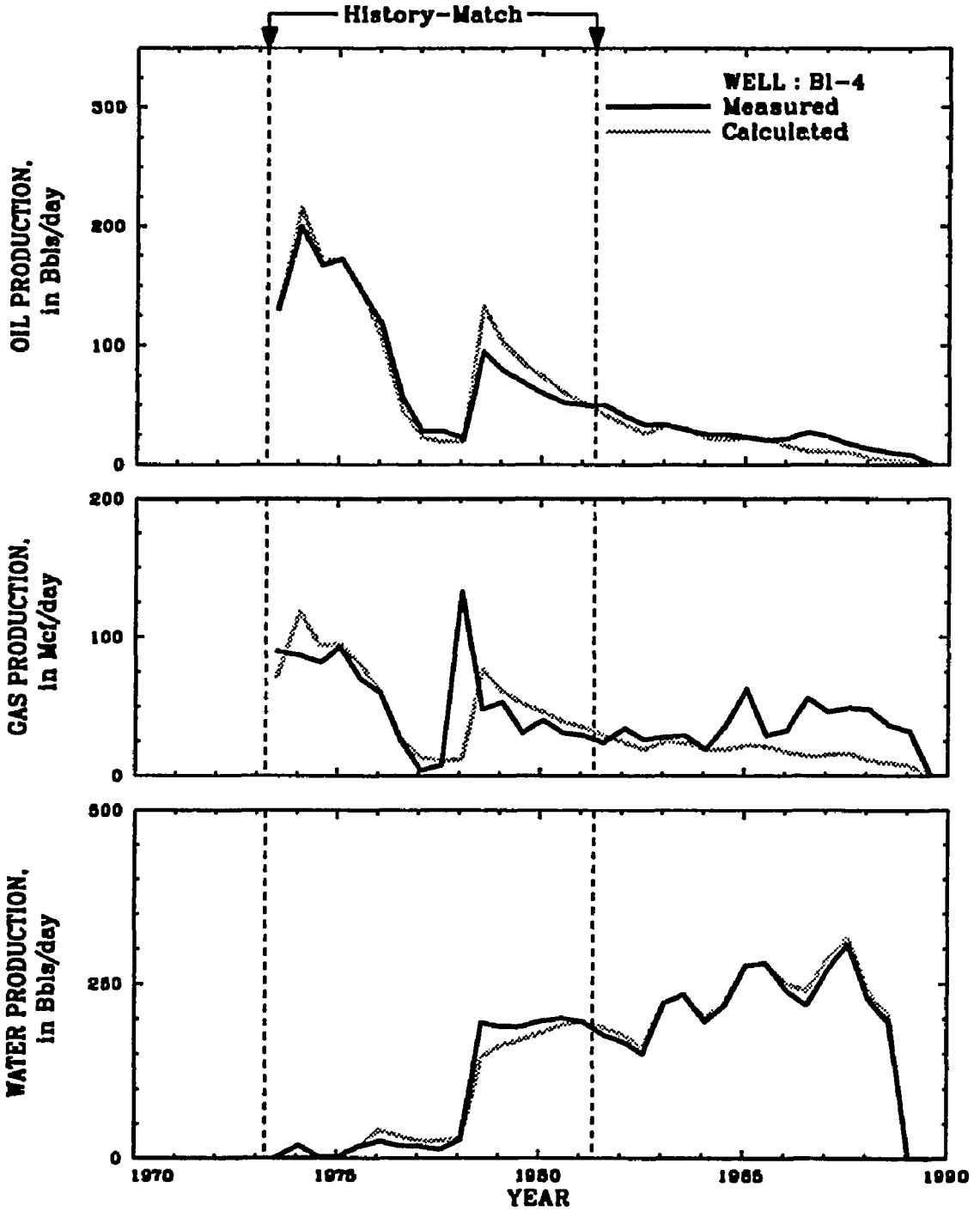

Figure 8.14--Production from well Bl-4 in the Sparta "B".

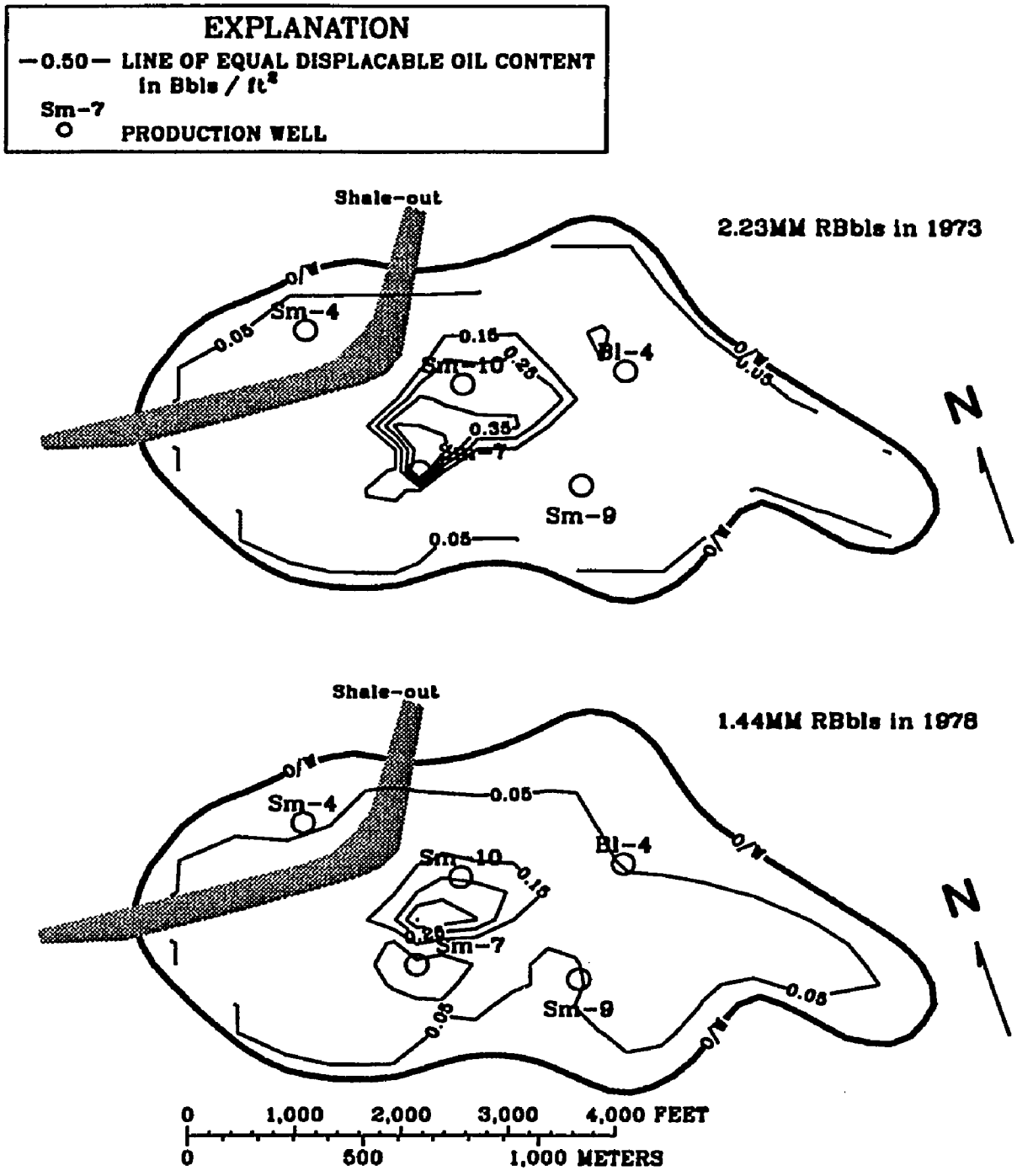

Figure 8.15--Displaceable oil distribution in the Sparta "B" in 1973 and 1978.

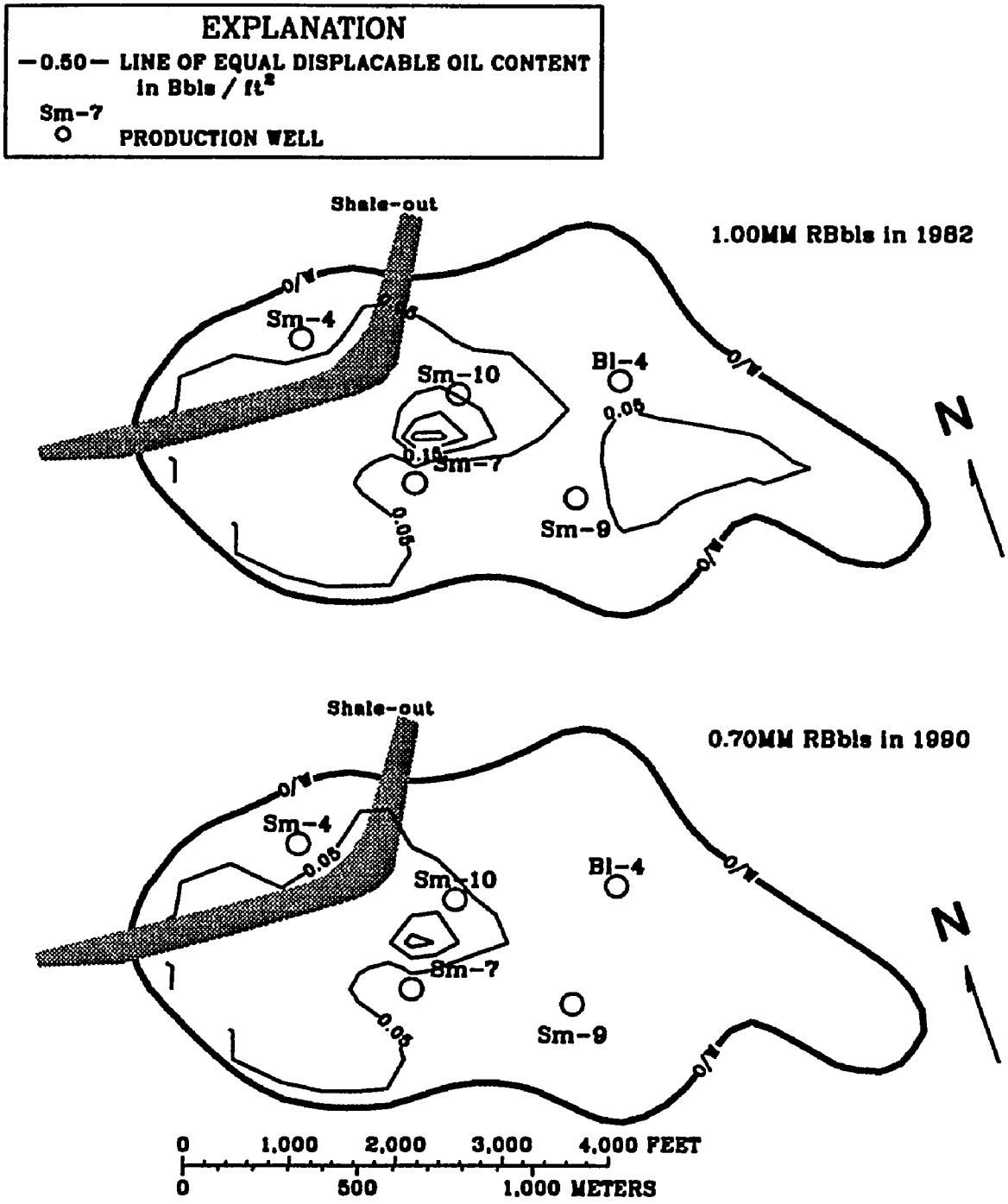

Figure 8.16--Displaceable oil distribution in the Sparta "B" in 1982 and 1990.

CHAPTER IX
CONCLUSIONS

Automatic history-matching is refined in this work by expanding the objective function and incorporating reservoir characteristics in the process of parameter selection. Adding more data types to the objective function made problems more unique. History-matching parameters based on reservoir characteristics constrained reservoir property estimates to believable values and distributions.

A sum-of-squares objective function is expanded to include permeability, porosity, saturation, and synthesized data in addition to pressure and production data. Permeability and porosity measurements provide direct feed-back that constrain nearby estimates of those properties. Additional data types are synthesized by approximating the temporal and spatial changes associated with the measured data types. Synthesized data allow an automatic history-matching program to mimic qualitative judgments made during trial-and-error history-matching.

The spatial variation of porosity, permeability, and aquifer influx characteristics are defined with weight matrices generated by iso-value contours. Iso-value contours allow inferred reservoir characteristics to be incorporated within history-matching parameters. Parameters defined in this manner are constrained to geologically plausible solutions.

Estimating log transformed values of reservoir properties is found to be suited to petroleum applications, particularly estimating

permeability distributions. Log transformed properties reduce scaling problems and prevent negative estimates of reservoir properties. A hyperbolic tangent function is used to define relative permeability curves because it provides a wide range of appropriate curves.

An automatic history matching algorithm, OPTIM, is coded with an expanded objective function and improved parameter formation tools. It is coupled with BOAST II, a 3-D oil and gas simulator. Parameter estimates are solved for iteratively using a Quasi-Newton method. Unless the Hessian update fails or there is no prior parameter change information, then a variant of the Levenberg-Marquardt method is used. The algorithm iterates until error reduction or net parameter change is less than a user defined minimum.

A hypothetical case representing a reservoir of known geometry and properties is used to demonstrate the effectiveness of the proposed history-matching approach. OPTIM is initially tested by history-matching a hypothetical reservoir with four parameters that could duplicate the true reservoir description. OPTIM reduced the root-mean-square error from 98 to 0.99 Bbls/d in 13 iterations. It also reduced the difference between parameter multipliers and their true values to less than a percent.

The same hypothetical reservoir was history matched but with a horizontal permeability distribution defined by an iso-value line. OPTIM reduced the root-mean-square error from 112 to 9.3 Bbls/d in 9 iterations. The error is not a reflection of the inability of the search algorithm, but of the imperfect approximation of the horizontal permeability distribution.

The Sparta "B" reservoir is history matched to test OPTIM on a field case that is representative of south Louisiana reservoirs. Oil, gas, and water production, and flowing pressure measurement are used in the objective function. The first eight years of production, 1973-1981 are used in the automatic history match. The data available for the 1982-1990 period is used to test the predictive ability of the history-matched model. Aquifer contact, horizontal permeability, vertical permeability, and oil and water relative-permeability curves are modified to history match the model. The history-matched model's permeability distribution qualitatively agreed with the reservoir's geologic characteristics. Overall, the calculated cumulative oil production is only 5% greater than the measured cumulative oil production.

Case histories of both hypothetical and real reservoirs demonstrated the effectiveness of OPTIM, an algorithm, incorporating reservoir characteristics in automatic history-matching.

REFERENCES

Begg, S.H. and Carter, R.R.: "Assigning Effective Values to Simulator Grid-Block Parameters in Heterogeneous Reservoirs," Paper SPE 16754 presented at the 62nd Annual Technical Conference, Dallas, TX, September 27-30, 1987.

Carrera, Jesus and Neuman, S.P.: "Estimation of aquifer parameters under transient and steady-state conditions: 3. Applications to synthetic and field data," Water Resources Research, v. 22, no. 2, pp. 228-242, February 1986.

Carrera, Jesus and Neuman, S.P.: "Estimation of aquifer parameters under transient and steady-state conditions: 1. Maximum likelihood method incorporating prior information," Water Resources Research, v. 22, no. 2, pp. 199-210, February 1986.

Carrera, Jesus and Neuman, S.P.: "Estimation of aquifer parameters under transient and steady-state conditions: 2. Uniqueness, stability, and solution algorithms," Water Resources Research, v. 22, no. 2, pp. 211-227, February 1986.

Chavent, G., Dupuy, M., and Lemonnier, P.: "History Matching by Use of Optimal Theory," Society of Petroleum Engineers Journal (February, 1975) 74-86.

Chen, W.H., Gavalas, G.R., Seinfeld, J.H., and Wasserman, M.L.: "A New Algorithm for Automatic History Matching," Society of Petroleum Engineers Journal (December, 1974) 593-608.

Coats, K.H., Dempsey, J.R., and Henderson, J.H.: "A New Technique for Determining Reservoir Description from Field Performance Data," Society of Petroleum Engineers Journal (March, 1970) pp. 66-74.

Combariza R., G.A: By-Passed Oil Due to Misinterpretation of Well Logs, M.S. Thesis, LSU, 1990.

Cooley, R.L.: "A method of estimating parameters and assessing reliability for models of steady state groundwater flow, 1, Theory and numerical properties," Water Resources Research, v. 13, no. 2, pp. 318-324, 1977.

Cooley, R.L.: "Incorporation of prior information into nonlinear regression groundwater flow models, 1, Theory," Water Resources Research, v. 18, no. 4, pp. 965-976, August 1982.

Cooley, R.L.: "Incorporation of prior information into nonlinear regression groundwater flow models, 2, Applications," Water Resources Research, v. 18, no. 4, pp. 662-676, June 1983.

Dietrich, J.K. and Bondor, P.L.: "Three-Phase Oil Relative Permeability Models," Paper SPE 6044 presented at the 51st Annual Fall Technical Conference, New Orleans, LA, October 3-6, 1976.

Durbin, T.J.: "Application of Gauss algorithm and Monte Carlo simulation to the identification of aquifer parameters," U.S. Geological Survey Open-File Report 81-688, 28 pp., 1983.

Farouq Ali, S.M. and Berkowitz, B.S.: "Limiting Aspects of Automatic History Matching," Paper Petroleum Society of CIM 88-39-03, presented at the 39th Annual Technical Meeting, Calgary, Canada, June 12-16, 1988.

Fletcher, R.: "A New Approach to Variable Metric Algorithms," Computer Journal (1970) 13, pp. 317-22.

Fanchi, J.R., Kennedy, J.E., and Dauben, D.L.: BOAST II: A Three-Dimensional, Three-Phase Black Oil Applied Simulation Tool, U.S. Department of Energy Report DOE/BC/-88/2/SP, December 1987.

Freyberg, D.L.: "An Exercise in Ground-water Model Calibration and Prediction," Ground Water, v. 26, no. 3, pp. 350-360, 1988.

Gavalas, G.R., Shah, P.C., and Seinfeld, J.H.: "Reservoir History Matching by Bayesian estimation," Society of Petroleum Engineers Journal, v. 16, no. 6, pp 337-350, 1976.

Gill, P.E., Murray W., and Wright, M.H.: Practical Optimization, Academic Press, San Diego, CA, 1981, 401 pp.

Goldfarb, D.: "A Family of Variable-Metric Methods Derived by Variational Means," Mathematics of Computation (1970) 24, 23-26.

Gomez-Hernandez, J.J. and Gorelik, S.M.: "Effective groundwater model parameter values: influence of spatial variability of hydraulic conductivity, leakance, and recharge," Water Resources Research, v. 25, no. 3, pp. 405-419, March 1989.

Hill, M.C.: "Analysis of accuracy of approximate, simultaneous, nonlinear confidence intervals on hydraulic heads in analytical and numerical test cases," Water Resources Research, v. 25, no. 2, pp. 177-190, February 1989.

Hoeksema, R. J. and Kitanidis, P. K.: "An application of the geostatistical approach to the inverse problem in two-dimensional groundwater modeling," Water Resources Research v. 20 no. 7, 1984 1003-1020p.

Jacquard, P., and C. Jain: "Permeability distribution from field pressure data," Society of Petroleum Engineers Journal. v. 5, pp. 281-294, 1965.

Jahns, H.O.: "A rapid method for obtaining a two-dimensional reservoir description from well response data," Society of Petroleum Engineers Journal. v. 6, no. 4, pp. 315-327., 1966.

Kirk, D.E.: Optimal Control Theory--An Introduction, Prentice-Hall, Inc., Englewood Cliffs, NJ, 1970, 452 pp.

Kitanidis, P. K.: "Parametric Estimation of Covariances of Regionalized Variables," Water Resources Bulletin v. 23 no. 4, 1987 557-567p.

Kuiper, L.K.: "A Comparison of Several Methods for the Solution of the Inverse Problem in Two-Dimensional Steady State Groundwater Flow Modeling," Water Resources Research, v. 22, no. 5, pp. 705-714, May 1986.

Kuniansky, E.L.:"Geohydrology and simulation of ground-water flow in the "400-foot," "600-foot," and adjacent aquifers, Baton Rouge area, Louisiana," Louisiana Department of Transportation and Development, Water Resources Technical Report No. 50., 1989

Lu, A.H., Schittroth, F., and Yeh, W.W.-G.: "Sequential estimation of aquifer parameters," Water Resources Research, v. 24, no. 5, pp. 670-682, May 1988.

Marquardt, D.W.:"An algorithm for least-squares estimation of nonlinear parameters," Journal of the Society for Industrial Applied Mathematics. v. 11, no. 2, pp. 431-441., 1963.

Martin, Angel, Jr., and Whiteman, C.D., Jr.:"Map showing generalized potentiometric surface of the Evangeline and equivalent aquifers in Louisiana, 1980," U.S. Geological Survey Water-Resources Investigations Report 84-4359, map (1 sheet), 1985.

Martin, Angel, Jr., and Whiteman, C.D., Jr.:"Geohydrology and regional ground-water flow of the coastal lowlands aquifer system in parts of Louisiana, Mississippi, Alabama, and Florida--a preliminary analysis," U.S. Geological Survey Water-Resources Investigations Report 88-4100, pp. 88, 1989

McDonald, M.G. and Harbaugh, A.W.: A modular three-dimensional finite-difference ground-water flow model, U.S. Geological Survey Techniques of Water-Resources Investigations, book 6, chap. A1, 576 pp., 1988.

Meyer, P.D., Valocchi, A.J., Ashby, S.F., and Saylor, P.E.: "A numerical investigation of the conjugate gradient method as applied to three-dimensional groundwater flow problems in randomly heterogeneous porous media," Water Resources Research, v. 25, no. 6, pp. 1440-1446, June 1989.

Neuman, S.P.: "A statistical approach to the inverse problem of aquifer hydrology, 3, Improved solution method and added perspective," Water Resources Research, v. 16, no. 2, pp. 331-346, April 1980.

Nghiem, L.X.: "A New Approach to Quasi-Newton Methods with Application to Compositional Modeling," Paper SPE 12242 presented at the Reservoir Simulation Symposium, San Francisco, CA, November 15-18, 1983.

Peaceman, D.W.: "Interpretation of Well-Block Pressures in Numerical Reservoir Simulation with Nonsquare Grid Blocks and Anisotropic Permeability," Society of Petroleum Engineers Journal (June, 1983) pp. 531-543.

Sage, Andrew P.: Optimum Systems Control, Prentice-Hall, Inc., Englewood Cliffs, NJ, 1968, 562 pp.

Selly, R.C.: An Introduction to Sedimentology, Academic Press, New York, NY, 408 pp., 1976.

Shah, P.C., Gavalas, G.R., and Seinfeld, J.H.: "Error Analysis in History Matching: The Optimum Level of Parameterization," Society of Petroleum Engineers Journal (June, 1978) 219-228.

Shanno, D.F.:"Conditioning of Quasi-Newton Methods for Function Minimization," Mathematics of Computation (1970) 24, 647-56.

Stone, H.L.: "Probability Model for Estimating Three-Phase Relative Permeability," Journal of Petroleum Technology, pp. 214-218, February 1970.

Thomas, L.K., Hellums, L.J., and Reheis, G.M.: "A Nonlinear Automatic History Matching Technique for Reservoir Simulation Models," Paper SPE 3475 presented at the 46th Annual Fall Meeting, New Orleans, LA, October 3-6, 1971.

Torak, L.J., and Whiteman, C.D., Jr.: "Applications of digital modeling for evaluating the ground-water resources of the "2,000-foot" aquifer of the Baton Rouge area, Louisiana," Louisiana Department of Transportation and Development, Office of Public Works Water Resources Technical Report No. 27, 87 p., 1982

Townley, L.R. and Wilson, J.L.: "Computationally efficient algorithms for parameter estimation and uncertainty propogation in numerical models of groundwater flow," Water Resources Research, v. 21, no. 12, pp. 1851-1860, December 1985.

Veatch, Jr., R.W. and Thomas, L.K.: "A Direct Approach for History Matching," Paper SPE 3515 presented at the 46th Annual Fall Meeting, New Orleans, LA, October 3-6, 1971.

Vecchia, A.V. and Cooley, R.L.: "Simultaneous confidence and prediction intervals for nonlinear regression models with application to a groundwater flow model," Water Resources Research, v. 23, no. 7, pp. 1237-1250, July 1987.

Wasserman, M.L., Emanuel, A.S., and Seinfeld, J.H.: "Practical Applications of Optimal-Control Theory to History-Matching Multiphase Simulator

Models," Society of Petroleum Engineers Journal (August, 1975) 347-355.

Watson, A.T. and Lee, W.J.: "A New Algorithm for Automatic History Matching Production Data," Paper SPE 15228 presented at the Unconventional Gas Technology Symposium, Louisville, KY, May 18-21, 1986.

Watson, A.T., Seinfeld, J.H., Gavalas, G.R., and Woo, P.T.: "History Matching in Two-Phase Petroleum Reservoirs," Society of Petroleum Engineers Journal (December, 1980) 521-532.

Wilson, J.L. and Metcalfe: "Illustration and verification of adjoint sensitivity theory for steady state groundwater flow," Water Resources Research, v. 21, no. 11, pp. 1602-1610, November 1985.

Yang, P.H., Armasu, R.V., and Watson A.T.: "Automatic History Matching with Variable-Metric Methods," Paper SPE 16977 presented at the 62nd Annual Technical Conference and Exposition, Dallas, TX September 27-30, 1987.

Yeh, W.W.-G. and Yoon, Y.S.: "Aquifer parameter identification with optimum dimension in parameterization," Water Resources Research, v. 17, no. 3, pp. 664-672, June 1981.

Yeh, W.W.-G. and Wang, Chuching: "Identification of Aquifer Dispersivities, Methods of Analysis and Parameter Uncertainty, Water Resources Bulletin (Urbana) v. 23 no. 4, 1987 569-580p.

Yeh, W.W.-G.: "Review of parameter identification procedures in groundwater hydrology," Water Resources Research, v. 22, no. 2, pp. 95-108, February 1986.

Yufeng, Qi and Xin, Zhang: "Parameter Estimation in a Naturally Fractured Reservoir by the Method of Cybernetics," Paper SPE 14864 presented at the International Meeting on Petroleum Engineering, Bejing, China, March 17-20, 1986.

APPENDIX A

SIMULATION OF THE "1,200-FOOT" AQUIFER

The "1,200-foot" aquifer and adjacent aquifers are comprised of a complex series of lenticular beds of sand and clay. Because the "1,200-foot" aquifer is hydraulically connected to the adjacent aquifers, a three-dimensional model is needed to quantitatively analyze the ground-water flow in the "1,200-foot" aquifer. MODFLOW (McDonald and Harbaugh, 1988) was used to simulate flow in the "1,200-foot" aquifer.

A.1 Model Grid

A 31 row by 29 column grid that covers 6,100 mi^2 (Fig. A.1) was used. The grid was oriented parallel to the Baton Rouge fault. Four layers were used to simulate the "1,200-foot" aquifer and adjacent aquifers (Fig. A.2). Layer 1 is a specified-head upper boundary representing a composite of water levels in the "400-foot" and "600-foot" aquifers and the water table altitudes in the unconfined, surficial deposits of Pleistocene age in the Southern Hills outcrop area. Layers 2, 3, and 4 represent the "800-foot" and "1,000-foot" aquifers, the "1,200-foot" aquifer, and the "1,500-foot" and "1,700-foot" aquifers, respectively (Fig. A.2).

The upper boundary, layer 1, acts as a source or sink for water entering or leaving the flow system, except for flow across the lower boundary and water removed by pumpage (Fig. A.3). Use of a specified-head upper boundary is acceptable because there has been no significant decline in the water levels in the unconfined, surficial deposits of

Pleistocene age in the Southern Hills outcrop area as a result of pumping through 1987. Streams draining the recharge areas have high base flows, indicating that recharge is being rejected by the unconfined, surficial deposits of Pleistocene age in the Southern Hills outcrop area (Kuniansky, 1989).

A.2 Model Boundaries

The lower model boundary is a set of specified-flow rates that approximate flow between the combined "1,500-foot" and "1,700-foot" aquifers (layer 4) and the "2,000-foot" aquifer (fig. A.2). These flow rates were varied from 1946 to 1988 and were held constant at 1988 rates from 1988 onward for all simulations. Torak and Whiteman (1982) showed there are appreciable flow rates between these two aquifers since the development of the "2,000-foot" aquifer. For this model, the flow rates between layer 4 and the "2,000-foot" aquifer were assumed to be negligible prior to pumping. The Gulf Coast Regional Aquifer-System Analysis (GCRASA) provided the most recent information for the specified fluxes between layer 4 and the "2,000-foot" aquifer (Martin and Whiteman, 1989).

All of the lateral model boundaries are impermeable. The northern edge of the model is impermeable to simulate the pinchout of the "1,500-foot" and "1,700-foot" aquifers. Layers 2 and 3 extend to the northern boundary although the aquifers modeled pinch out before the northern edge of model. This is only to provide continuity between layer 1, the upper specified-head boundary, and lower layers that model aquifers still present. The southern boundary in all layers of the model is treated as impermeable, because the aquifers modeled have a dissolved-solids concentration of 10,000 mg/L or

greater. This water is considered immobile relative to the time scale of the model and not considered as part of the simulated flow system. The eastern boundary parallels a groundwater divide present in all layers that is shown by Martin and Whiteman (1985). This constitutes an impermeable boundary because water will flow parallel to but not across the boundary. The western boundary lies along the present Atchafalaya River basin, which lies above an ancestral path of the Mississippi River, and serves as an impermeable boundary because the basin is a regional drain for all the aquifers (Martin and Whiteman, 1985).

A.3 Period Investigated

The "1,200-foot" aquifer was simulated from 1946 to 1988 to incorporate the major development that began in 1953. Prior to 1953, the "1,200-foot" aquifer was a minor water supply, providing less than 1.5 million gallons per day within the modeled area. In 1985 the pumping rates were 18 million gallons per day. Stress periods were selected so that the assumption of constant pumping rates within a period was valid. The pumpage from 1946 to 1988 was divided into nine stress periods: 1946-52, 1953-57, 1958-62, 1963-67, 1968-69, 1970-75, 1976-79, 1980-83, and 1984-88. Pumpage data for 1985 were used for the last stress period, 1984-88. The pumping rates per stress period in "1,200-foot" and adjacent aquifers are shown in Figure A.4.

A.4 History Match and Sensitivity Analysis

The model was history-matched by adjusting values for transmissivity, vertical leakance, and storage coefficient to minimize differences between

calculated and measured water levels. The history-matched model root-mean-square error was 12.15 ft overall and 11.18 ft for all stress periods in layer 3, the "1,200-foot" aquifer. The greater number of water-level measurements available in 1988 biased model calibration towards the last stress period (1984-88). The comparisons for the optimization program were averages of the hydrograph records during the last year in a stress period. Record periods of most of the hydrographs used were for only a part of the total simulation period. Simulated water levels compared favorably to hydrograph records with most showing better agreement from 1975 to 1985 (Figs. A.5-6).

The model was most sensitive to changes in transmissivity (Fig. A.7) throughout the range examined because the Baton Rouge fault was modeled as a low transmissivity zone and large stresses are imposed at nearby pumping centers in Baton Rouge. The decreasing model sensitivity, as transmissivity values were increased to 10 times or greater than the calibrated values, was due to the lack of resistance to flow in the fault and near pumping centers (Fig. A.7).

The model was more sensitive to vertical leakance decreases than increases (Fig. A.7) since large decreases cut-off the model's water supply (layer 1). This asymmetrical model sensitivity to vertical leakance changes exists for transmissivity values other than the calibrated values (Fig. 3.1). Overall, the model was least sensitive to changes in storage coefficient (Fig. A.7) and showed a greater sensitivity to storage coefficient increases.

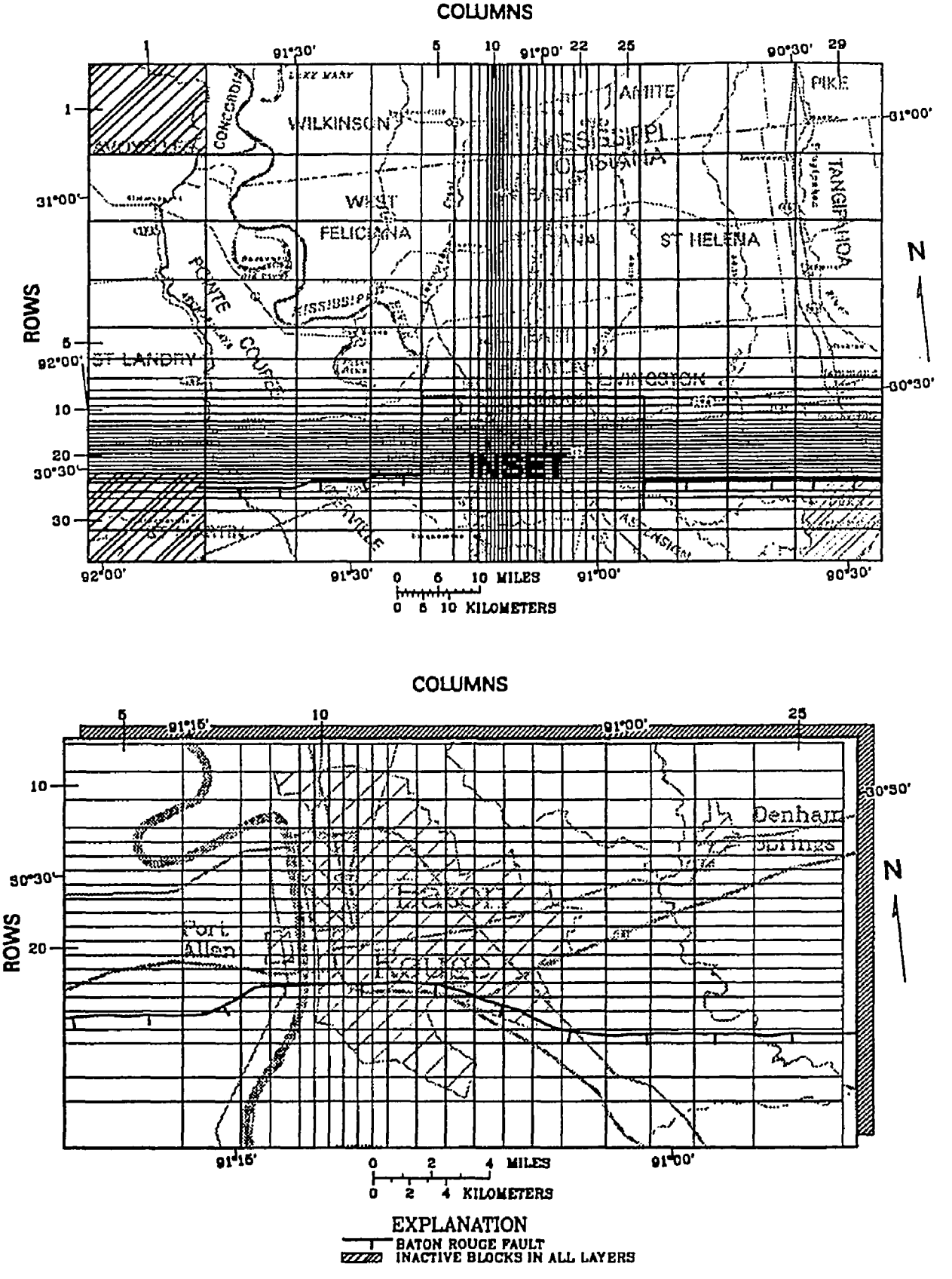

Figure A.1--Model grid and extent.

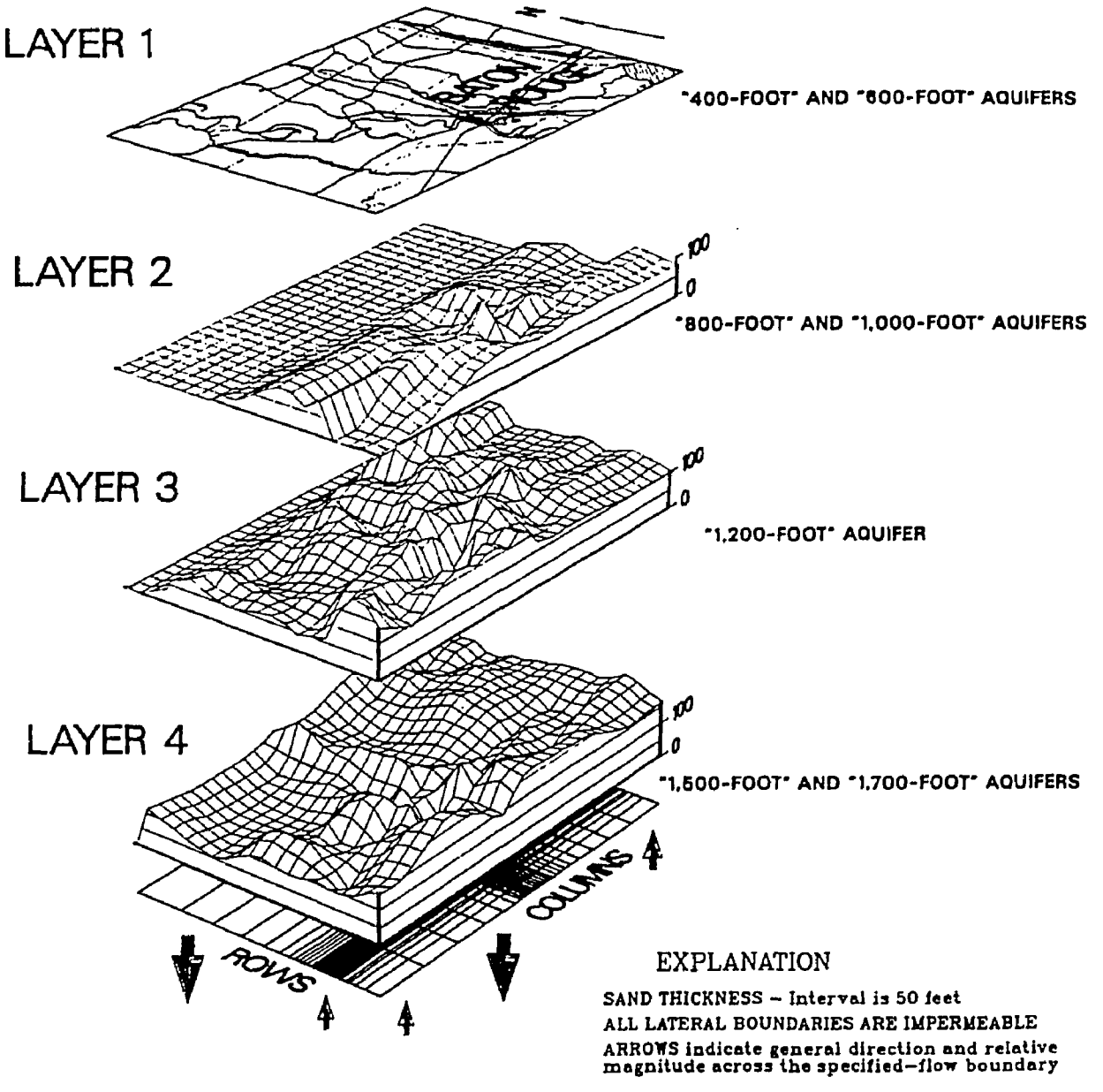

Figure A.2––Conceptual model for the "1,200–foot" aquifer and adjacent units.

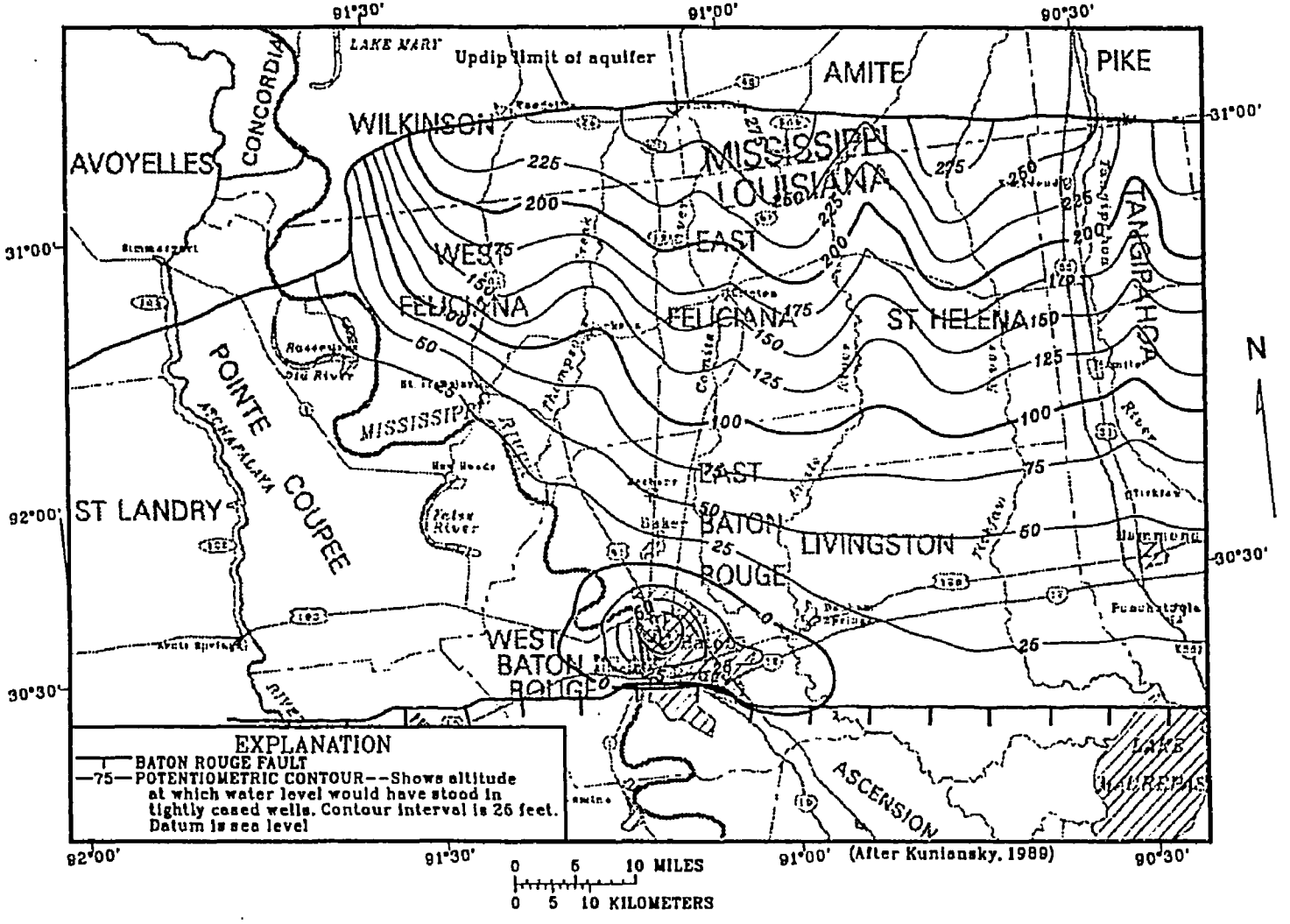

Figure A.3--Simulated potentiometric surface of the "400- and 600-foot" aquifers (layer 1) in 1984.

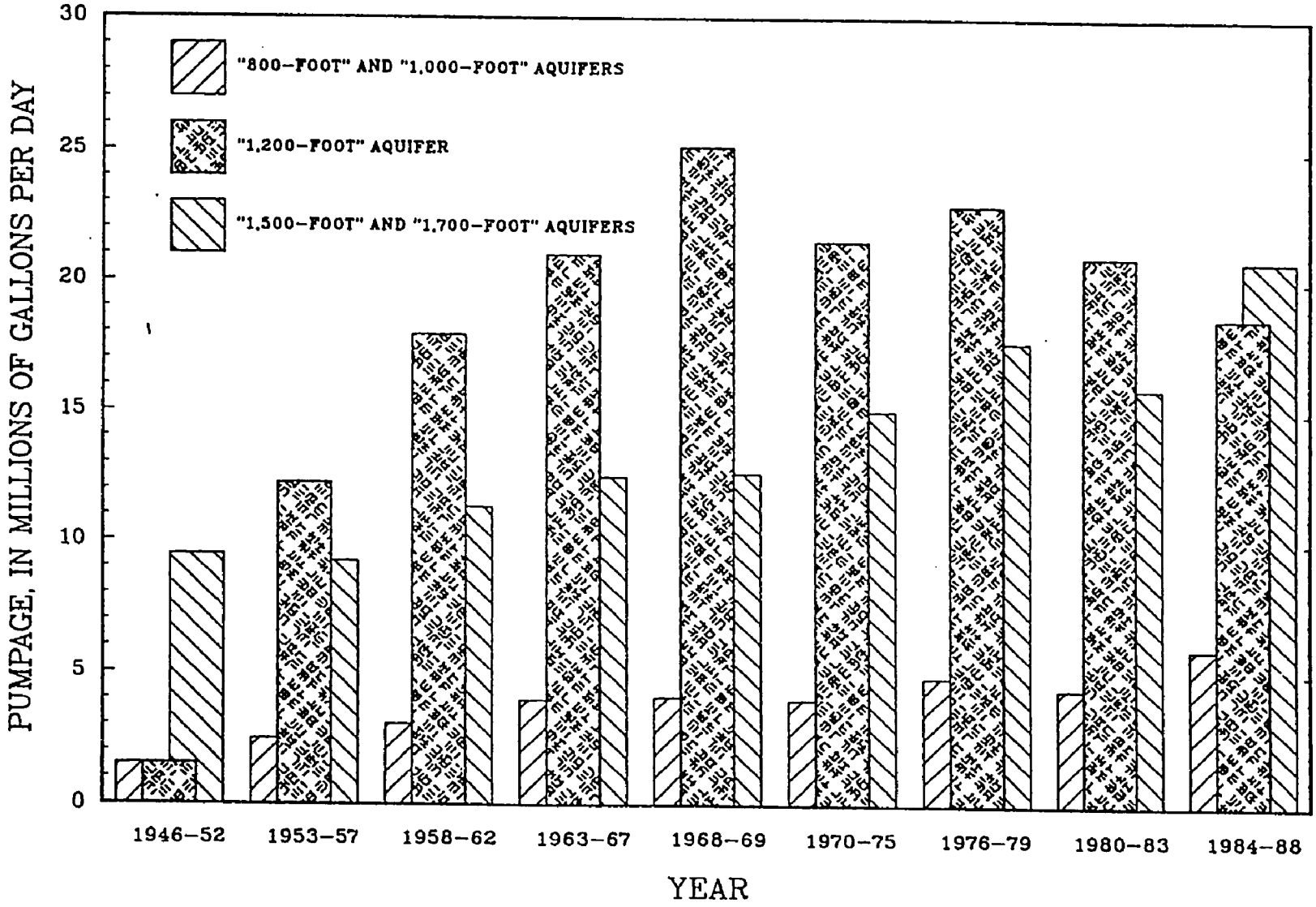

Figure A.4--Pumpage by aquifer from 1946 through 1988.

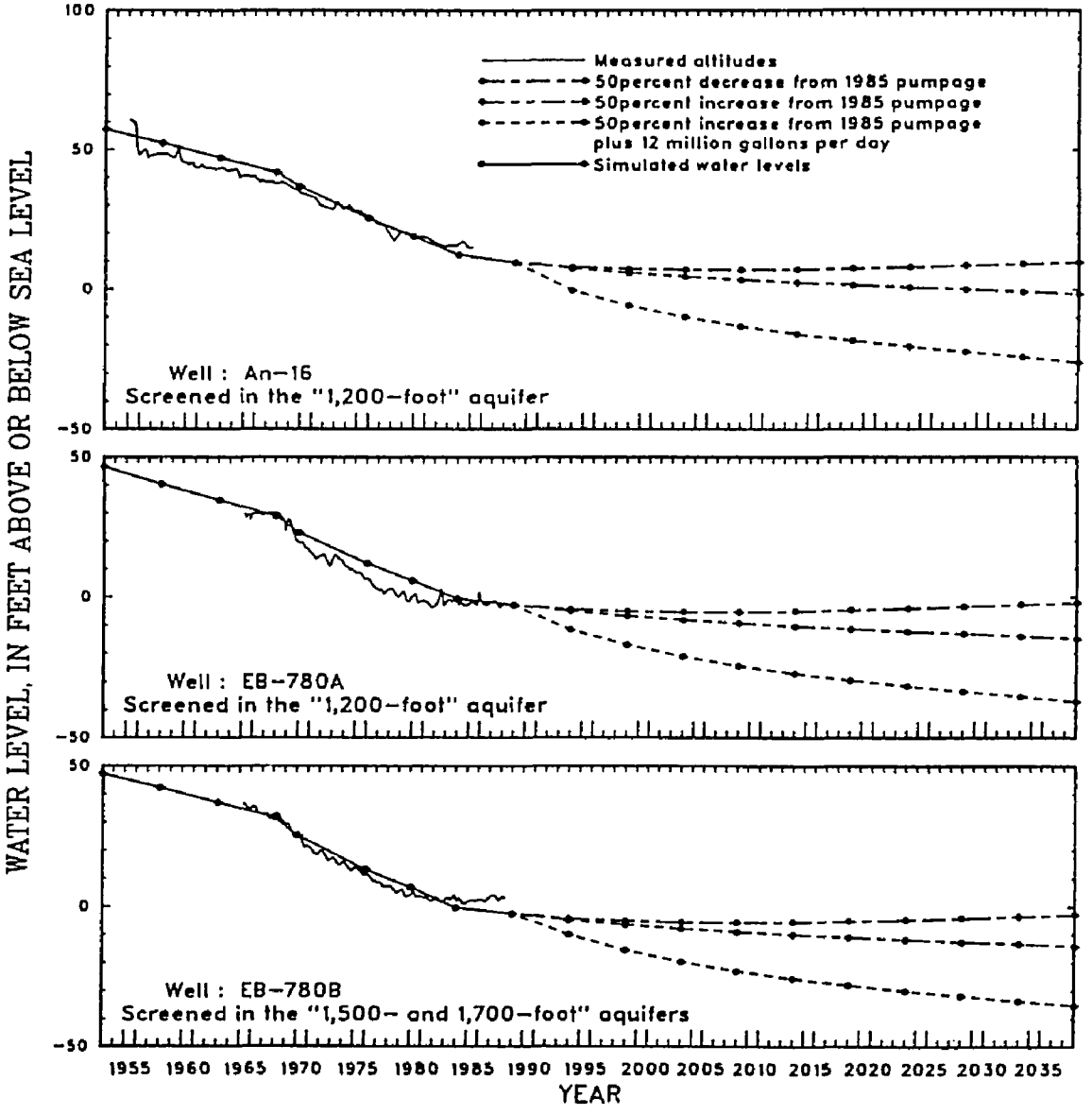

Figure A.5--Simulated and measured water levels for wells An-16, EB-780A, and EB-780B south of the Baton Rouge fault.

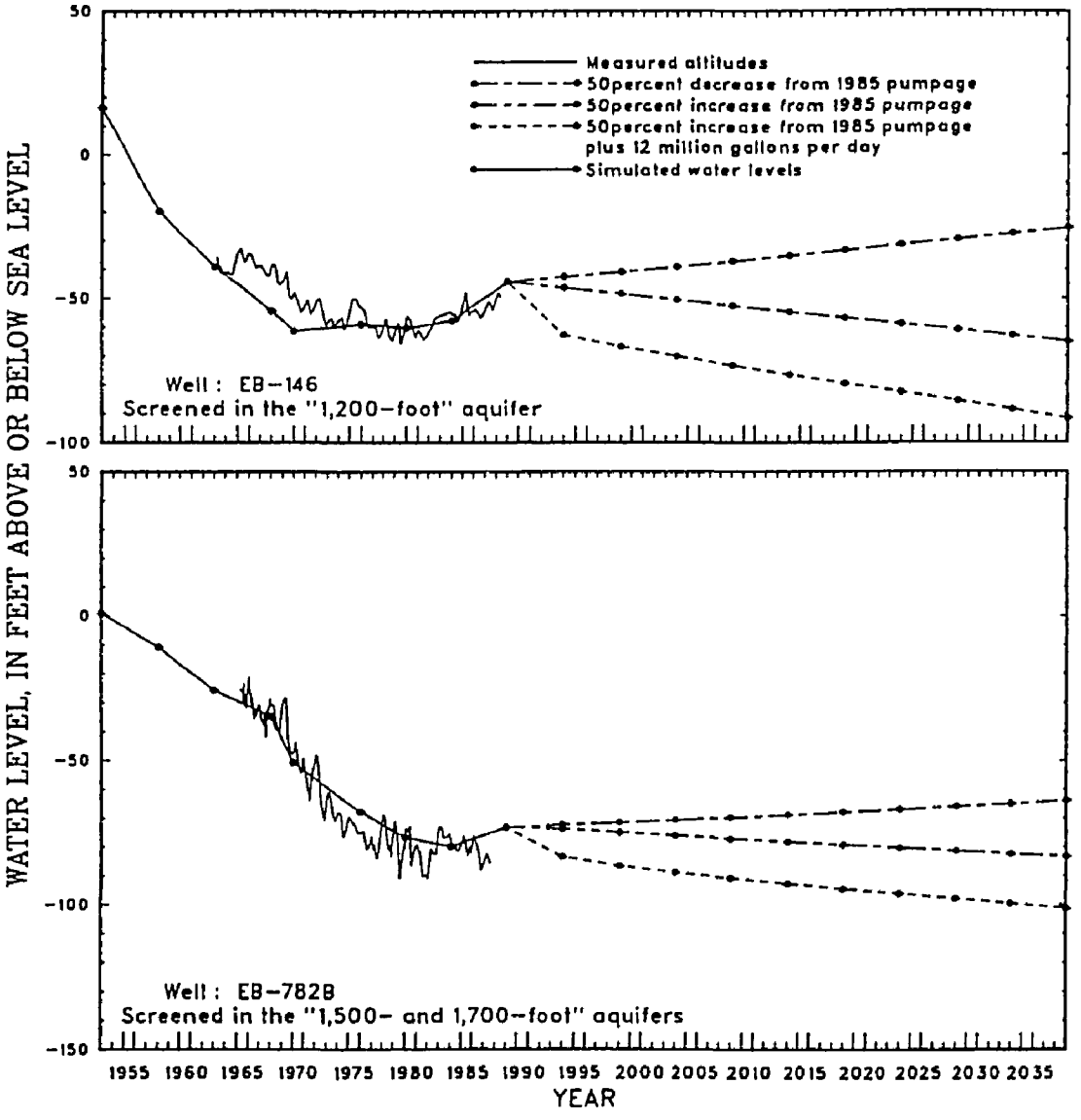

Figure A.6--Simulated and measured water levels for wells EB-146 and EB-782B in Baton Rouge.

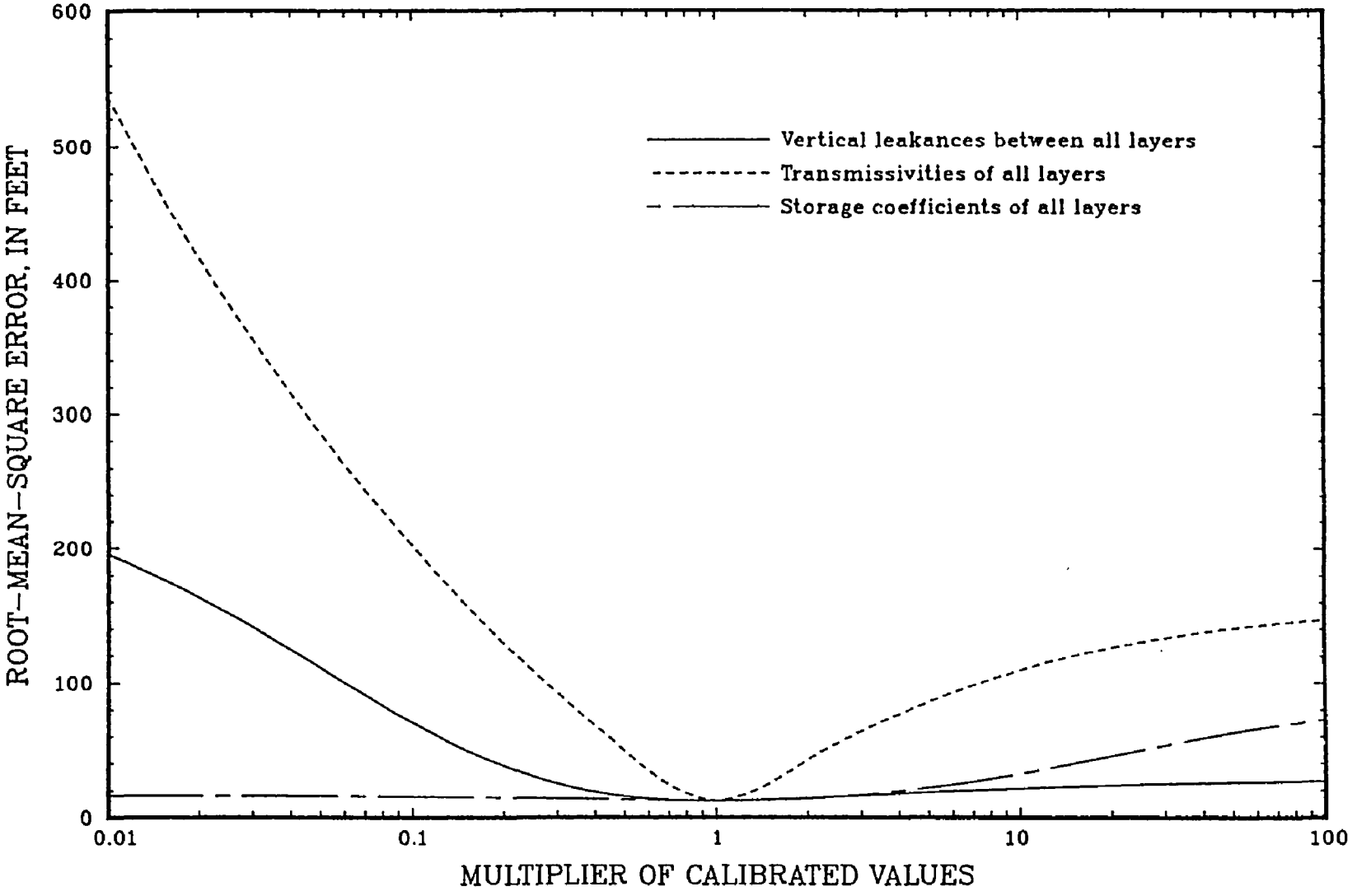

Figure A.7--Model sensitivity to changes in transmissivity, vertical leakance, and storage coefficient.

APPENDIX B
MODIFICATIONS TO BOAST II

B.1 BOAST as a Subroutine

BOAST II was divided into two parts, a main program that read the reservoir description and a subroutine that executed the simulation. This was done to avoid re-reading the reservoir description during the recurrent simulations needed during automatic history matching. An additional routine was added to reinitialize the starting pressures and saturations with each subsequent simulation.

B.2 SIP, Strongly Implicit Procedure, Matrix Solver Added

BOAST II's matrix solvers are inadequate. They are unstable when used over a wide range of property estimates and are very likely to fail. A more robust matrix solver, SIP (Strongly Implicit Procedure), was adapted from the USGS's MODFLOW groundwater model (McDonald and Harbaugh, 1988, ch. 12). As its name implies, SIP solves the matrix as a whole instead of in parts as is done in SSOR, Slice Successive Over Relaxation, algorithms.

B.3 Subroutines SOLONE and SOLTWO

SOLONE and SOLTWO subroutines update the conductances between nodes that change over time as a function of oil, gas, and water relative permeabilities, oil, gas, and water viscosities, and saturation change.

SOLTWO differs form SOLONE in how effective, internode, relative permeabilities, are treated.

Each model node has six flow faces associated with it. Using BOAST II nomenclature, the six flow faces are east, west, north, south, top, and bottom. The flow across each face is proportional to the internode conductance and potential difference between each node. The conductance of all external flow faces is zero.

The original SOLONE and SOLTWO subroutines formulated the internode conductance for all six flow faces at each node. The modified subroutines only calculate the internode conductance of a nodes eastern, northern, and bottom faces. The western, southern, and top conductances are taken from the appropriate eastern, northern, and bottom neighbors, respectively.

Internode conductance matrices are formed with only half the computational effort. For a given model and matrix solver, BOAST II using the modified SOLONE or SOLTWO subroutines executed in 75% of the time needed while using the original subroutines. In addition, the internode conductance between two nodes is identical for each node, as it should be. Discrepancies appeared in the fourth significant figure using the original SOLONE and SOLTWO subroutines. Although seemingly slight, these discrepancies contribute to model instability.

B.4 Subroutine QRATE

Total fluid voidage rate is handled as a special specified oil production rate in QRATE. Consequently, the well is shut-in automatically if it waters-out. For automatic history matching, a comparable production history is needed between simulations. QRATE was altered to handle total fluid voidage rates as a specified water rate well when the WOR exceeded one.

Large flow rate oscillations in a well can occur as it begins to water-out. This occurs when the cell oil and water saturations are close to the values that produce a mobility ratio of one. When the mobility ratio is less than one and favors oil production, the water saturation of the cell increases during that time step. In the next time step, the mobility ratio is greater than one, water production is favored, and the oil saturation of the cell increases. BOAST II tries to compensate by decreasing the size of time steps, but this makes simulations take much longer.

An average of the previous flow rates and the new flow rates are specified as an alternate solution. This damps out production rate oscillations without using prohibitively small time steps.

B.5 No Free Gas Option

For unsaturated reservoirs, an option was added to BOAST II to force the gas saturation to zero at all times. This enhances model stability and reduces computational effort if the reservoir pressure in an intermediate model falls below the bubble point.

APPENDIX C

HISTORY MATCH OF SPARTA "A" RESERVOIR -- FORDOCHE FIELD

C.1 The Sparta "A"

The Sparta "A" reservoir is formed by an anticline (Fig. C.1) and is composed of three laterally continuous sands separated by thin shales. The thickness of the upper, middle, and lower sands averaged 8, 10, and 9 ft, respectively. The isopach of each sand and the net pay are shown in Figures C.2 and C.3. The intermediate shales are absent near well Sm-7 (Figs. C.4 and C.5). Both shales thicken toward the northern shale-out and southern oil/water contact. The porosity distributions of each sand are shown in Figures C.6 and C.7.

Using the isopach and porosity maps, an initial oil/water contact at 11,350 ft subsea (Fig. C.5), and an irreducible water saturation of 0.44, the initial oil in place is 7.16 MMSTB. No free gas was initially in place and no gas came out of solution during production since the initial reservoir pressure was 8,200 psia and no flowing-well pressures dropped below the bubble point, 2,450 psia.

Horizontal permeability distributions were not estimated due to a lack of data. The vertical permeability, K_z, distribution is assumed to be inversely proportional to the intermediate shale thickness (McDonald and Harbaugh, 1988). The gross reservoir characteristics and fluid properties are summarized in Table C.1.

Table C.1--Summary of Sparta "A" reservoir, fluid properties, and aquifer characteristics.

Discovery well	N. Smith Jr. #7, Sm-7
Initial oil in place	7.16 MMSTB
Initial solution gas in place	4.4 BCF
Average net sand thickness	27 ft
Average permeability	370 md
Average porosity	0.24
Irreducible water saturation	0.44 Residual oil saturation 0.23
Reservoir temperature	226 ^{o}F
Initial reservoir pressure	8,200 psia
Bubble point pressure	2,450 psia
Initial oil/water contact	11,350 ft subsea
Formation compressibility	15 μsips

Fluid properties @ 8,200 psia and 226 ^{o}F

	Oil	Gas	Water
FVF	1.38	0.0035	1.03
Viscosity, cp	0.36	0.011	0.41
Gas in Solution SCF/BBl	610	---	18
Density, lb/ft^3	51.7	0.05	62.7

Radial aquifer characteristics*

t_D = 0.01 t, from:		Aquifer contact, B, =	ft^2,
Compressibility	8 μsips	from:	
Viscosity	0.40 cp	Oil/water interface**	ft^2
Permeability	80 md	Fraction connected	
Porosity	0.25		
Reservoir radius	12,000 ft		
re/rw	∞		

* Modified Van Everdingen and Hurst radial aquifer model where,

$$\text{Aquifer influx} = B \sum_{0}^{t} (p_{t_0} - p_t)\, Q(t_D)$$

** The oil/water interface is the vertical area open to flow along the oil/water contact.

C.2 Production History

Production started in May of 1968 with the Sm-6 which was completed in the upper and middle sand. The first year and a half of production was not used since production records did not begin until January 1970.
The cumulative production for each well draining the Sparta "A" from 1970 to 1990 is summarized in Table C.2. Production is simulated by specifying the total rate of all three phases, i.e. oil, gas, and water, in reservoir barrels, RBbls.

C.3 Automatic History Matching

The Sparta "A" is simulated as a three layer model (Fig. C.5) based on stratigraphy. A 29 column by 25 row grid is used to define the model laterally (Fig. C.1). Sm-7 is the reference well where node <15,16> is defined as x,y location <10,000, 10,000>. The northern boundary is assumed to be impermeable since it is a shale-out (Fig. C.1). The oil/water contact defines the model's southern boundary in all layers. This boundary is simulated as an infinite, radial aquifer characterized by the properties listed in table C.1. The initial aquifer contact, B, for each node was proportional to the area of the vertical, external block faces.

Aquifer contact, horizontal permeability, and oil and water relative-permeability curves are the four reservoir properties modified and estimated. The horizontal permeability, K_{xy}, is modified with a weight matrix as an exponential, scaled parameter, PINFO = WVES. The aquifer contact, B, is modified with a constant and the same weight matrix used to modify K_{xy}. It

is also treated as an exponential, scaled parameter, PINFO = BVES. Both the oil and water relative permeability curves are modified as constant, multiplicative, scaled parameters, PINFO = CVMS.

The history-matched model of the Sparta "A" had a root-mean-square error of 28 Bbls/d based on all production from 1970 to 1990. The history-matched permeability distribution increases from east to west (Fig. 8.7). The fitted relative permeability coefficients produced the curves shown in Figure 8.8.

Total production differences between the history-matched model and reality are shown in Figure C.9. The calculated and measured production from An-2, Sm-5, Sm-6, and Sm-7 is shown in Figures C.10-C.13. The difference between calculated and measured cumulative oil production is 10% in 1979 at the end of the history-match and 1% in 1990 at the end of production (Table C.3)

Most of the oil migration is from southeast to northwest (Figs. C.14-16). Most of the by-passed oil is located west of wells Sm-7 and An-2 (Fig. C.16).

Table C.2--Production from the Sparta "A" by well from January 1970 to September 1989.

Well	Date			Oil	Gas	Water	Sand
	Comp.	Start	Shut-In	MSTB	MMCF	MSTB	
Sm-5	6/68	1/70	9/89	997	861	2,742	Upper, Middle
Sm-6	5/68	1/70	12/74	217	113	175	Upper, Middle
Sm-7	5/69	1/70	9/89	848	520	812	Upper, Middle
An-2	11/68	1/70	5/89	870	500	1,079	Upper, Middle
TOTAL				2,932	1,994	4,807	

Table C.3--Cumulative calculated and measured production from the Sparta "A".

	Oil, MSTB		Gas, MMCF		Water, MSTB	
From 1970 to:	$\hat{\psi}$	ψ	$\hat{\psi}$	ψ	$\hat{\psi}$	ψ
1974	1,471	1,633	898	790	559	436
1978	2,083	2,348	1,274	1,180	1,329	1,034
1979	2,204	2,448	1,348	1,258	1,522	1,271
1982	2,479	2,653	1,517	1,475	2,174	2,069
1986	2,759	2,823	1,690	1,807	3,275	3,381
1990	2,972	2,932	1,823	1,994	4,453	4,807

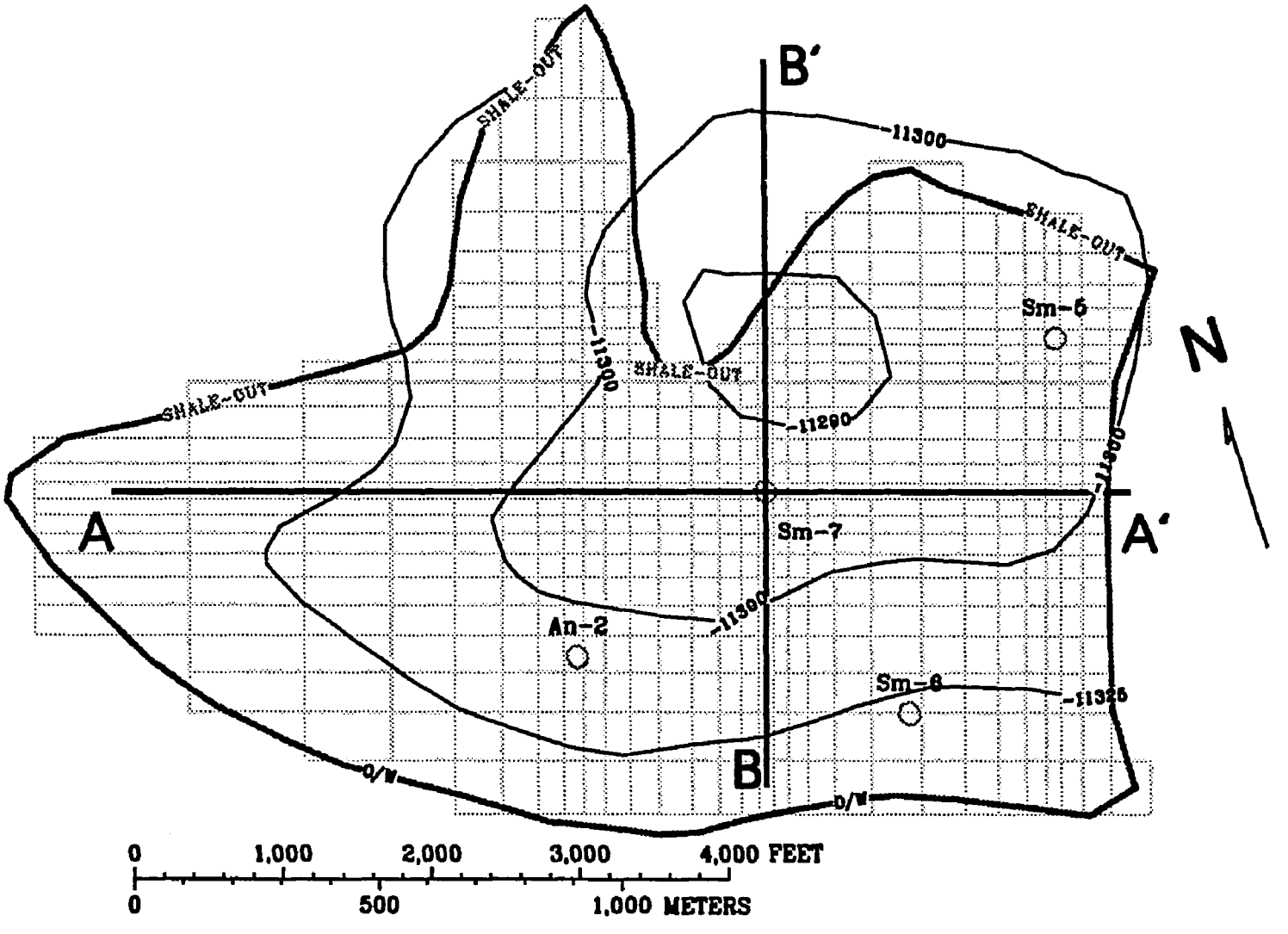

Figure C.1--Structure map and model grid for the Sparta "A".

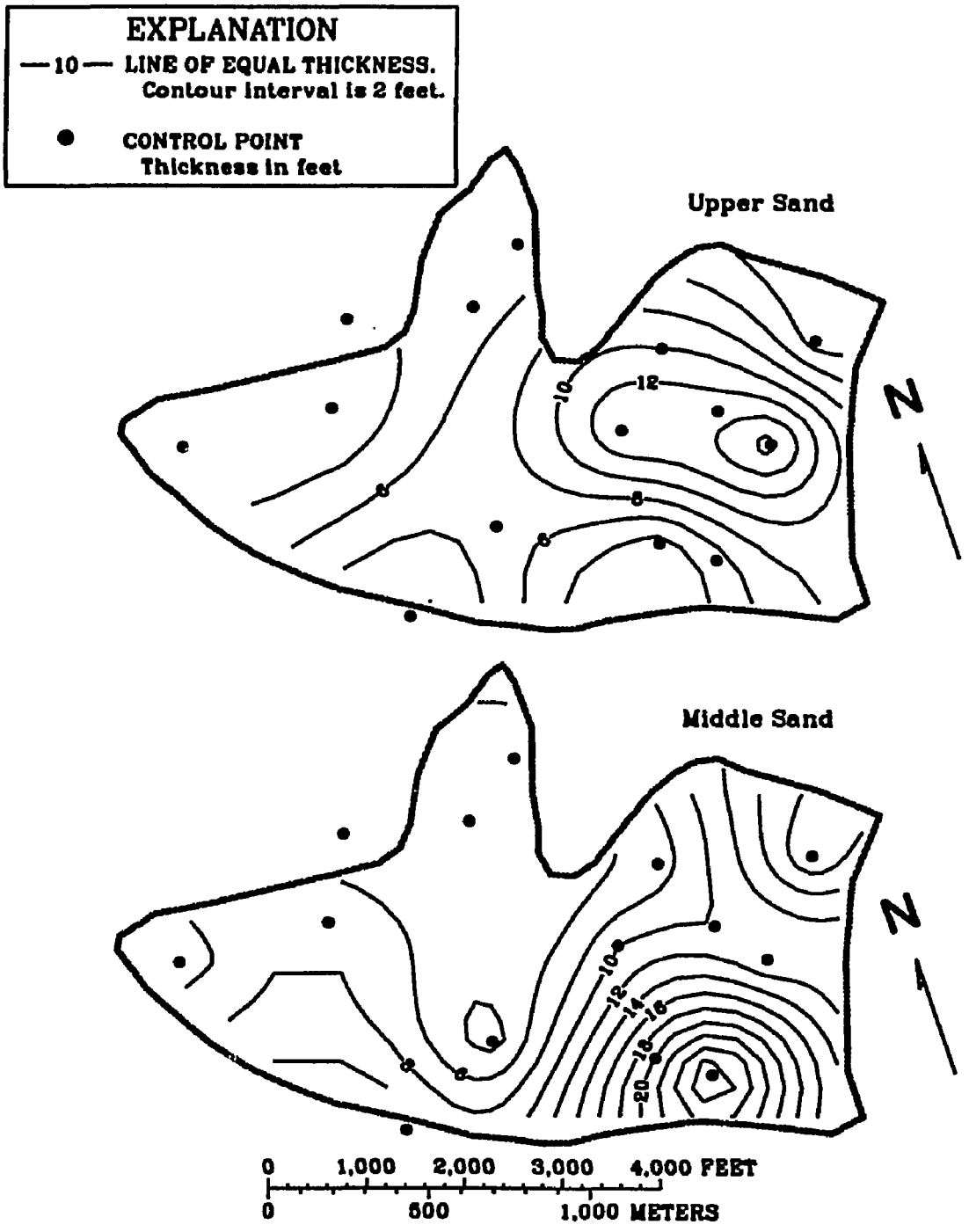

Figure C.2--Isopach maps of Sparta "A" upper sand and middle sand.

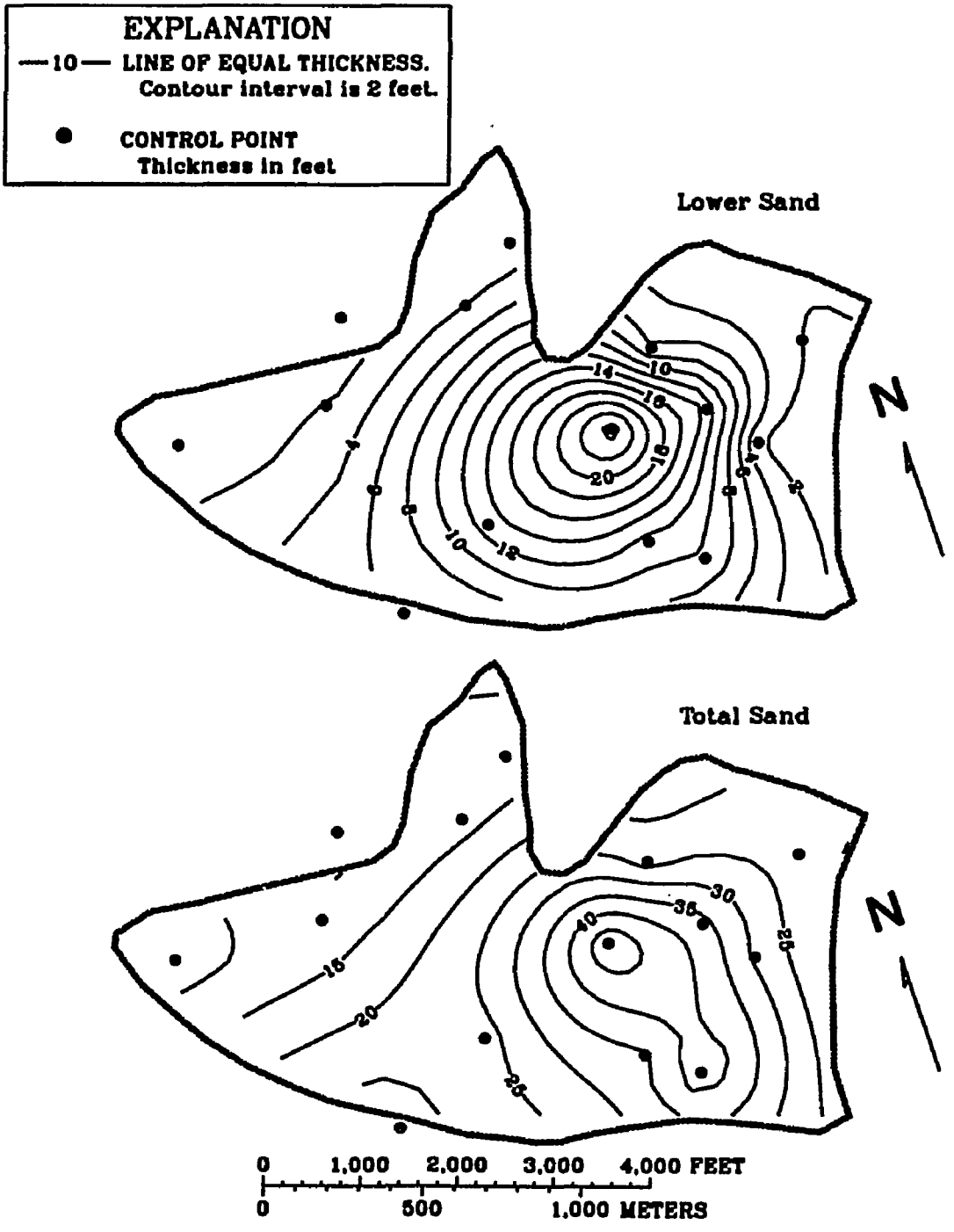

Figure C.3--Isopach maps of Sparta "A" lower sand and total sand.

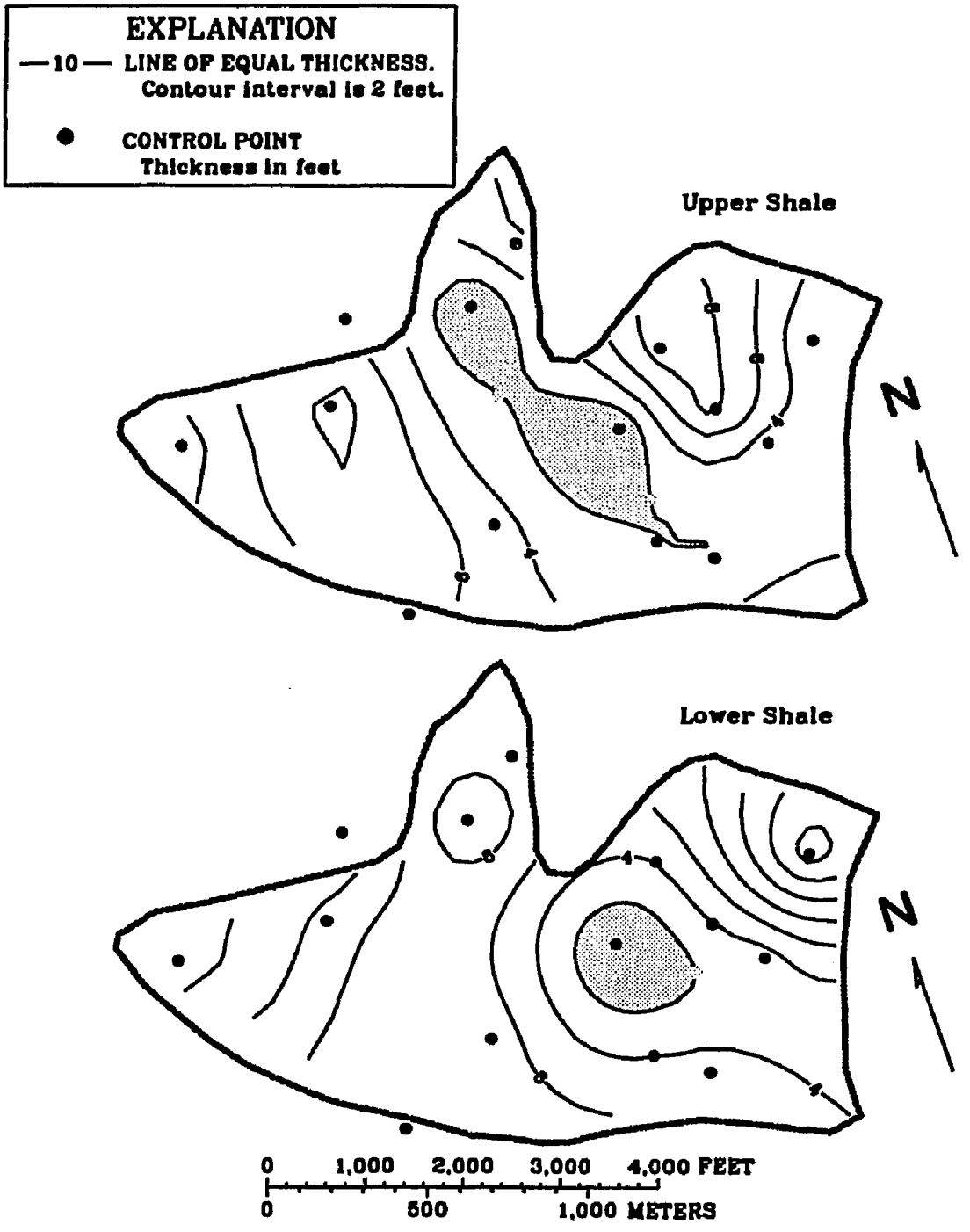

Figure C.4--Isopach maps of Sparta "A" upper shale and lower shale.

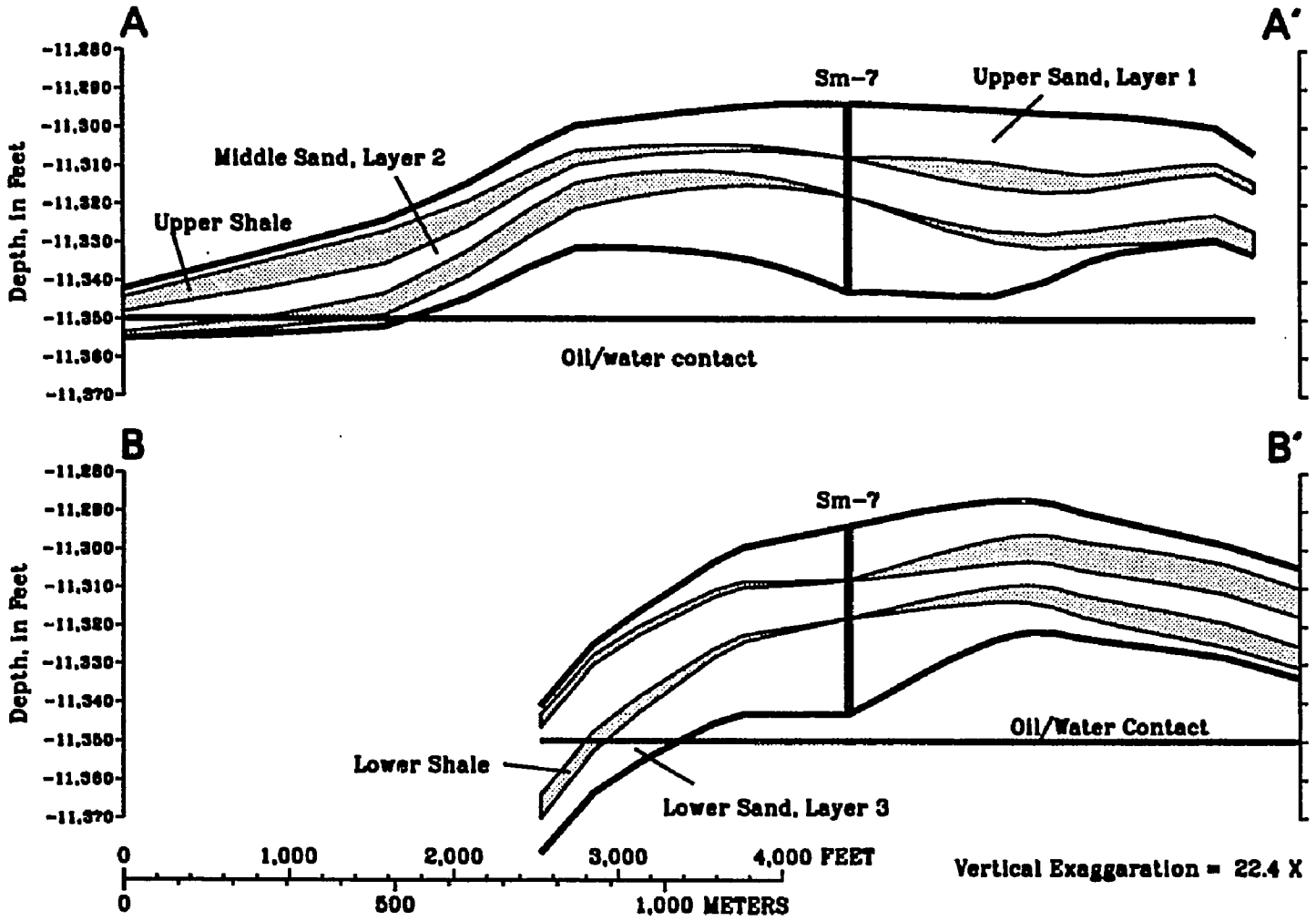

Figure C.5--Cross-sections A-A' and B-B' through the Sparta "A".
See figure C.1 for sections traces.

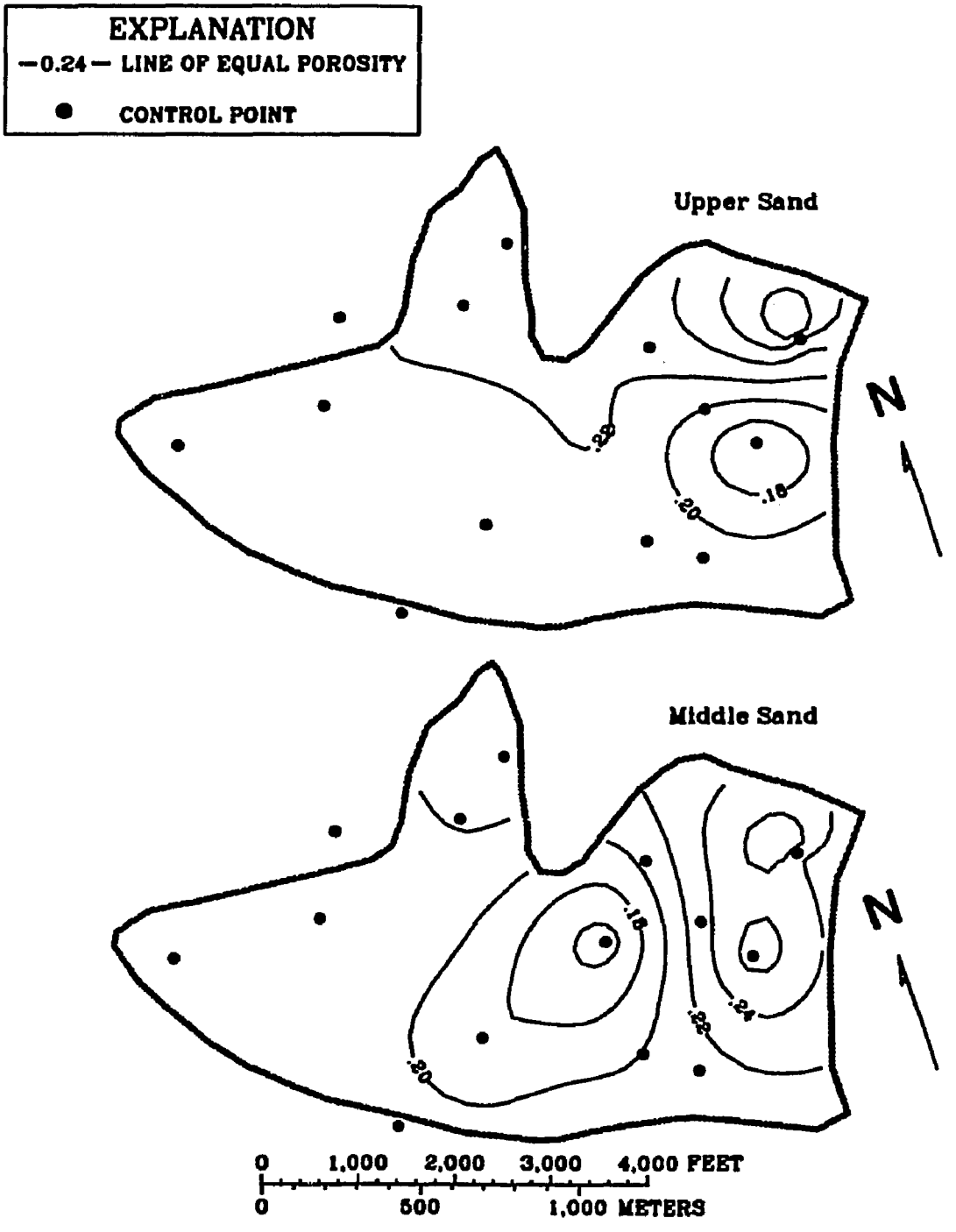

Figure C.6--Porosity maps of Sparta "A" upper and middle sands.

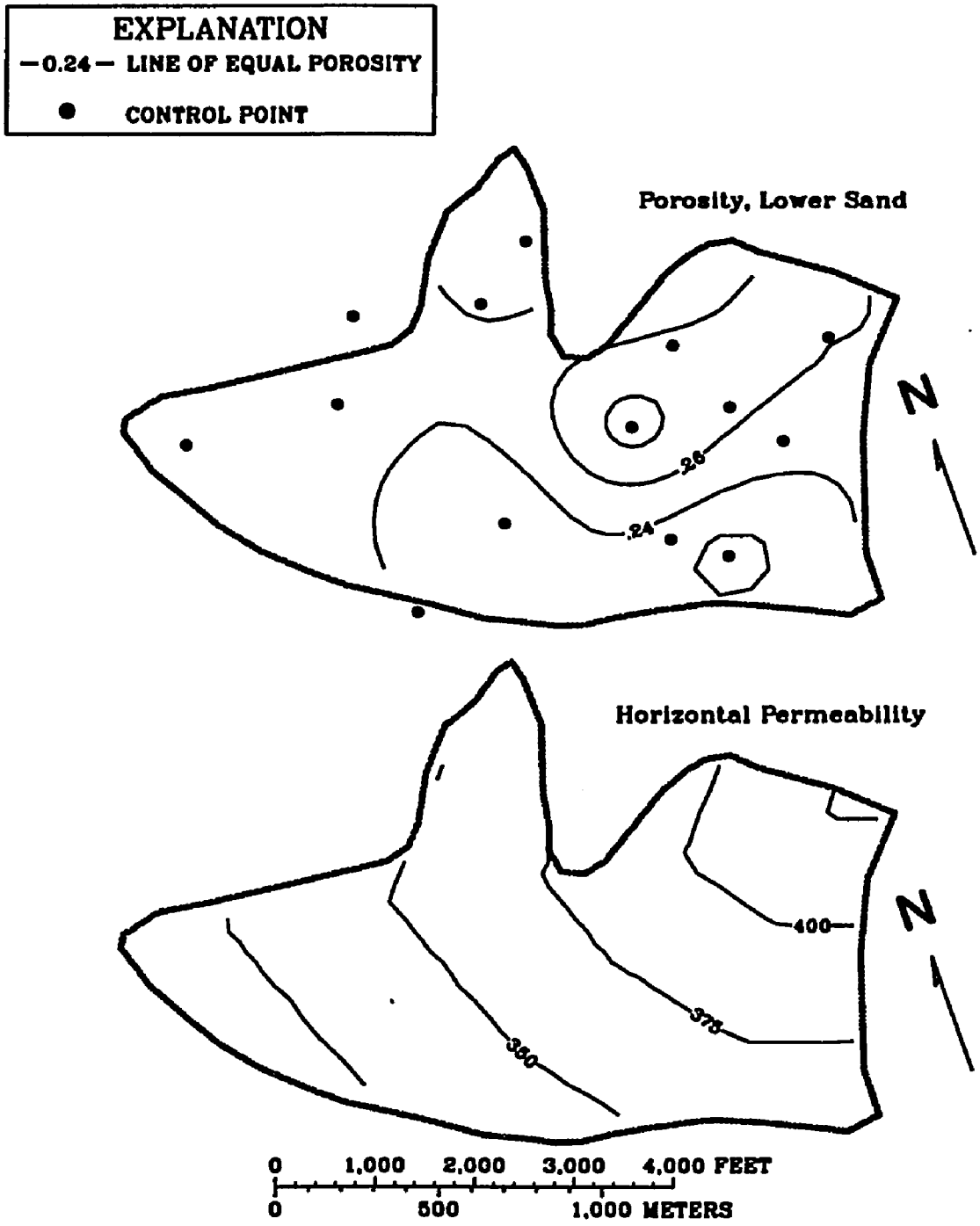

Figure C.7--Porosity map of Sparta "A" lower sand and the history-matched permeability map of all sands in the Sparta "A" reservoir.

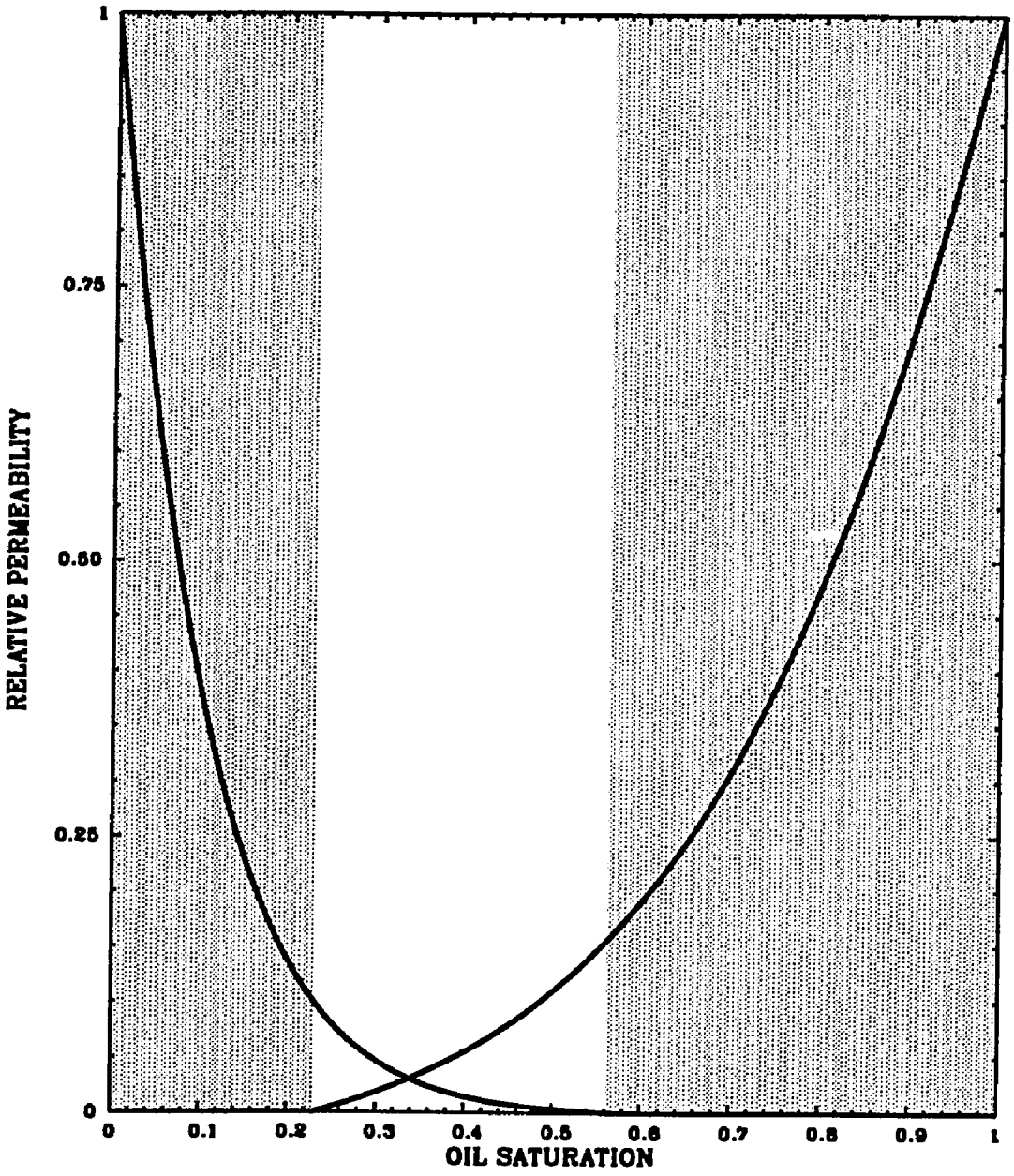

Figure C.6--Relative permeability curves for the Sparta "A".

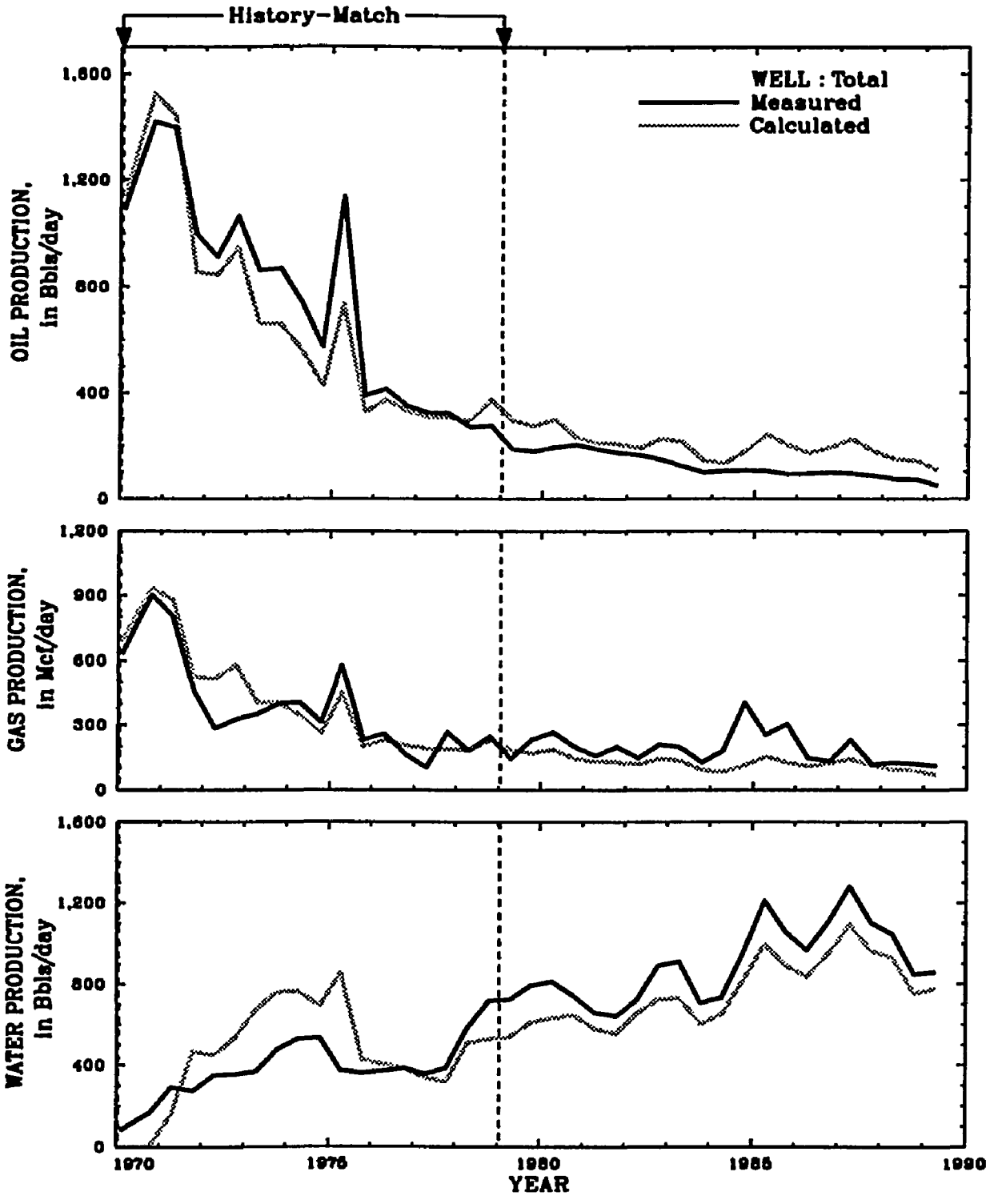

Figure C.9--Total production from the Sparta "A".

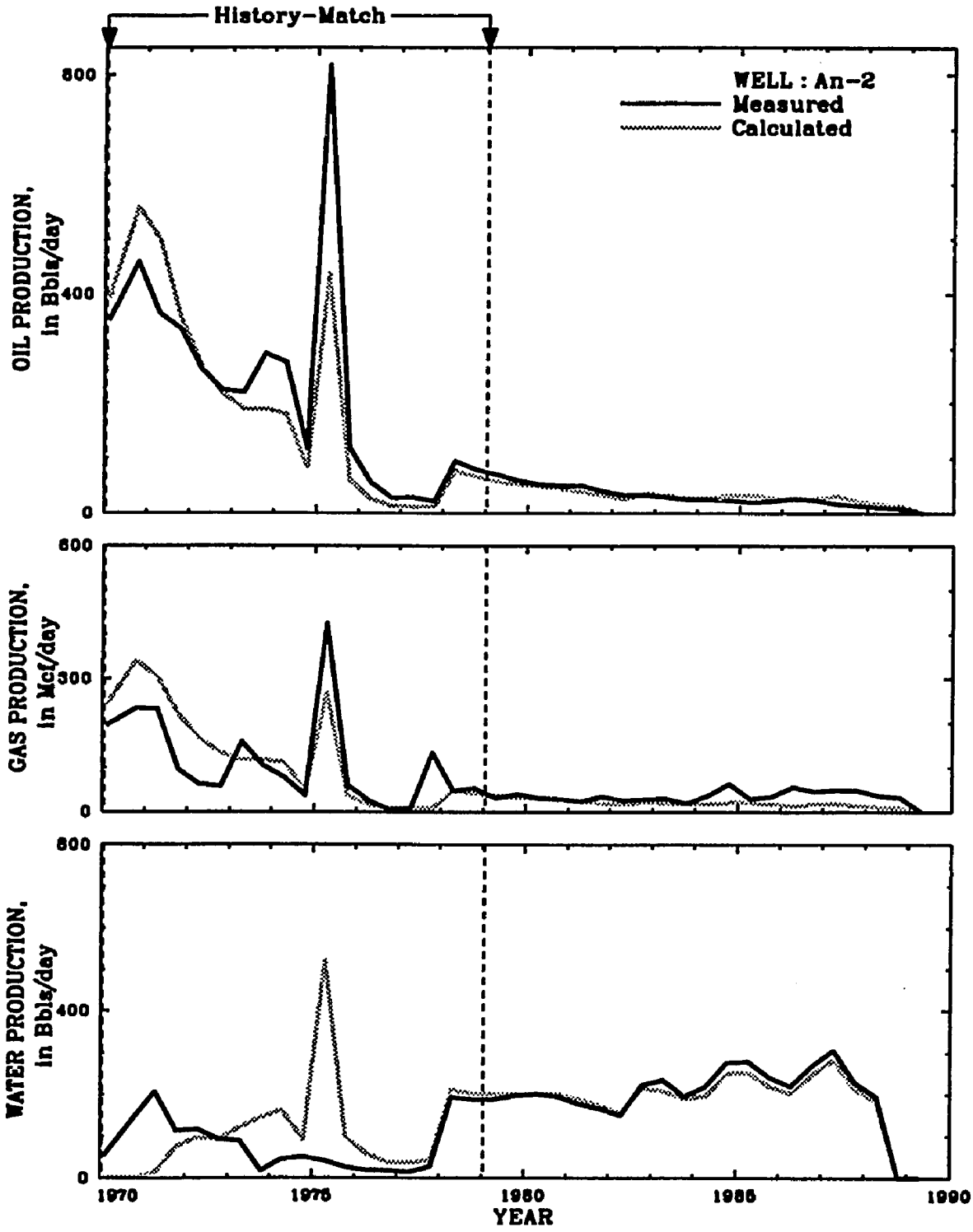

Figure C.10--Production from well An-2 in the Sparta "A".

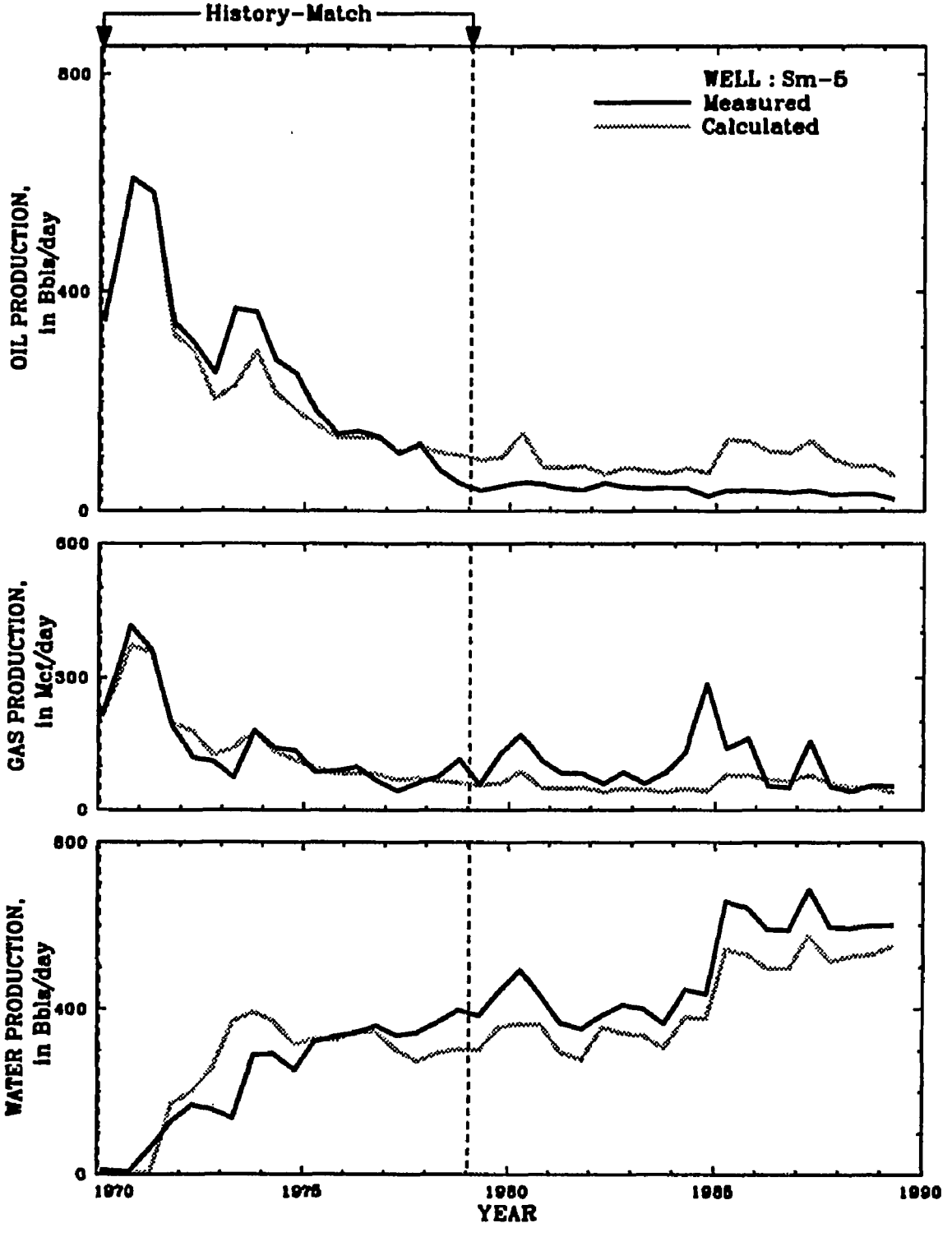

Figure C.11--Production from well Sm-5 in the Sparta "A".

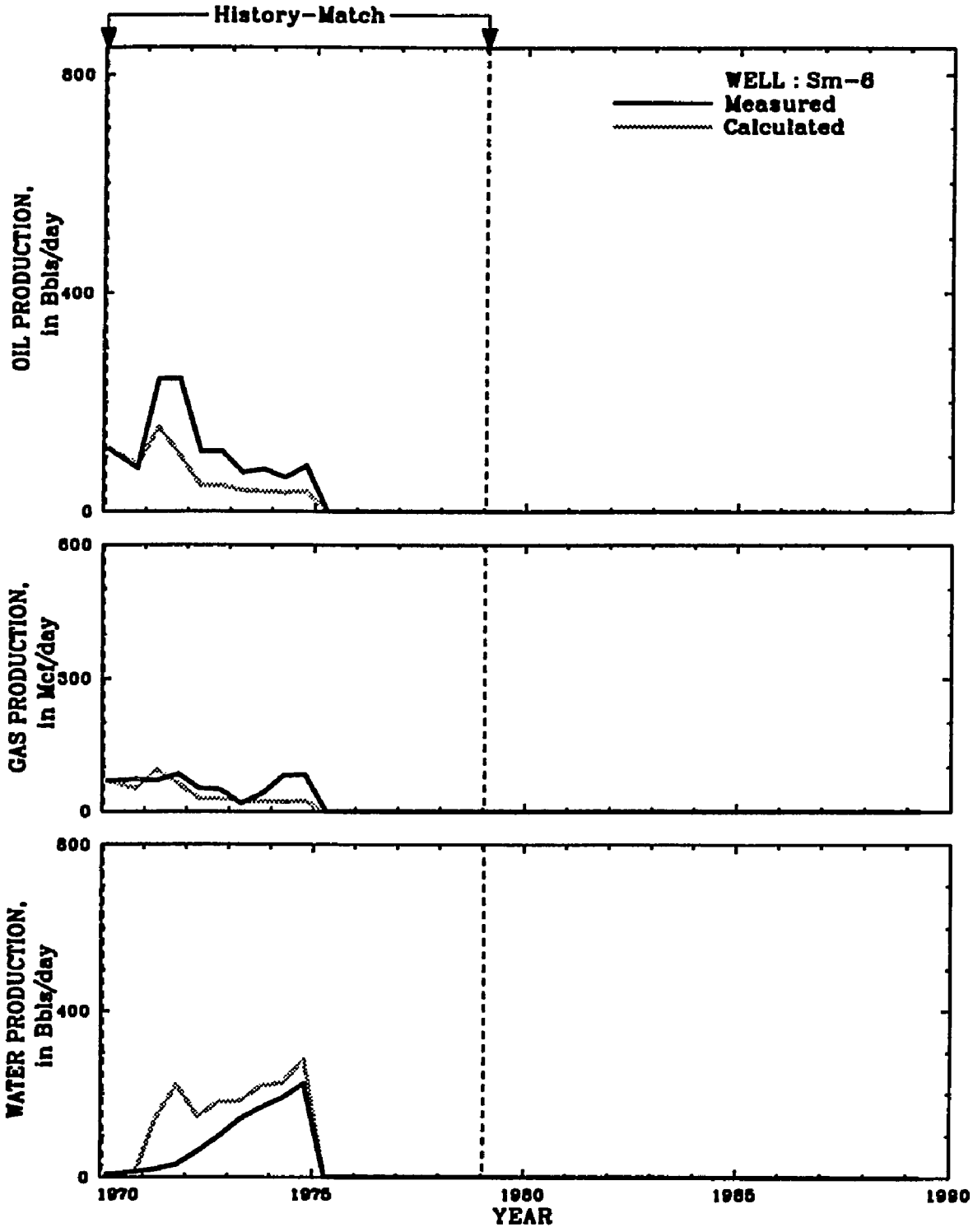

Figure C.12--Production from well Sm-6 in the Sparta "A".

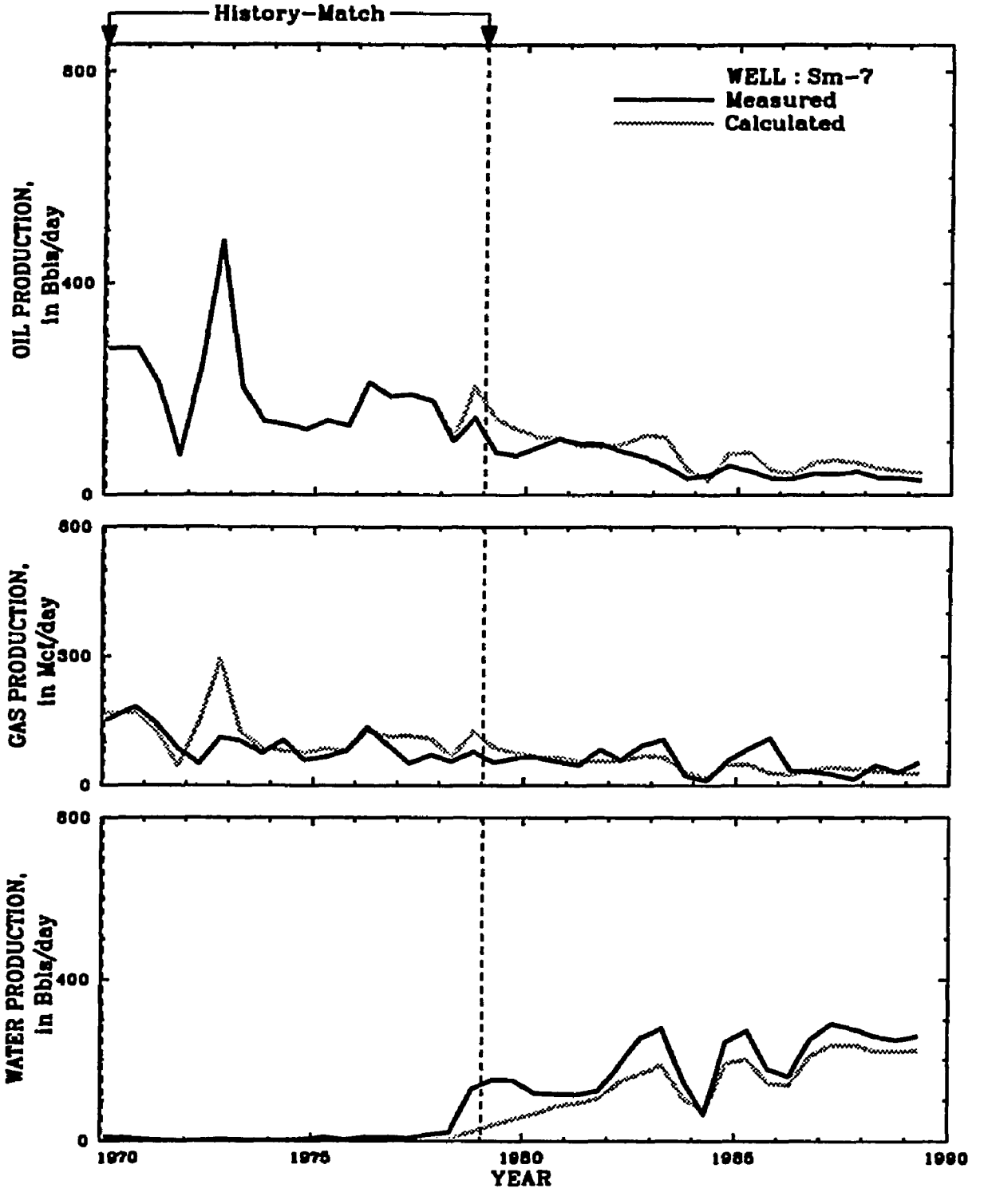

Figure C.13--Production from well Sm-7 in the Sparta "A".

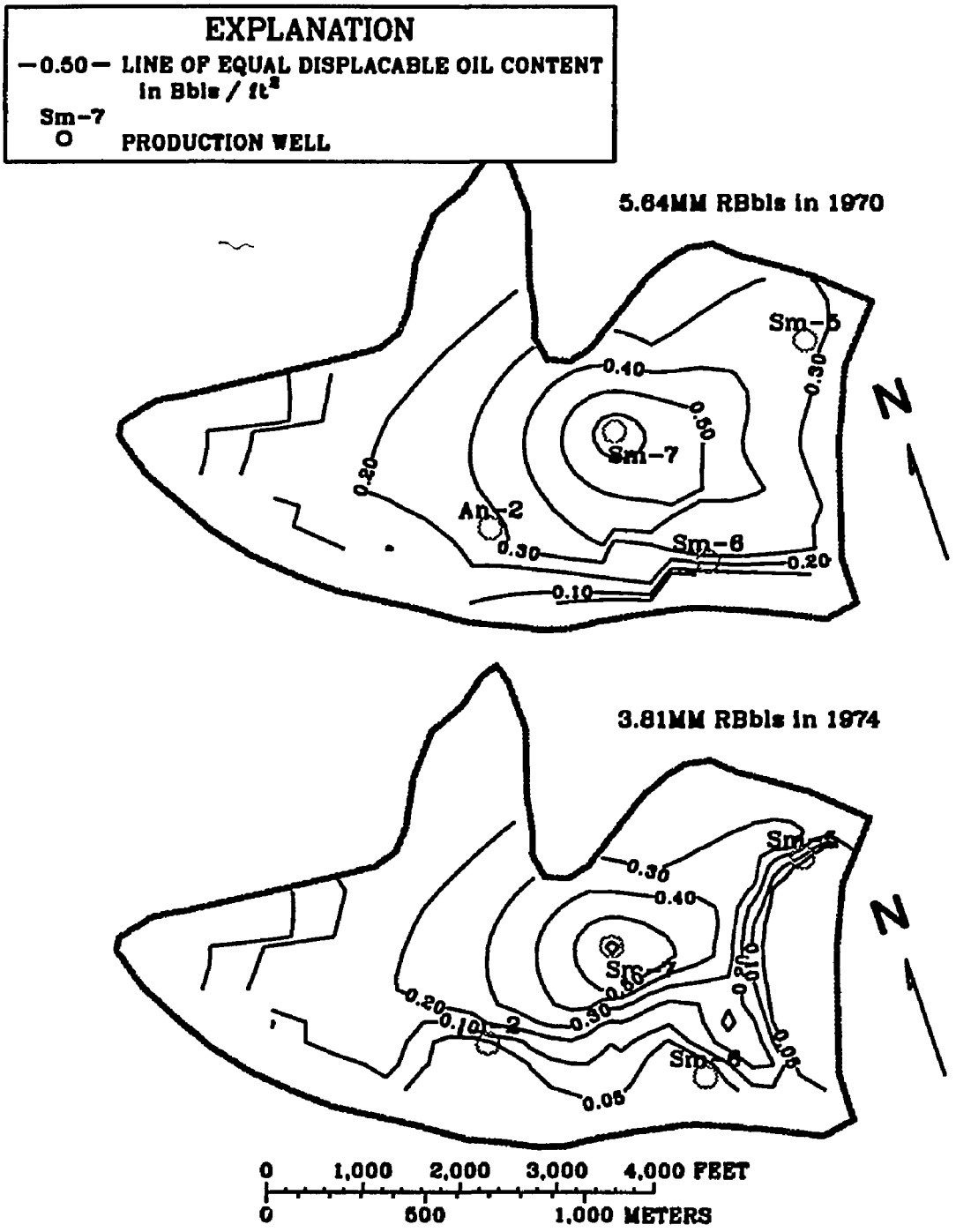

Figure C.14--Displaceable oil distribution in the Sparta "A" in 1970 and 1974.

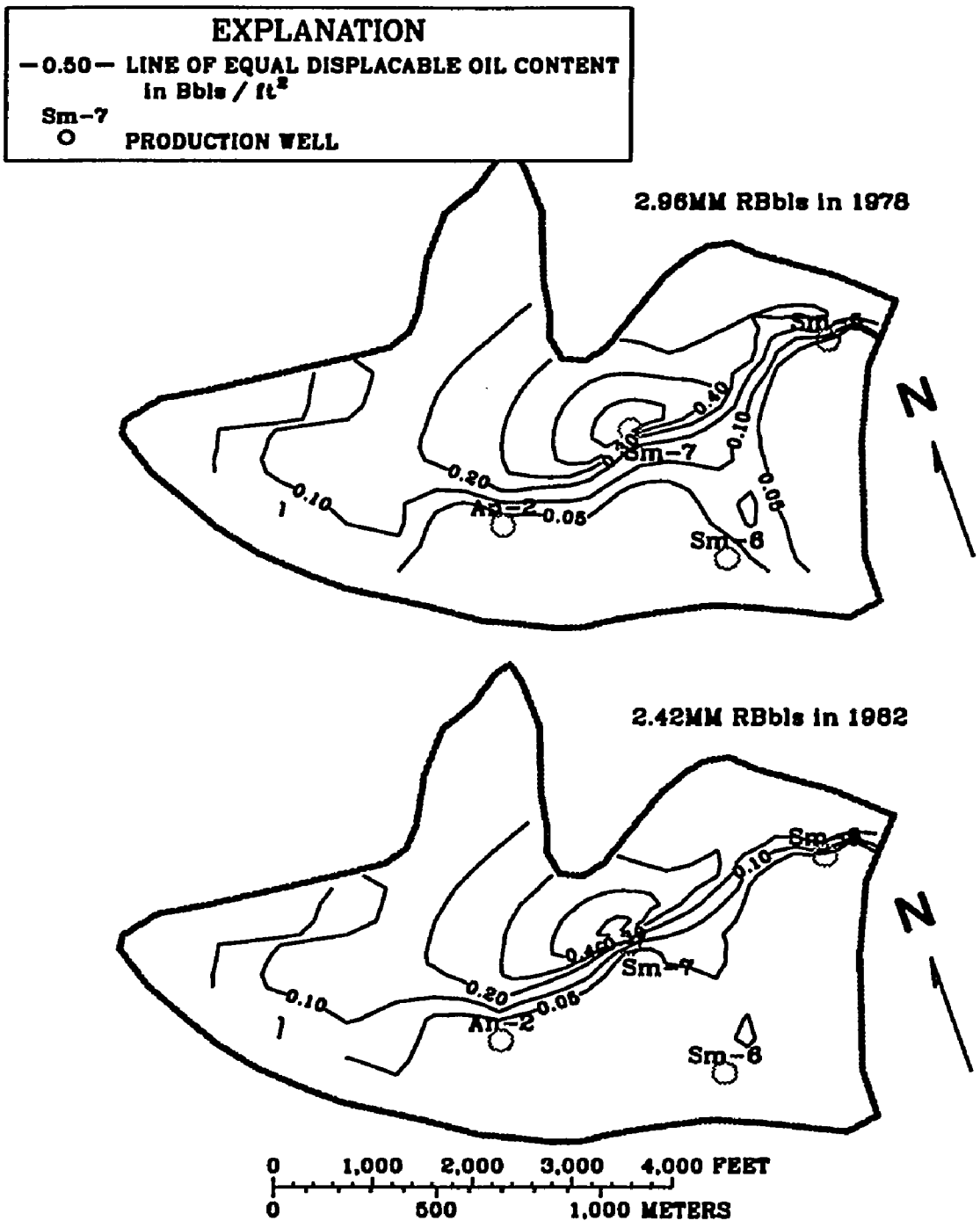

Figure C.15--Displaceable oil distribution in the Sparta "A" in 1978 and 1982.

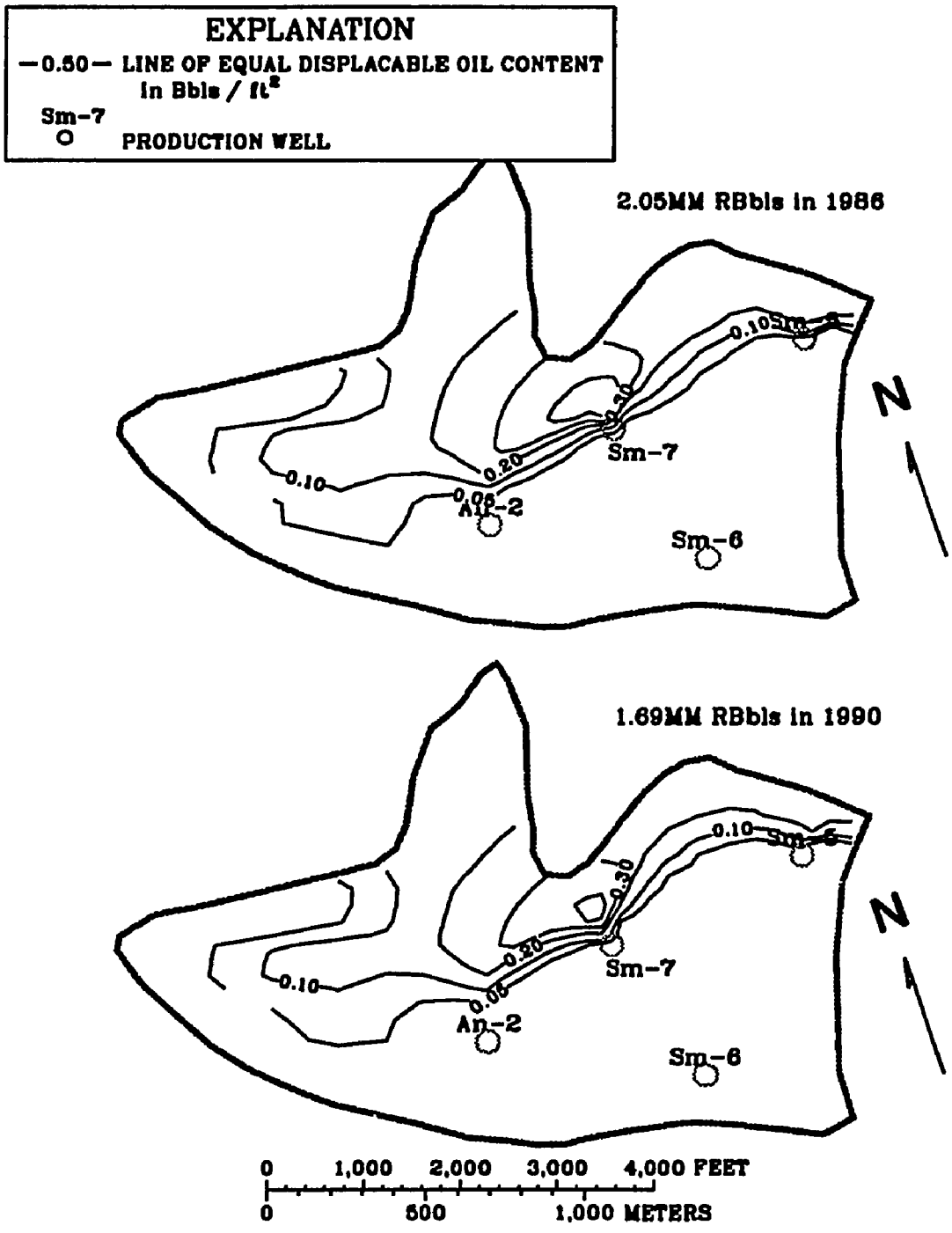

Figure C.16--Displaceable oil distribution in the Sparta "A" in 1986 and 1990.

VITA

Keith J. Halford was born in New Orleans, Louisiana on August 12, 1962, the son of Jerome P. and Elsie B. Halford. He received his official B.S. in Petroleum Engineering from Louisiana State University in May, 1984. Deja vu, he received his Master of Science in Petroleum Engineering from Louisiana State University in December, 1985.

Unlike the pursuit of his M.S., he did not strive non-stop and directly toward the degree of Doctor of Philosophy. He frittered away the days in blissful ignorance while working for the U.S. Geological Survey. The pace accelerated in May, 1989 after marrying Beryl Annette Swarzenski. In November, 1991, the cows had come home and PhuD work became paramount.

DOCTORAL EXAMINATION AND DISSERTATION REPORT

Candidate: Keith J. Halford

Major Field: Petroleum Engineering

Title of Dissertation: "Incorporating Reservoir Characteristics for Automatic History Matching"

Approved:

Major Professor and Chairman

Daniel Fogel

Dean of the Graduate School

EXAMINING COMMITTEE:

James Erwin

Kenneth Loh

Adam T. Bourgoyne Jr

Philip D. Shenewerk

Robert Desbrandes

Charles R. Dekell

Date of Examination:

April 14, 1992